Garnet- and clinopyroxene-liquid equilibria at high pressure: an experimental study in part of the system $CaO-MgO-FeO-Al_2O_3-SiO_2$ with relevance to garnet-lherzolites.

by

Derek Armshaw

Ph.D.

University of Edinburgh

1987

ABSTRACT

Melting experiments were conducted on 12 compositions in part of the system $CaO-MgO-FeO-Al_2O_3-SiO_2$, and electron microprobe analyses were obtained of the coexisting phases (liquid plus one or more of garnet, clinopyroxene, orthopyroxene, olivine and spinel).

Garnet-liquid and clinopyroxene-liquid equations were derived which expressed the distribution coefficents of mineral end-member components between crystal and liquid phases as functions of temperature, pressure and liquid composition using an ideal mixing liquid model and a regular mixing liquid model. The equations were written in the form of linear regression models and the partial regression coefficients were derived by fitting the equations to the experimental data by the method of least squares.

For any liquid in equilibrium with garnet and/or clinopyroxene, the derived mineral-melt equations can be used to predict the equilibrium temperature and the compositions of the coexisting crystals, provided that the pressure and liquid composition are known. The mineral-melt equations were tested by using them to predict temperature and composition values for the experimental liquids. Equations using the ideal mixing liquid model gave agreement between the predicted and the experimentally determined values to within 17°C, 9.2mol% Py, 17.2mol% Gr and 1.8mol% Alm (all 2σ). The greatest discrepancies were for grossular-rich garnets and calcic liquids. The existence of an experimentally determined minimum on the garnet-clinopyroxene cotectic shows that the ideal mixing liquid model is not appropriate for these compositions. Mineral-melt equations incorporating the regular mixing liquid model for the liquid phase recover the expeimental dataset to within 29.4°C,

3.4mol% Py, 5.2mol% Gr and 1.6mol% Alm (all 2σ), but cannot be used to predict values for other liquids due to numerical instability in their partial regression coefficients. It is suggested that this is a consequence of the least-squares fitting of equations with interrelated variables.

Mineral-melt equations using the ideal mixing liquid model were used to generate partial phase diagrams of part of the plane CS-MS-A, contoured for temperature and garnet composition. These enable the composition of the garnet predicted to coexist with any liquid, and the equilibrium temperature, to be obtained graphically. Diagrams are drawn for liquids with Mg'=85 and Mg'=100. In both diagrams, the predicted position of the garnet-clinopyroxene cotectic is close to the position of that determined experimentally. Temperature and composition values extracted from the Mg'=100 diagram are compared with experimental data on the pyrope-grossular join and are shown to agree to within 30°C and 5wt% Py.

Mineral-melt equations (ideal mixing liquid model) were also used to predict the temperature and pressure dependencies of the mineral end-member partition coefficients. Pyrope, grossular, almandine, diopside, enstatite and ferrosilite partition coefficients ($K_i=X_i^{xtal}/X_i^{liq}$) all decrease with increasing temperature, but the opposite behaviour is shown by Ca-tschermak pyroxene. The experimental data agree with these predictions.

TABLE OF CONTENTS

CHAPTER 1

INTRODUCTION

Basaltic magmas originate by partial melting of the upper mantle and may be modified by crystal fractionation during their ascent. Depths of melting of 50–200km are suggested by the seismic characteristics of the "low-velocity zone". In this depth range the dominant mantle lithology is garnet-lherzolite (*e.g.* Ringwood, 1975; Yoder, 1976), which suggests that the chemical equilibria between garnet, clinopyroxene, orthopyroxene, olivine and silicate liquids control the generation and early evolution of basic and ultrabasic magmas. To understand these equilibria and the processes and products of garnet-lherzolite partial melting and high-pressure crystallisation, a knowledge of the compositions of crystals and liquids which coexist at different temperatures and pressures is required.

Early high-pressure melting studies of lherzolites, basaltic rocks and related systems could not report liquid compositions because these could not be directly measured before the advent of the electron microprobe (*e.g.* Ito & Kennedy, 1967; Cohen *et al.*, 1967). Later studies were often affected by experimental problems of iron-loss and quench modification (*e.g.* Cawthorn *et al.*, 1973; Stern & Wyllie, 1975; Jaques & Green, 1979). Consequently, known compositions of coexisting garnets, clinopyroxenes, orthopyroxenes, olivines and silicate liquids at high pressures are few.

Several recent studies have been able to use crystal-liquid compositions from low pressure melting experiments on basaltic rocks and related simple systems to approximate the thermodynamic relationships between minerals and silicate melts and to model low to moderate pressure crystallisation and magmatic differentiation (Ford *et al.*, 1983; Ghiorso *et al.*, 1983; Berman &

Brown, 1984). The success of this approach suggests that it should be extended to higher pressures and that sufficient high-pressure data could yield a general model for upper mantle partial melting and crystal fractionation of primary magmas.

1.1. Previous work

1.1.1. Partial melting of garnet-lherzolite

Experiments at mantle pressures and temperatures became possible after the development of the solid-media high pressure apparatus (Boyd & England, 1958, 1960). The melting and phase relations of simple systems involving pyrope, diopside, enstatite and forsterite were determined at 30-40kb, and their relevance to natural systems demonstrated (*e.g.* Kushiro, 1964; O'Hara, 1963a; Davis, 1964; Boyd & England, 1964; Davis & Schairer, 1965). High-pressure experiments on garnet-lherzolite (O'Hara, 1963b; Ito & Kennedy, 1967) and basaltic rocks (*e.g.* Cohen *et al.*, 1967) supported the hypothesis that basaltic magma could be obtained by partial melting of the assemblage garnet + clinopyroxene + orthopyroxene + olivine.

In these early studies, the composition of the crystalline phases could be determined by X-ray diffraction (*e.g.* O'Hara, 1963b; Davis, 1964) but there was no technique to directly measure the liquid composition. The electron microprobe made this possible and several authors conducted partial melting experiments on natural spinel- and garnet-lherzolites (*e.g.* Kushiro *et al.*, 1972; Nehru & Wyllie, 1975; Mysen & Boettcher, 1975a,b; Mysen & Kushiro, 1977) but two major difficulties were encountered. These were chemical reaction between the partial melt and the container and modification of the liquid composition by growth of quench crystals.

1.1.2. Experimental problems

The problem of iron-loss to noble metal containers is well known (*e.g.* Stern & Wyllie, 1975; Biggar, 1977; Johannes & Bode, 1978). Jaques & Green (1979) emphasised that since iron is lost prefentially in the order liquid > olivine > pyroxene, significant iron-loss produces non-equilibrium assemblages. More recent studies (*e.g.* Scarfe *et al.*, 1979; Takahashi & Kushiro, 1983) have used graphite capsules to avoid this problem. The choice of graphite capsules for the present study is discussed in section 2.2.1..

Growth of metastable crystals from the liquid during quenching of a partially melted lherzolite can significantly alter the composition of the glass away from that of the equilibrium melt (Cawthorn *et al.*, 1973). Most previous studies have reported the presence of olivine or pyroxene quench crystals and quench overgrowths to stable crystalline phases. Jaques & Green (1979) examined the quench phases in their experiments by scanning electron microscopy and concluded that quench modification of their own and previous melt compositions precluded the direct determination of the compositions of partial melts. They determined the compositions of residual crystalline phases and the modal proportions of all phases (counting glass and quench as melt) and attempted to obtain the equilibrium melt compositions by mass balance calculations. Such calculations were shown to be unsatisfactory by Mysen & Boettcher (1975b, pp.576-578) because a small error in estimation of the modal proportions caused significant errors in the calculated compositions of small degree partial melts.

The problem of quench modification arises because the liquids to be analysed are typically the products of low to moderate degrees of partial melting. The small amounts of liquid produced are particularly susceptible to quench modification because they occur as films along grain boundaries and as

pockets at grain junctions. They have a high surface area in contact with the solid phases and formation of even thin quench overgrowths represents significant crystallisation from the liquid. Takahashi & Kushiro (1983) used an experimental technique with a basalt disc in a lherzolite–basalt–lherzolite "sandwich" to ensure a sufficiently large ~~area~~ volume of glass in the result to obtain the liquid composition with confidence. The latest studies (Takahashi & Scarfe, 1985; Takahashi, 1986) have analysed only segregated melts for the same reason.

Experiments on lherzolite melting are complemented by high-pressure crystallisation studies on lavas thought to represent primary magmas – *i.e.* liquids unaltered since separation from the crystalline residue of their source. Green & Ringwood (1967) identified garnet and clinopyroxene as the liquidus phases of three different basalt compositions at 27kb and an experiment on a picrite at the same pressure crystallised garnet, clinopyroxene, orthopyroxene and olivine together near the liquidus. Further studies have mainly concentrated on crystallisation at pressures up to 20kb and the genesis of oceanic basalts (*e.g.* Presnall *et al.*, 1979; Stolper, 1980). Elthon & Scarfe (1984) however, included one experiment on a high-Mg basalt at 25kb which gave the assemblage gt+cp+op+ol on the liquidus and reported the compositions of the coexisting phases. Analyses from results of high-pressure crystallisation experiments are also subject to the problem of quench modification discussed above. Again some authors have tried to design their experiments to minimise this by ensuring a large ~~area~~ volume of glass for analysis (*e.g.* Presnall *et al.*, 1979; Stolper, 1980).

1.1.3. Thermodynamics of minerals and melts

A number of models for the thermodynamic properties of mineral solid solutions have been proposed (reviewed by Grover, 1976). Component activities may be related to phase compositions by models based on the occupancy of crystal lattice sites. For non-ideal solutions, the excess free energy of mixing can be expressed by a mixing model using one or more "interaction parameters". The absolute value of the interaction parameters can be derived from experimental data. Rigorous thermodynamic models of sub-solidus phase equilibria are possible (*e.g.* Saxena & Eriksson, 1983, 1985; Wood & Holloway, 1984).

The main obstacle to a rigorous thermodynamic treatment of crystal-liquid equilibria is lack of knowledge of the thermodynamic properties of silicate liquids. Polymer theory has been applied to binary silicate liquids (Masson, 1965; Hess, 1979), but it is difficult to extend this to multicomponent systems. Bottinga & Weill (1972) considered silicate melts to consist of a polymerised irregular network of tetrahedrally coordinated Si and Al cations linked by bridging oxygen anions. This network is modified by larger cations which occupy high coordination sites. Cations are therefore classed as network formers or network modifiers. By assuming that network formers and network modifiers mix idealy amongst themselves and that there is no interaction between the two types, the activities of oxide melt components can be expressed in terms of their mole fractions. Expressions of melt component activities from Bottinga & Weill's "two lattice" model have been used by Nielsen & Drake (1979) and Nielsen & Dungan (1983) to calculate crystal-liquid equilibria in mafic systems at low pressures.

Burnham (1975, 1979, 1981) developed a model in which complex "quasi-crystalline" components mix ideally. These components have the same

stoichiometry as the phases which appear on the liquidus of the melt. Melt components are normalised to eight oxygen atoms and the aluminosilicate components $NaAlSi_3O_8$, $KAlSi_3O_8$ and $CaAl_2Si_2O_8$ together with silica, Si_4O_8, are regarded as a multicomponent solvent in which the other components behave as solutes according to Henry's Law (*i.e.* the activity of a component is equal to its mole fraction). This model has successfully described the behaviour of water in granitic melts but has not yet been extended to more basic liquids because of a lack of the required thermochemical data.

Ghiorso & Carmichael (1980) and Ghiorso *et al.* (1983) also used stoichiometric mineral-like components normalised to eight oxygens, choosing a set related to network, orthosilicate and chain-type structures. The activities of these components were described by a regular solution model with the interaction parameters derived by regression techniques from a database of published experimental results on natural silicate liquids at low to moderate pressures. Berman & Brown (1984) also used a regular solution model for the liquid and derived interaction parameters from an experimental database but chose the simple oxides as melt components. This allowed the whole compositional space to be represented with non-negative proportions of these components. Ghiorso & Carmichael (1980) and Ghiorso *et al.* (1983) were concerned with the more restricted compositional space occupied by natural silicate liquids. Ford *et al.* (1983) chose oxide melt components in their study of olivine-liquid equilibria and derived equations to express single-component partition coefficients as functions of temperature, pressure and liquid composition. These equations were then fitted to an experimental database by regression.

A major goal of the numerical treatment of crystal-liquid equilibria must be the calulation of phase equilibria, especially the compositions and proportions

of coexisting crystals and liquids during partial melting and crystallisation. Nathan & Van Kirk (1978) designed a computer model of atmospheric pressure fractional crystallisation. Equations relating temperature and crystal compositions to liquid compositions were empirically derived from a database of published analyses. Langmuir & Hanson (1981) also used an empirical approach, deriving single-component partition coefficients from a database of published experimental results, and combining these with mass balance equations and stoichiometric constraints imposed by the crystalline phases to calculate phase equilibria in some simple and natural systems. More recent attempts (Nielsen & Dungan, 1983; Ghiorso *et al*, 1983; Berman & Brown, 1984; Ford, 1984) have been thermodynamically based according to one of the models already discussed. Both empirical and thermodynamically based approaches have been successful in reproducing some experimentally determined phase equilibria and crystallisation sequences. However, only the thermodynamically based models have the potential to make predictions considerably beyond their database and are therefore to be preferred.

1.2. Aims of this study

The aims of this study are twofold:

- to conduct high-pressure melting experiments involving particularly garnet, but also clinopyroxene, orthopyroxene and olivine and to obtain the compositions of coexisting crystal and liquid phases.

- to use this data to approximate a thermodynamically based model to describe crystal-liquid equilibria in the assemblage liquid+gt+cp+op+ol at high pressures and to apply this model to simple and natural systems

1.3. Approach adopted

In this study melting experiments were carried out on synthetic compositions in the system $CaO-MgO-FeO-Al_2O_3-SiO_2$. These oxides constituted over 94wt% in each of 161 whole rock analyses of mantle-derived garnet-lherzolites found in a literature search; the average sum exceeded 97wt% (Appendix). The work of Presnall *et al.* (1979) on lherzolite melting at pressures up to 20kb used a simplified lherzolite composition in the system $CaO-MgO-Al_2O_3-SiO_2$. The same system was used by Maaloe & Petersen (1976) to consider the possible effects of high-pressure crystal fractionation from primary magmas. In the present study, FeO has been included because almandine ($Fe_3Al_2Si_3O_{12}$) is a significant component of garnets in natural lherzolites and since iron-magnesium partitioning between solid and liquid phases is an important petrological tool (*e.g.* Roeder & Emslie, 1970; Mysen, 1975).

The choice of a synthetic system allows greater control over the experimentation. Compositions can be chosen to generate results over a range of temperature, pressure and composition. In addition, the problem of quench modification can be overcome by choosing compositions to yield a large proportion of liquid. The choice of a relatively simple system also facilitates the numerical treatment of the results since the thermodynamic description of the system is more straightforward than for a complex natural system. As already discussed however, a simple model, if properly formulated can have applications to natural systems.

CHAPTER 2

EXPERIMENTAL PROCEDURE AND ANALYSIS OF RESULTS

2.1. Choice of starting materials

The five component system $CaO-MgO-FeO-Al_2O_3-SiO_2$ chosen for this study can be represented graphically with four components if FeO is recalculated as its molar equivalent of MgO as in the CMAS projection scheme of O'Hara (1968). Figure 2-1 is a sketch of the CMAS tetrahedron showing the plotting parameters used and the compositions of the mineral end-members of interest to this study. Note that direct representation of the iron-magnesium ratio is lost in this projection.

Several authors have noted that the system $CaSiO_3-MgSiO_3-Al_2O_3$ provides a good model for garnet-pyroxene equilibria in ultramafic rocks since it contains the mineral end-members pyrope, grossular, enstatite, diopside and Ca-tschermak pyroxene and solid solutions between them (*e.g.* Boyd, 1970; Thompson, 1979). The corresponding system in this study is represented by the plane CS-MS-A in Figure 2-1. Since olivine-liquid equilibria had already been studied by Ford *et al.* (1983) and Ford (1984), the first efforts of this study were directed towards coexisting garnets, pyroxenes and liquids in the plane CS-MS-A. Later experiments were performed on compositions on either side of this plane in the volumes M_2S-CS-MS-A and S-CS-MS-A.

The iron-magnesium ratio of the starting compositions was chosen to be Mg'= 85 (Mg'= mol.props. MgO/MgO+FeO) because the most iron-rich (*i.e.* "fertile") mantle-derived garnet-lherzolites found in a literature search had Mg'= 85-90 (Appendix). The liquidus projection of part of the system $CaSiO_3-MgSiO_3-Al_2O_3$ was deduced by Maaløe & Wyllie (1979) from phase relations in the joins diopside-pyrope and pyrope-grossular. Melting and phase

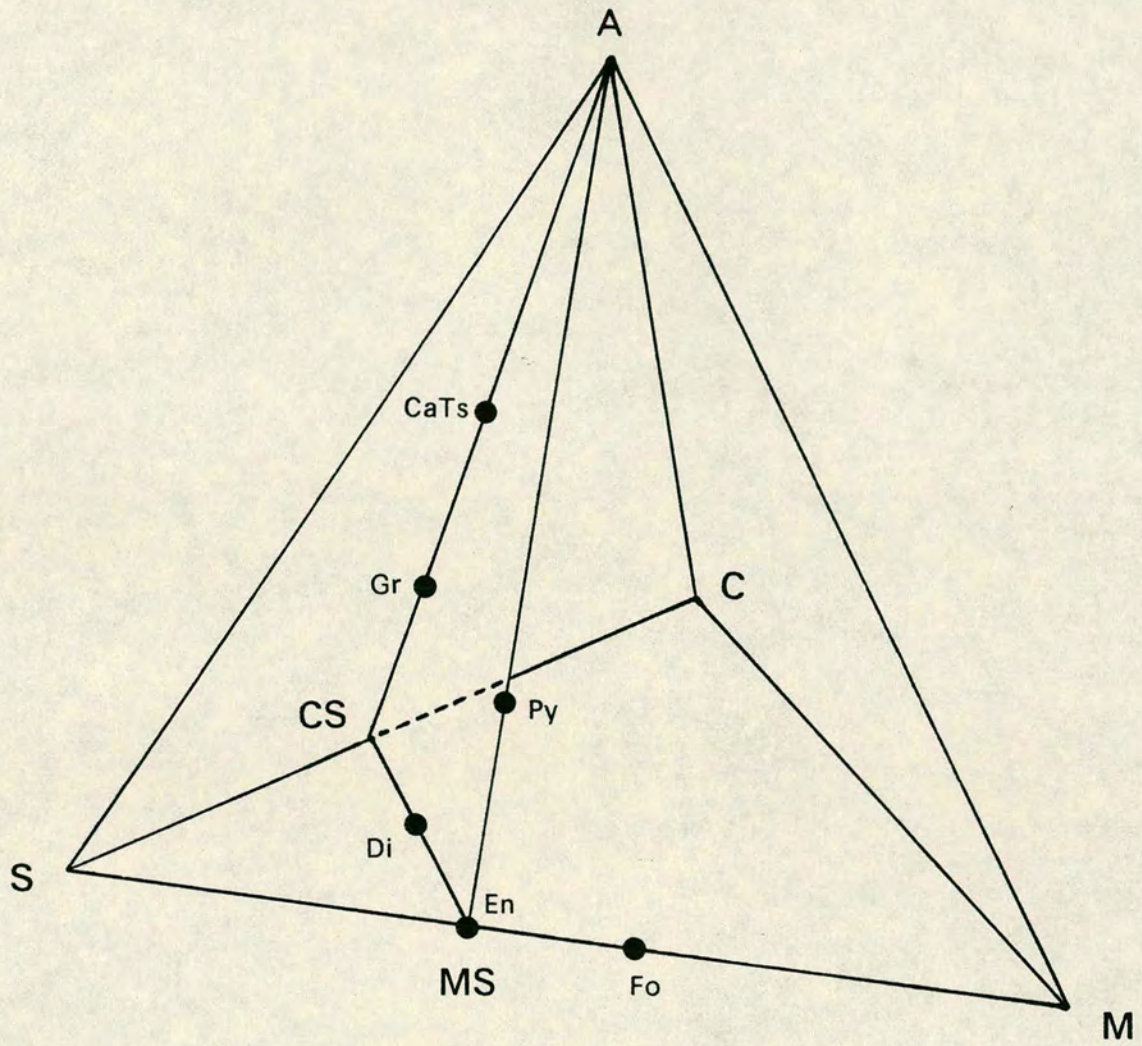

Figure 2-1 : CMAS tetrahedron and CS-MS-A plane. Pyrope (Py), grossular (Gr), diopside (Di), enstatite (En), Ca-tschermak pyroxene (CaTs) and forsterite (Fo) are plotted. Plotting parameters are calculated as follows, then expressed as percentages:

C = wt% CaO
M = 40.3 x (mol. props. MgO + FeO)
A = wt% Al_2O_3
S = wt% SiO_2

relations in the CS-MS-A plane of this study were assumed to be broadly similar to those known from $CaSiO_3$-$MgSiO_3$-Al_2O_3 because of the comparatively low FeO content, and four starting material compositions were chosen to lie fairly close to the presumed positions of the garnet-clinopyroxene and garnet-orthopyroxene cotectic curves in order to generate a large melt fraction close to the solidus (Figure 2-2).

Calculated compositions of the four chosen points in the plane CS-MS-A are given in Table 2-1. These compositions were prepared as gels according to the technique of Biggar & O'Hara (1969). One gram of each gel was dried and reduced as a pressed pellet held at 1100°C for 24 hours in a H_2-CO_2 gas mixture at the oxygen fugacity of the iron-wüstite buffer.

For experiments on compositions on either side of the plane CS-MS-A starting materials were made by addition of either silica or olivine to the in-plane gels. Silca was obtained from a Brazilian quartz crystal from the departmental collection; olivine from material separated from a garnet-lherzolite nodule by O'Hara & Mercy (1963) and designated A1 by them. The quartz was essentially pure silica (P. Aspen, pers.comm.) and analyses of olivine A1 are given in Table 2-2. Quartz and olivine crystals were ground for 1 minute in an agate Tema mill and for five minutes by hand under acetone in an agate mortar. The final grainsize of the crushed material was less than 20 µm. Sufficient quartz or olivine was added to the in-plane gels to give mixtures containing about 15 mol% of the added material. Mixtures were ground together under acetone for 5 minutes. Actual compositions of these materials are given in Table 2-3 and are discussed below.

The twelve starting compositions thus comprised four in the plane CS-MS-A, four in the volume S-CS-MS-A and four in the volume

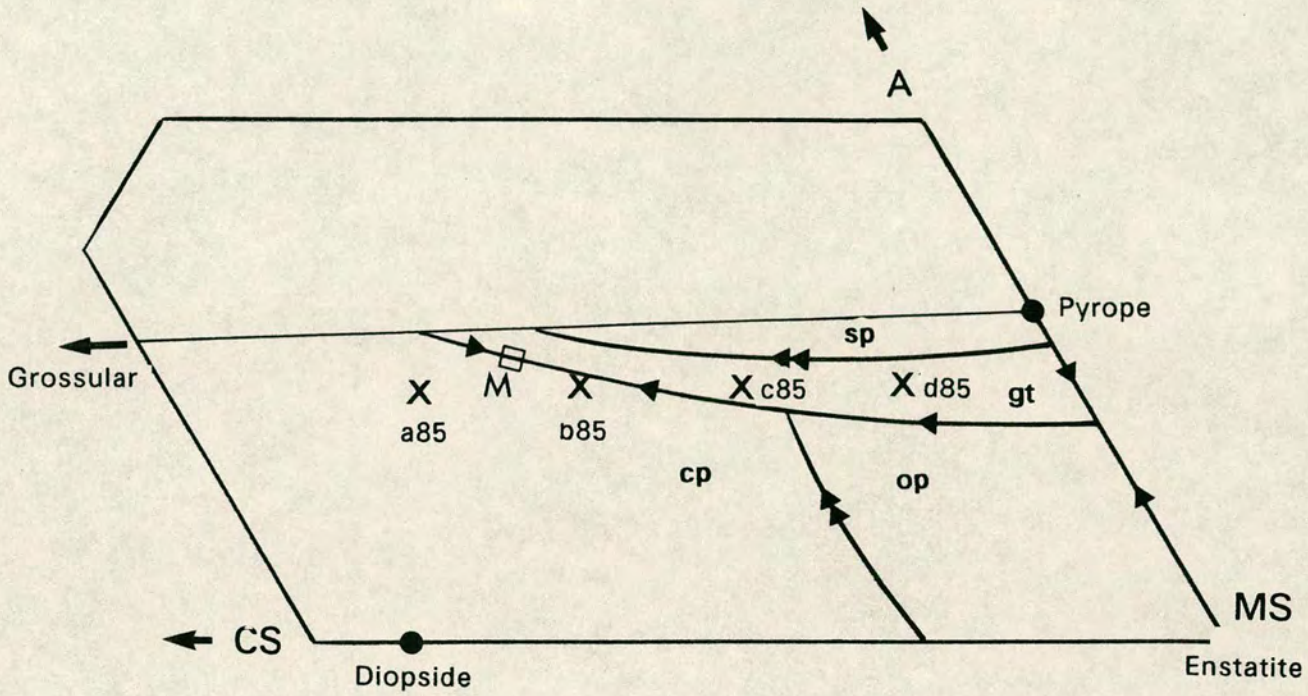

Figure 2–2 : Part of the plane CS–MS–A showing the compositions of the starting materials a85, b85, c85 and d85, and the phase relations of part of the system $CaSiO_3$–$MgSiO_3$–Al_2O_3 from Maaløe & Wyllie (1979). Primary phase fields are garnet solid solution (**gt**), clinopyroxene solid solution (**cp**), orthopyroxene solid solution (**op**) and spinel (**sp**). Double arrows represent reaction curves. The point M represents a minimum on the garnet–clinopyroxene cotectic.

Table 2-1 : Calculated compositions of starting materials in the plane CS-MS-A.

	a85	b85	c85	d85
SiO_2	44.14	44.59	45.05	45.52
Al_2O_3	18.72	18.92	19.11	19.31
FeO	3.96	5.00	6.06	7.14
MgO	12.58	15.89	19.27	22.71
CaO	20.60	15.61	10.51	5.31
total	100.00	100.01	100.00	99.99
Mg'	0.85	0.85	0.85	0.85

Table 2-2 : Analyses of Olivine A1

1 O'Hara & Mercy (1963) wet chemistry
2 this study - average of 6 probe analyses

	1	2
SiO_2	-	41.00
FeO	6.28	6.30
MgO	51.61	52.32
MnO	0.10	0.11
NiO	0.38	0.39
others	0.07	-
total	-	100.12
Fo	93.6	93.7

Table 2-3 : Analysed compositions of starting materials

	a85	a85+S	a85+Ol	b85	b85+S	b85+Ol
SiO_2	43.15	49.27	43.21	44.32	46.98	43.51
Al_2O_3	18.96	16.94	14.28	19.06	17.66	15.76
FeO	3.71	3.33	4.58	4.76	4.50	4.85
MgO	12.40	10.90	17.93	15.33	15.08	20.67
CaO	20.79	18.78	18.62	15.51	15.42	14.22
total	99.01	99.22	98.62	98.98	99.64	99.01
Mg'	0.86	0.85	0.87	0.85	0.86	0.88

	c85	c85+S	c85+Ol	d85	d85+S	d85+Ol
SiO_2	44.48	48.61	43.74	45.43	50.13	44.45
Al_2O_3	18.90	17.71	16.24	19.50	16.94	14.87
FeO	5.74	5.25	5.85	6.78	6.14	6.86
MgO	19.01	17.66	23.91	22.92	20.49	28.43
CaO	10.64	9.86	8.86	5.50	4.93	4.28
total	98.77	99.09	98.60	100.13	98.63	98.89
Mg'	0.85	0.86	0.88	0.86	0.86	0.88

M_2S-CS-MS-A. The actual compositions of these materials when prepared were checked by electron microprobe analysis of glass beads produced on a hot-stage microscope. In this device, about 1mg of starting material was held in a loop of platinum wire through which a current was passed. The sample could be observed through the microscope and complete melting took place in 2-3 seconds depending on the size of the sample. The liquid was quenched to a glass almost instantaneously by switching off the power. Two or three beads were made from each starting composition and analysed by electron microprobe. Results are given in Table 2-3. These analyses are taken to be the actual compositions of the starting materials used in the experiments.

The possibility that the prepared gels were inhomogeneous was examined by making 12 glass beads of starting composition d85 on the hot-stage microscope as described above. Four analyses of each bead were obtained by electron microprobe. Variations between beads were similar to variations between analyses of the same bead and it was concluded that the gels used as starting materials were homogeneous, at least in samples of 1mg or more. Possible inhomogeneity of the silica- and olivine-added mixtures was not investigated. It was considered that since the object of the experiments was to obtain the compositions of coexisting crystals and liquids, a knowledge of the exact composition of the starting material was unnecessary provided that each experiment reached equilibrium.

2.2. Solid media apparatus

2.2.1. Equipment and materials

All experiments were carried out using a single stage piston-in-cylinder solid media pressure apparatus similar to that described by Boyd & England (1960). Two such devices were used and there were no mechanical or

operational differences between them. Labels by which experiments are refered to (*e.g.* A364, B707 *etc.*) are derived from a letter A or B to denote which solid-media device was used and a number continuing from a sequence previously used in the laboratory.

All experiments at 30kb were conducted using the pressure cell shown in Figure 2-3. Several 40kb experiments with this cell gave a result in which the capsule was badly deformed and penetrated by the thermocouple. Satisfactory results were obtained when the lower alumina ceramic filler rod of the pressure cell was replaced with one made of boron nitride, and a 0.5mm thick ceramic disc was used between the thermocouple tip and the capsule. In all experiments, a thin coat of a MoS_2 based lubricant ("Molykote") was used between the lead foil and the carbide core.

Tungsten / tungsten74%-rhenium26% alloy thermocouples were used to measure and control the furnace temperature. Thermocouple tips were welded in a stream of argon gas using a tungsten electrode. Temperature control was maintained by a Eurotherm stepless temperature controller and temperatures were checked using a Pye precision decade potentiometer. No correction was made for the effect of pressure on the thermocouple emf. Possible errors in reported temperatures may include a slight thermal gradient between the thermocouple tip and the sample, and possible temperature fluctuation too rapid to register on the controller or potentiometer. Reported temperatures are believed accurate to within ±10°C.

In each experiment 4-5mg of sample was contained in a graphite capsule. The use of graphite to overcome the problem of iron-loss to noble metal capsules was discussed in section 1.2.2. Presnall *et al.* (1973) reported that occasional leakage of graphite capsules allowed ingress of Al_2O_3 from

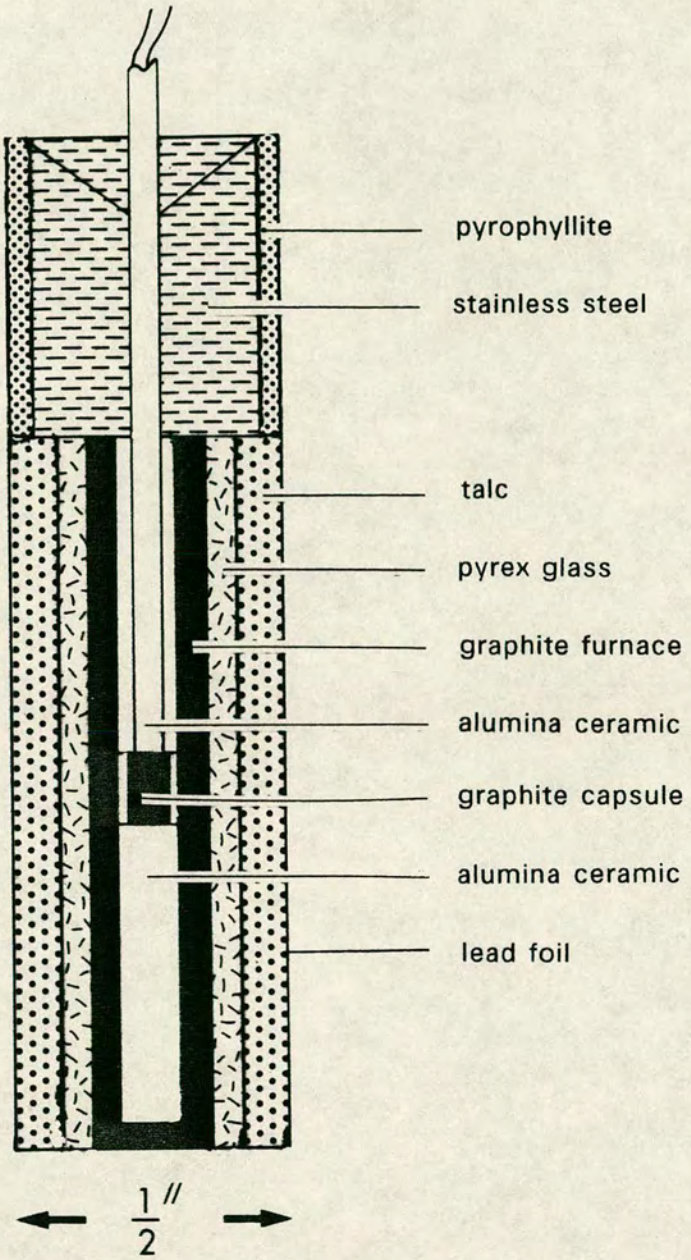

Figure 2–3 : Pressure cell.

surrounding furnace parts. In the present study, the capsule recovered from experiment was examined optically before and after mounting. Experimental products with broken or badly deformed capsules were discarded. Capsule breakage became a serious problem at 40kb and some experiments were conducted with graphite capsules within platinum outer capsules to ensure their integrity.

Thompson & Kushiro (1972) performed experiments on hematite-graphite mixtures in graphite capsules at 1100-1600°C and 10-20kb and obtained wüstite as the experimental product over most of this range. They concluded that the use of graphite capsules maintained the oxygen fugacity of the sample within the wüstite stability field. Bickle (1978) contained samples of magnesiowüstite in graphite capsules at 1700°C and 30kb for up to 24 hours. The composition of magnesiowüstite is sensitive to oxygen fugacity. Bickle (1978) detected no change in the compositions of the magnesiowüstite charges and concluded that there was insufficient oxygen available in a dry graphite capsule to oxidise an initially reduced charge. The starting materials used in the present study contained only ferrous iron and it is belived that the oxygen fugacity was maintained within the stability field of wüstite for the majority of the experiments. In four experiments, some of the iron was reduced to iron metal ; this is discussed further in Section 3.2.

A careful drying procedure was followed to ensure that all experiments were performed under anhydrous conditions. Starting materials were stored either in a drying oven at 110°C or in a dessicator. Graphite furnaces were assembled with a loaded capsule and the packing pieces, and dried at 110°C overnight or longer. Immediately prior to the experiment, each furnace assembly was dried for 20-30 minutes at 600°C in a stream of dry nitrogen in a muffle furnace.

All experiments were carried out using the piston-out technique of Richardson *et al.* (1968) with an overpressure of 5kb. No corrections have been applied to the reported pressures. A number of tungsten carbide pistons broke during pumping up at 35-45kb. Each breakage caused the loss of the pressure vessel carbide core as well as the experiment. The problem was reduced with the use of a 0.005 inch thick steel shim between the large and small pistons, but the risk of breakage could not be completely eliminated and it was suspected that the quality of the carbide used for the pistons was below the required specification. This problem resulted in only a few 40kb experiments being successfully completed.

2.2.2. Calibration

The melting point of diopside was determined in both graphite and platinum capsules at 25kb and in graphite capsules at 40kb. The starting material for all 25kb experiments was a diospide gel made by Dr. G.M. Biggar according to the method of Biggar & O'Hara (1969). The 40kb experiments were conducted on finely ground crystalline diopside prepared by hydrothermal synthesis from a gel by M. Welch. Results of melting point determinations are given in Table 2-4. Most experiments were of 5 minutes duration and the products were mounted in oil and examined in transmitted light. The presence of glass and quench crystals with no remaining crystals of primary diopside was taken to indicate that the liquidus had been crossed. Three experiments of 24 hours duration were conducted, mounted in epoxy resin, sectioned and analysed by electron microprobe to check for possible Al_2O_3 entry to the graphite capsules. One capsule was found to be cracked on recovery and contained a glass with almost 3wt% Al_2O_3. The two successful experiments were analysed as pure diopside glass or crystals within the analytical precision of the electron microprobe. Table 2-4 shows that there is good agreement in this study

Table 2-4 : Diopside melting point determinations for the two solid media pressure devices used in this study.

	Run no.	Temp	Result
Apparatus A	A351	1710°C	quench >> glass
Platinum capsules	A350	1700°C	> 95% crystalline
25kb 5mins duration			
Apparatus B	B536	1720°C	quench >> glass
Platinum capsules	B535	1710°C	quench >> glass
25kb 5mins duration	B538	1700°C	> 95% crystalline
	B539	1690°C	> 95% crystalline
Apparatus A	A358	1720°C	quench >> glass
Graphite capsules	A356	1710°C	crystalline > quench
25kb 5mins duration	A353	1700°C	crystalline > quench > glass
	A354	1690°C	> 95% crystalline
Apparatus B	B556	1720°C	quench >> glass
Graphite capsules	B549	1710°C	quench > crystalline
25kb 5mins duration	B546	1700°C	> 95% crystalline
	B547	1690°C	> 95% crystalline
Apparatus B	B710	1710°C	glass >> quench
Graphite capsules	B708	1700°C	crystalline > quench
25kb 24hrs duration			
Apparatus B	B788	1820°C	> 95% glass
Graphite capsules	B790	1810°C	crystalline >> quench > glass
40kb 5mins duration	B789	1800°C	crystalline >> quench > glass

Table 2-5 : Previous diopside melting point determinations.

Boyd & England (1963) 25.1kb	: between 1675 and 1700°C graphite capsules temperature uncertainty ±10°C "floating piston" - experiment brought to temperature at pressure no corrections applied
Williams & Kennedy (1969) 25kb	: 1687±15°C molybdenum capsules corrected for friction and pressure effect on emf.
Howells (1975) Edinburgh laboratory 25kb	: 1710±10°C platinum capsules uncorrected piston-out pressure
Bickle et al. (1977) Edinburgh laboratory 25kb	: 1720±20°C both graphite and platinum capsules uncorrected piston-out pressures
Boyd & England (1963) 39.5kb	: between 1775 and 1800°C
Williams & Kennedy (1969) 40kb	: 1822±15°C

between 25kb melting point determinations in graphite and platinum capsules, and between experiments of 5 minutes and 24 hours duration.

Previous determinations of the diopside melting point at 25 and 40kb from this and other laboratories are given in Table 2-5. There is good agreement between the results of this study and others from the Edinburgh laboratory. Discrepancies between Edinburgh determinations and Williams & Kennedy (1969) can be explained by a 1-2kb difference between the uncorrected piston-out pressure values of the former and the friction-corrected values of the latter. Good agreement between Williams & Kennedy (1969) and this study at 40kb suggests that piston-cylinder friction may be negligible in the Edinburgh apparatus at 40kb and 1800°C.

It is believed that there are no major differences between the temperature and pressure scales of this study and of previous studies in this and other laboratories.

2.3. Analysis of results

After recovery from the pressure cell, each capsule was mounted whole in epoxy resin and sectioned by grinding by hand on silicon carbide discs of various grades. When the desired section through the capsule was reached, this surface was polished on mechanical laps using diamond pastes down to 1/4µm grade. The polished mount was examined by reflected light microscopy. Garnet and spinel were readily identified by their high reflectance and characteristic shape. Lower reflectance crystals were identified as pyroxene but whether they were clinopyroxene or orthopyroxene could not be determined optically. Olivine had a reflectance intermediate between that of garnet and pyroxene. Identification of phases was confirmed by electron microprobe.

Electron microprobe analyses were initially carried out using a Cambridge Instruments Microscan 5 with two crystal spectrometers. The take-off angle was 75° and operating conditions were an accelerating potential of 20KV and a probe current of 30nA. All analyses from this instrument were performed with a focussed electron beam of 1-2 µm diameter. In 1985, a new Cameca Camebax instrument with four crystal spectrometers was installed and approximately two-thirds of the analyses were carried out with this instrument. The take-off angle was 40° and an accelerating potential of 20KV was used. The probe current of the Camebax was maintained automatically at about 25nA. Most analyses from this instrument were carried out using a focussed electron beam of approximately 1µm diameter. Some analyses of areas of quench crystals were made using an electron beam rastered over an area of approximately $50\mu m^2$. All analyses from both instruments were performed by wavelength dispersive spectrometry (WDS) where the number of X-rays from an element in an unknown is related to the number of X-rays from a standard for that element, read in the same session. Calculations of the ZAF correction procedure (Sweatman & Long, 1969) were performed automatically by both instruments. Several analyses performed with the Microscan 5 were repeated with the Camebax and no significant differences were observed.

Precision determinations are presented in Tables 2-6, 2-7 and 2-8. Three methods were used. Firstly (Table 2-6), precision calculations were made according to the formula:

$$\text{Precision} = \sigma = 100 / [\, Tp^{0.5} \,.\, (\, Rp^{0.5} - Rb^{0.5} \,)\,]$$

Where the calculated precision is at the 1σ level, the result is expressed as a percentage of the wt% oxide and:

Table 2-6 : Microprobe precision calculations based on one analysis. Same sample analysed in both instruments

Glass unknown

	Microscan 5		Camebax	
	wt%	2σ wt%	wt%	2σ wt%
SiO_2	45.85	0.55	46.52	0.20
Al_2O_3	16.17	0.27	16.24	0.12
FeO	9.00	0.25	8.40	0.14
MgO	19.21	0.29	19.92	0.11
CaO	8.05	0.22	8.07	0.07
total	98.28		99.15	

Garnet unknown

	Microscan 5		Camebax	
	wt%	2σ wt%	wt%	2σ wt%
SiO_2	43.21	0.54	43.38	0.23
Al_2O_3	24.46	0.33	24.69	0.17
FeO	5.24	0.21	5.05	0.15
MgO	23.80	0.31	23.85	0.17
CaO	3.46	0.16	3.14	0.08
total	100.17		100.11	

Clinopyroxene unknown

	Microscan 5		Camebax	
	wt%	2σ wt%	wt%	2σ wt%
SiO_2	47.11	0.55	46.58	0.17
Al_2O_3	14.25	0.25	14.66	0.09
FeO	3.10	0.18	2.71	0.07
MgO	14.51	0.25	14.94	0.10
CaO	20.08	0.34	20.59	0.11
total	99.05		99.48	

Table 2–6 : continued

Orthopyroxene unknown

	Microscan 5		Camebax	
	wt%	2σ wt%	wt%	2σ wt%
SiO_2	52.42	0.58	53.25	0.25
Al_2O_3	8.56	0.21	8.45	0.11
FeO	5.24	0.21	4.76	0.15
MgO	31.06	0.35	32.15	0.19
CaO	1.66	0.12	1.57	0.06
total	98.94		99.78	

Olivine unknown

		Camebax	
		wt%	2σ wt%
SiO_2		41.10	0.20
Al_2O_3	no olivine	0.24	0.03
FeO	analyses taken	6.42	0.12
MgO	with Microscan	52.24	0.18
CaO		0.53	0.02
total		100.53	

Spinel unknown

	Microscan 5		Camebax	
	wt%	2σ wt%	wt%	2σ wt%
SiO_2	0.41	0.24	0.38	0.04
Al_2O_3	69.00	0.53	69.07	0.27
FeO	6.17	0.23	5.96	0.16
MgO	23.96	0.30	24.71	0.17
CaO	0.13	0.13	0.06	0.02
total	99.69		100.18	

Table 2–7 : Repeat analyses of approximately the same point. Camebax instrument

	Glass unknown 9 analyses		Garnet unknown 8 analyses		Clinopyroxene unknown 8 analyses	
	wt%	2σ wt%	wt%	2σ wt%	wt%	2σ wt%
SiO_2	46.12	0.98	42.67	0.21	46.39	0.28
Al_2O_3	16.06	0.43	24.41	0.23	15.00	0.16
FeO	8.48	0.16	4.87	0.14	2.77	0.07
MgO	20.01	0.34	24.47	0.78	14.91	0.21
CaO	8.12	0.11	3.08	0.88	20.42	0.27
total	98.79		99.50		99.49	

	Orthopyroxene unknown 5 analyses		Olivine unknown 6 analyses		Spinel unknown 6 analyses	
	wt%	2σ wt%	wt%	2σ wt%	wt%	2σ wt%
SiO_2	52.35	0.28	41.03	0.63	0.43	0.02
Al_2O_3	9.18	0.29	0.25	0.02	69.17	0.62
FeO	4.84	0.13	6.49	0.09	5.90	0.09
MgO	31.43	0.29	52.06	0.49	24.03	0.21
CaO	1.76	0.07	0.53	0.02	0.10	0.02
total	99.56		100.36		99.63	

Table 2–8 : Analyses of National Bureau of Standards (NBS) microprobe standard glass K412 taken with Microscan 5 over a period of six months

	NBS wet chemical analysis wt%	average of 24 analyses wt%	2σ wt%
SiO_2	45.35	45.27	0.42
Al_2O_3	9.27	9.23	0.24
FeO	9.96	9.85	0.12
MgO	19.33	19.35	0.32
CaO	15.25	15.07	0.32
total	99.16	98.77	

Rp = peak count rate per second
Rb = background count rate per second
Tp = time on peak

Secondly, repeated analyses of approximately the same point are presented (Table 2-7). This gives some idea of the precision for each element when operational factors other than counting statistics are considered. Analyses are presented for the Camebax instrument. Thirdly, to assess the longer term effects of fluctuation in standard counts, calibrations, microprobe stability and operator behaviour, analyses of a National Bureau of Standards microprobe standard glass (K412) as an unknown were made during 10 different sessions on the Microscan 5 over a period of six months (Table 2-8). Agreement of these analyses and the wet chemical analysis of the National Bureau of Standards is good.

2.4. Equilibrium and the duration of experiments

Most experiments were run for 20 hours. This choice of duration was governed by the need to 1) achieve chemical equilibrium between crystals and liquids and 2) form an area of liquid sufficiently large to be unaffected by quench modification.

The importance of an area of segregated liquid is illustrated by Figure 2-4. The same starting material (d85) was used for two experiments with the same conditions of temperature and pressure (1620°C, 30kb) but different durations. Both experiments yielded the assemblage liquid + garnet + orthopyroxene, but in the shorter experiment (2 hours) all the liquid occurred as intergranular pools whereas in the longer experiment (24 hours) it formed a segregated area in the upper part of the charge. Compositions of garnet and orthopyroxene crystals from the two experiments were very similar and suggested that chemical equilibrium might be achieved within 2 hours, but there was a considerable

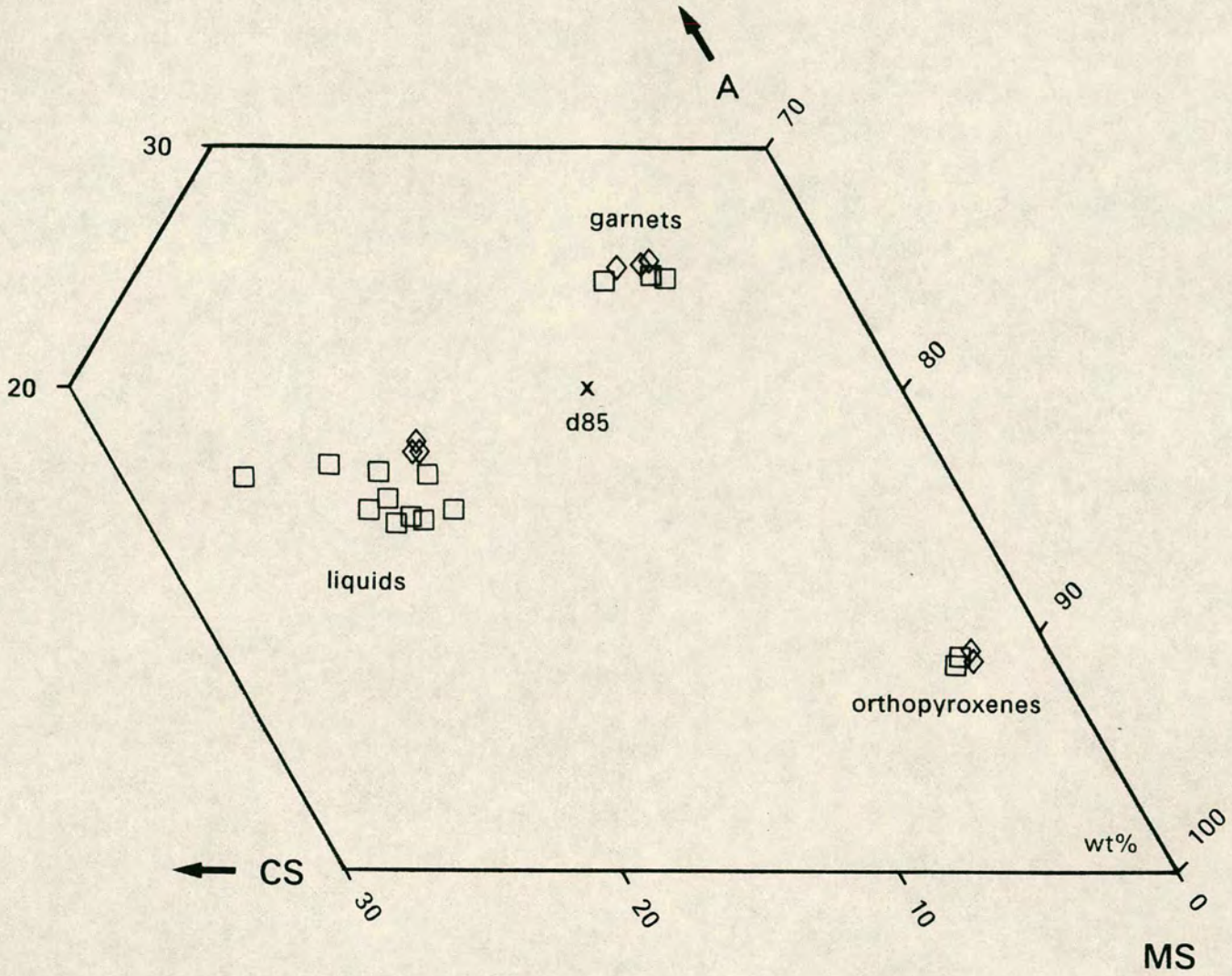

Figure 2-4 : Comparison of results of two experiments on the same starting material (d85) at the same temperature and pressure, but of different durations. Squares - 2 hours, glass analyses taken from small intergranular pools. Diamonds - 24 hours, glass analyses from a large area of segregated glass. Note the wide scatter in the glass analyses taken from the small pools. Garnet and orthopyroxene compositions are very similar in both experiments. All compositions lie in the plane CS-MS-A.

scatter amongst the glass analyses from the 2 hour experiment compared to those from the 24 hour experiment which formed a tight group. Glass analyses from the 24 hour experiment are taken to represent the equilibrium melt composition. Analyses from the intergranular pools of the 2 hour experiment are displaced from this equilibrium composition and record the quench crystallisation of various proportions of garnet and pyroxene.

An attempt was made to demonstrate chemical equilibrium by conducting a crystallisation experiment (cooling from an initially all-liquid charge) to reproduce the result of a straightforward melting experiment at the same temperature and pressure. At 30kb, a sample of starting composition d85 was held at 1700°C (approximately 50°C above the liquidus) for 10 minutes to ensure complete melting, then cooled to 1620°C (approximately 30°C below the liquidus) and held for 24 hours. The result of a melting experiment at the same temperature and pressure was the assemblage liquid + garnet + orthopyroxene, but the result of the crystallisation experiment was all liquid (glass + quench). The glass was checked by electron microprobe analysis and the bulk composition was found to be unchanged. It was concluded that garnet and orthopyroxene crystals had failed to nucleate and that demonstaration of equilibrium by reversal of melting and crystallisation experiments was not possible. Dr. C.E. Ford (pers. comm.) has observed similar behaviour melting and crystallising diopside on a hot-stage microscope. Diopside crystals coexisting with molten diopside can be made to shrink or grow by increasing or decreasing the temperature slightly, but if the crystals are completely melted, the liquid may be supercooled by several hundred degrees before any crystals reappear.

An approach was devised to demonstrate chemical equilibrium without complete melting. An experiment (B701) was conducted in which the charge

(d85) was held at 1640°C (30kb) for 2 hours, then cooled to 1620°C and held for 20 hours. Figure 2-5 shows analyses of the phases from this experiment compared to straightforward melting experiments of 24 hours at 1620°C (B707), 2 hours at 1640°C (B689) and 24 hours at 1640°C (B747). Glass analyses from experiment B747 show the composition of the liquid which would have existed in experiment B701 after 2 hours at 1640°C. (Note that glass analyses from B689 which had to be taken from intergranular pools are scattered due to quench modification). The analysed liquid from experiment B701 matches the liquid from experiment B707, the straightforward melting experiment at 1620°C. This is taken to indicate that experiment B701 re-equilibrated at 1620°C within 20 hours. The presence of orthopyroxene in experiment B689 but its absence from experiment B747 suggested that experiments of 2 hours duration or less might not represent equilibrium conditions due to the persistence of metastable phases.

Individual crystals from experiments of 20 or 24 hours duration showed no zoning, either in backscattered electron images or by taking several analyses across crystals and this is taken as further evidence that chemical equilibrium was attained.

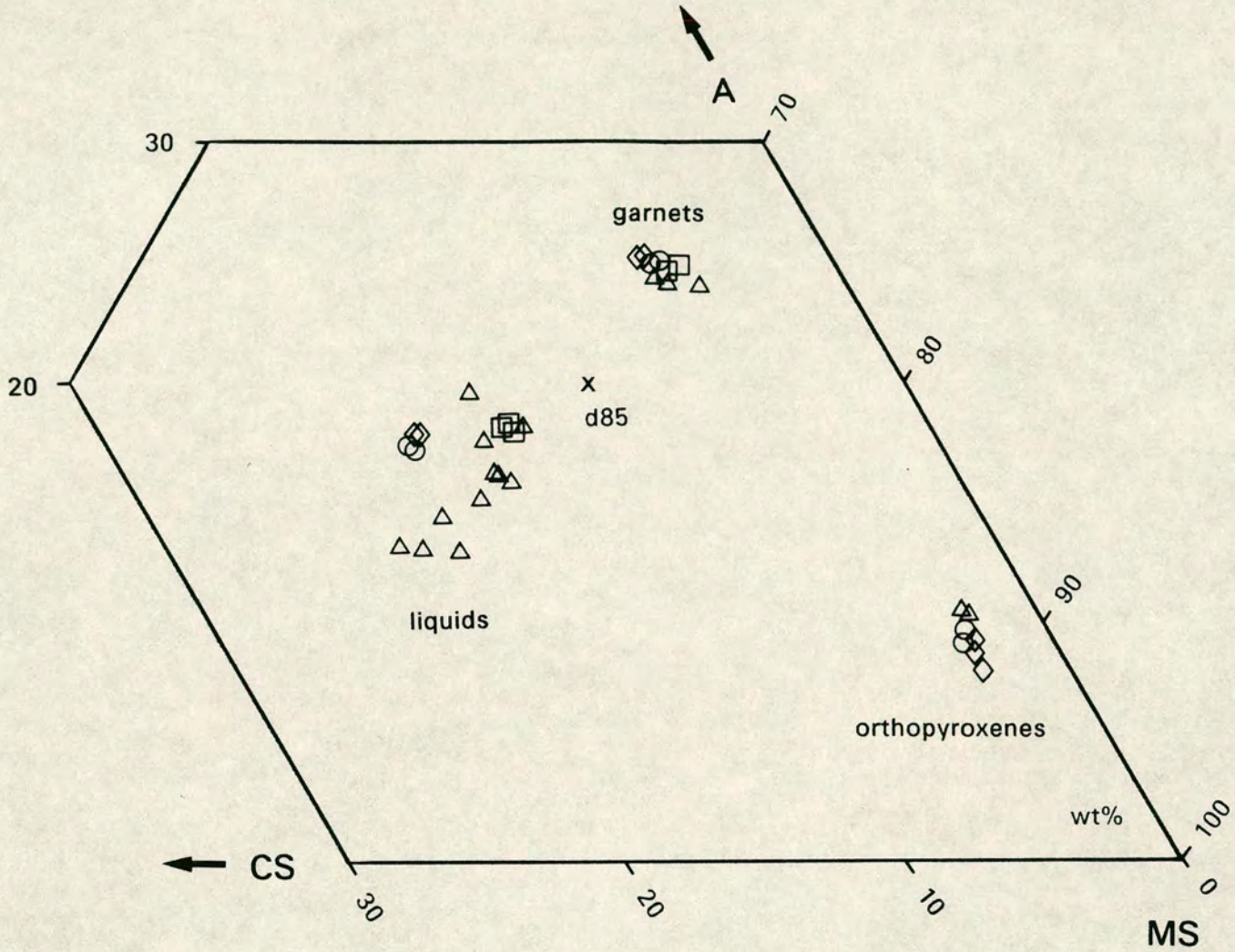

Figure 2–5 : Comparison of melting and reversal experiments to demonstrate chemical equilibrium – see text. Diamonds – B707 (1620°C, 30kb, 24 hours). Squares – B747 (1640°C, 30kb, 24 hours). Triangles – B689 (1640°C, 30kb, 2 hours). Circles – B701 (1640°C, 30kb, 2 hours; then 1620°C, 30kb, 20 hours). Note that the liquid from B701 plots beside that from B707 and not beside those from B747 or B689. All compositions lie in the plane CS–MS–A.

CHAPTER 3

EXPERIMENTAL RESULTS

3.1. Appearance of experimental products

Most experiments contained a significant liquid fraction which formed a discrete area of glass and quench crystals in the upper part of the charge. The liquid usually coexisted with garnet and either clinopyroxene or orthopyroxene. Spinel and olivine were present in some experiments. Garnet, orthopyroxene and clinopyroxene crystals were in the size range 10–50μm and were typically 20–30μm across in all experiments. Spinel crystals were generally 10–20μm across and olivine crystals 20–50μm. The appearance of a typical experimental product, mounted, sectioned and polished, is shown in Figure 3–1.

3.2. Analyses of coexisting phases

Details of the expriments conducted and the assemblages produced are given in Table 3–1. Electron microprobe analyses of the phases in all of the experiments are presented in Table 3–2.

For each experiment a check was made that the phases present and their analysed compositions were consistent with the composition of the starting material. Phase compositions were plotted in the plane CS–MS–A or projected into it from silica (S) or olivine (M2S). Results from experiments on the silica- and olivine-added starting materials were also plotted in the plane C–M–S by projection from alumina (A). These diagrams showed whether or not the starting composition of an experiment lay on a tie-line between the phases in the case of a two-phase assemblage, within the three-phase triangle in the case of a three-phase assemblage, or within the four-phase volume in the case of a four-phase assemblage. Experiments B797 and B811 were identified as suspect by this procedure. Both experiments were on starting composition

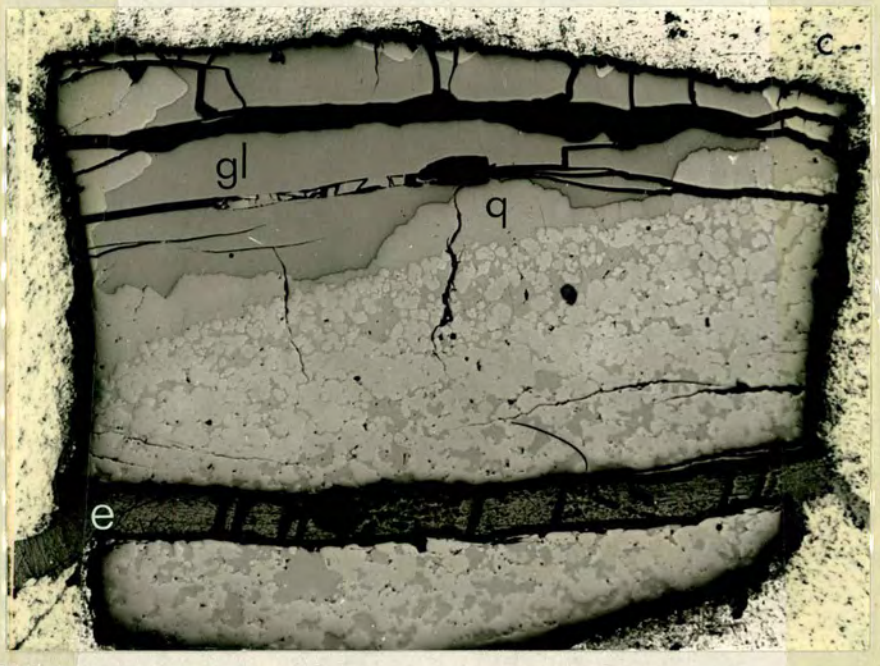

Figure 3–1 : Reflected light photomicrograph of a typical experimental result when mounted and sectioned. Crystals and small pools of glass/quench occupy the lower part of the charge, with an area of segregated glass (gl) in the upper part. Between the crystals and the glass there is a fringe of quench crystals (q). The surrounding graphite capsule (c) is also seen. The area marked e is epoxy resin. The width of the field of view is 1.1mm.

Table 3-1 : Conditions and products of experiments conducted.

Run no.	Comp.	T °C	P kb	Time hours	Assemblage
B748	a85	1620	30	20	gl,q
B739	a85	1600	30	20	gl,q,gt,cp,sp
B740	a85	1580	30	21.5	gl,q,gt,cp,sp
B745	a85	1560	30	20	gt,cp,sp
B735	b85	1600	30	20	gl,q
B736	b85	1580	30	20	gl,q,gt,cp,sp
B768	b85	1560	30	20	gl,q,gt,cp
B731	b85	1540	30	20	gt,cp
B704	c85	1620	30	24	gl,q
B705	c85	1600	30	24	gl,q,gt
B727	c85	1580	30	21.5	gl,q,gt,cp
A364	c85	1560	30	20	gl,q,gt,cp
B723	d85	1660	30	20	gl,q
B747	d85	1640	30	20	gl,q,gt
B707	d85	1620	30	24	gl,q,gt,op
B695	d85	1600	30	24	gl,q,gt,op
B734	d85	1580	30	20	gl,q,gt,op
B738	d85	1560	30	20	gt,op
B779	a85+S	1550	30	20	gl,q,cp
B776	b85+S	1550	30	20	gl,q,gt,cp, Fe metal
A366	c85+S	1550	30	20	gl,q,gt,cp
B780	d85+S	1550	30	17	gl,q,gt,op
B782	a85+Ol	1580	30	20	gl,q,cp,ol,sp
B781	b85+Ol	1580	30	20	gl,q,gt,cp,ol,sp
B775	b85+Ol	1550	30	20	gt,cp,ol,sp
B777	c85+Ol	1550	30	20	q,gt,cp,ol, Fe metal
B797	d85+Ol	1580	30	20	gl,q,gt
B773	d85+Ol	1550	30	20	gt,op,ol
B792	a85	1620	38	20	gl,q,gt,cp
B809	c85	1630	40	20	q,gt,cp
B807	d85	1675	40	20	q,gt,op
B784	b85+S	1600	40	20	gl,q,gt,cp
B811	d85+Ol	1640	40	21	q,gt,op

gl - glass
q - quench
gt - garnet
cp - clinopyroxene
op - orthopyroxene
ol - olivine
sp - spinel

Table 3–2 : Compositions of coexisting liquids and crystals. The starting material, experimental conditions, and resultant assemblage of each experiment are given. Each phase composition is reported as the mean ($\bar{x}$) and standard deviation (σ) of n microprobe analyses.

B739, a85, 1600°C, 30kb, 20hrs, liq+gt+cp+sp

	liq		gt		cp		sp	
wt%	$\bar{x}$	σ	$\bar{x}$	σ	$\bar{x}$	σ	$\bar{x}$	σ
SiO_2	43.68	0.08	42.31	-	44.30	0.30	0.44	0.09
Al_2O_3	18.91	0.09	23.09	-	18.19	0.20	69.77	0.44
FeO	5.44	0.04	3.07	-	1.94	0.07	5.14	0.06
MgO	12.27	0.10	13.47	-	12.20	0.09	24.66	0.16
CaO	19.29	0.06	18.42	-	22.86	0.19	0.26	0.04
total	99.59		100.36		99.49		100.27	
n	6		1		5		3	
Mg'	0.80		0.89		0.92		0.90	

B740, a85, 1580°C, 30kb, 21.5hrs, liq+gt+cp+sp

	liq		gt		cp		sp	
wt%	$\bar{x}$	σ	$\bar{x}$	σ	$\bar{x}$	σ	$\bar{x}$	σ
SiO_2	43.74	0.12	41.40	-	44.42	0.18	0.32	-
Al_2O_3	19.52	0.08	23.00	-	19.05	0.25	69.44	-
FeO	5.57	0.01	2.42	-	2.32	0.32	5.29	-
MgO	11.79	0.04	12.55	-	12.05	0.08	24.66	-
CaO	18.64	0.05	20.61	-	22.32	0.12	0.24	-
total	99.26		99.98		100.16		99.95	
n	3		1		3		1	
Mg'	0.79		0.90		0.90		0.89	

B736, b85, 1580°C, 30kb, 20hrs, liq+gt+cp+sp

	liq		gt		cp		sp	
wt%	$\bar{x}$	σ	$\bar{x}$	σ	$\bar{x}$	σ	$\bar{x}$	σ
SiO_2	44.84	0.31	42.21	0.09	46.49	0.37	0.41	0.02
Al_2O_3	17.44	0.26	24.12	0.08	14.79	0.32	69.28	0.21
FeO	7.43	0.33	5.39	0.22	2.84	0.13	5.93	0.04
MgO	14.66	0.32	18.93	0.38	14.79	0.16	24.40	0.23
CaO	15.11	0.19	9.51	0.33	20.40	0.19	0.09	0.02
total	99.48		100.16		99.31		100.11	
n	7		5		5		3	
Mg'	0.78		0.86		0.90		0.88	

Table 3-2 : continued

B768, B85, 1560°C, 30kb, 20hrs, liq+gt+cp

	liq		gt		cp	
wt%	$\bar{x}$	σ	$\bar{x}$	σ	$\bar{x}$	σ
SiO_2	43.80	0.43	41.77	0.35	46.40	0.30
Al_2O_3	17.66	0.15	23.89	0.27	14.96	0.23
FeO	7.55	0.39	5.99	0.22	3.10	0.12
MgO	13.25	0.46	18.64	0.45	14.28	0.29
CaO	15.77	0.25	9.46	0.40	20.66	0.48
total	98.03		99.75		99.40	
n	6		6		5	
Mg'	0.76		0.85		0.89	

B705, c85, 1600°C, 30kb, 24hrs, liq+gt

	liq		gt	
wt%	$\bar{x}$	σ	$\bar{x}$	σ
SiO_2	46.04	0.28	42.86	0.51
Al_2O_3	17.22	0.15	23.92	0.50
FeO	6.36	0.30	5.09	1.02
MgO	17.87	0.35	21.35	0.96
CaO	13.08	0.12	6.54	0.75
total	100.57		99.76	
n	4		10	
Mg'	0.83		0.88	

B727, c85, 1580°C, 30kb, 21.5hrs, liq+gt+cp

	liq		gt		cp	
wt%	$\bar{x}$	σ	$\bar{x}$	σ	$\bar{x}$	σ
SiO_2	46.73	0.13	42.90	0.45	50.00	0.38
Al_2O_3	17.29	0.14	24.31	0.72	9.95	0.40
FeO	6.95	0.05	5.33	0.35	3.29	0.06
MgO	15.07	0.16	20.68	0.59	18.54	0.36
CaO	13.94	0.05	7.16	0.51	17.25	0.28
total	99.98		100.38		99.03	
n	4		6		3	
Mg'	0.79		0.87		0.91	

Table 3–2 : continued

A364, c85, 1560°C, 30kb, 20hrs, liq+gt+cp

	liq		gt		cp	
wt%	$\bar{x}$	σ	$\bar{x}$	σ	$\bar{x}$	σ
SiO_2	45.87	0.02	42.18	0.52	49.18	0.06
Al_2O_3	16.44	0.04	23.89	0.26	10.47	0.16
FeO	9.33	0.23	6.20	0.31	3.75	0.10
MgO	13.48	0.27	19.46	0.25	17.65	0.04
CaO	14.34	0.11	8.23	0.70	18.70	0.17
total	99.46		99.96		99.75	
n	3		4		3	
Mg′	0.72		0.85		0.89	

B747, d85, 1640°C, 30kb, 20hrs, liq+gt

	liq		gt	
wt%	$\bar{x}$	σ	$\bar{x}$	σ
SiO_2	46.14	0.44	43.43	0.29
Al_2O_3	17.41	0.17	24.56	0.12
FeO	7.51	0.32	4.43	0.13
MgO	21.58	0.30	25.18	0.28
CaO	6.93	0.20	2.72	0.28
total	99.57		100.32	
n	4		6	
Mg′	0.84		0.91	

B707, d85, 1620°C, 30kb, 24hrs, liq+gt+op

	liq		gt		op	
wt%	$\bar{x}$	σ	$\bar{x}$	σ	$\bar{x}$	σ
SiO_2	45.70	0.10	43.11	0.21	52.76	0.28
Al_2O_3	16.47	0.11	24.59	0.15	8.51	0.46
FeO	8.50	0.03	5.00	0.13	4.68	0.06
MgO	18.93	0.11	23.73	0.30	32.24	0.28
CaO	8.27	0.04	3.46	0.24	1.50	0.08
total	97.87		99.89		99.69	
n	6		4		4	
Mg′	0.80		0.89		0.92	

Table 3–2 : continued

B695, d85, 1600°C, 30kb, 24hrs, liq+gt+op

	liq		gt		op	
wt%	$\bar{x}$	σ	$\bar{x}$	σ	$\bar{x}$	σ
SiO_2	47.24	0.17	43.00	0.19	55.25	0.47
Al_2O_3	16.93	0.08	24.13	0.09	10.09	0.24
FeO	7.42	0.06	5.35	0.16	5.02	0.03
MgO	17.78	0.14	23.57	0.20	30.76	0.20
CaO	10.10	0.05	3.83	0.25	2.12	0.26
total	99.65		99.88		100.24	
n	3		7		2	
Mg'		0.81		0.89		0.92

B734, d85, 1580°C, 30kb, 20hrs, liq+gt+op

	liq		gt		op	
wt%	$\bar{x}$	σ	$\bar{x}$	σ	$\bar{x}$	σ
SiO_2	47.07	0.20	43.57	0.31	53.16	0.22
Al_2O_3	15.49	0.09	23.69	0.79	8.01	0.18
FeO	9.46	0.05	6.80	0.34	6.25	0.03
MgO	16.77	0.10	21.66	0.23	30.10	0.24
CaO	10.17	0.04	5.30	0.16	2.49	0.09
total	98.96		101.02		100.01	
n	4		6		3	
Mg'		0.76	0.85		0.90	

B779, a85+S, 1550°C, 30kb, 20hrs, liq+cp

	liq		cp	
wt%	$\bar{x}$	σ	$\bar{x}$	σ
SiO_2	50.03	0.26	46.65	0.23
Al_2O_3	19.11	0.15	14.65	0.14
FeO	4.12	0.02	2.03	0.02
MgO	9.28	0.03	14.04	0.06
CaO	16.56	0.10	22.29	0.11
total	99.10		99.75	
n	4		4	
Mg'	0.80		0.92	

Table 3–2 : continued

B776, b85+S, 1550°C, 30kb, 20hrs, liq+gt+cp+Fe metal

	liq		gt		cp	
wt%	$\bar{x}$	σ	$\bar{x}$	σ	$\bar{x}$	σ
SiO_2	50.37	0.21	43.57	0.38	50.35	0.12
Al_2O_3	17.99	0.24	24.36	0.17	10.87	0.44
FeO	2.63	0.04	2.16	0.18	1.14	0.10
MgO	13.18	0.18	23.37	0.30	18.04	0.18
CaO	15.14	0.11	7.31	0.19	20.00	0.12
total	99.31		100.77		100.40	
n	5		3		5	
Mg'	0.90		0.95		0.97	

A366, c85+S, 1550°C, 30kb, 20hrs, liq+gt+cp

	liq		gt		cp	
wt%	$\bar{x}$	σ	$\bar{x}$	σ	$\bar{x}$	σ
SiO_2	54.34	0.08	42.30	0.50	52.69	0.45
Al_2O_3	16.75	0.12	24.38	0.12	7.45	0.23
FeO	5.20	0.05	5.37	0.03	4.58	0.05
MgO	11.79	0.10	22.70	0.10	24.72	0.19
CaO	11.74	0.06	5.35	0.10	10.06	0.27
total	99.82		100.10		99.50	
n	4		4		4	
Mg'	0.80		0.88		0.91	

B780, d85+S, 1550°C, 30kb, 17hrs, liq+gt+op

	liq		gt		op	
wt%	$\bar{x}$	σ	$\bar{x}$	σ	$\bar{x}$	σ
SiO_2	55.77	0.24	42.78	0.43	53.61	0.21
Al_2O_3	17.25	0.16	24.53	0.20	8.20	0.13
FeO	5.90	0.05	6.59	0.23	5.98	0.03
MgO	11.42	0.06	22.94	0.76	31.00	0.11
CaO	9.25	0.10	3.62	0.71	1.40	0.08
total	99.59		10.46		100.19	
n	6		5		4	
Mg'	0.78		0.86		0.90	

Table 3–2 : continued

B782, a85+Ol, 1580°C, 30kb, 20hrs, liq+cp+ol+sp

	liq		cp		ol		sp	
wt%	$\bar{x}$	σ	$\bar{x}$	σ	$\bar{x}$	σ	$\bar{x}$	σ
SiO_2	44.25	0.44	48.89	0.43	40.91	0.50	0.59	0.06
Al_2O_3	15.40	0.25	10.93	0.32	1.00	0.35	69.01	0.34
FeO	6.01	0.20	2.18	0.07	6.44	0.16	4.90	0.02
MgO	17.48	0.30	17.01	0.20	49.44	0.84	25.73	0.15
CaO	16.29	0.37	21.35	0.18	2.54	0.83	0.17	0.03
total	99.43		100.36		100.33		100.40	
n	3		5		5		3	
Mg′	0.84		0.93		0.93		0.90	

B781, b85+Ol, 1580°C, 30kb, 20hrs, liq+gt+cp+ol+sp

	liq		gt		cp		ol		sp	
wt%	$\bar{x}$	σ	$\bar{x}$	σ	$\bar{x}$	σ	$\bar{x}$	σ	$\bar{x}$	σ
SiO_2	44.58	0.45	42.57	0.04	48.46	0.06	40.62	0.24	0.57	0.02
Al_2O_3	15.92	0.27	23.90	0.01	10.49	0.04	0.27	0.01	69.60	0.05
FeO	6.57	0.22	4.11	0.01	2.41	0.04	6.46	0.03	4.75	0.06
MgO	18.58	0.23	20.90	0.06	18.23	0.15	51.71	0.52	25.42	0.02
CaO	14.40	0.07	7.92	0.02	19.42	0.24	0.52	0.03	0.14	0.03
total	100.05		99.40		99.01		99.58		100.48	
n	4		2		3		5		3	
Mg′	0.83		0.90		0.93		0.93		0.91	

B777, c85+Ol, 1550°C, 30kb, 20hrs, liq+gt+cp+ol+Fe metal

	liq		gt		cp		ol	
wt%	$\bar{x}$	σ	$\bar{x}$	σ	$\bar{x}$	σ	$\bar{x}$	σ
SiO_2	46.31	0.13	42.94	0.27	50.13	0.03	41.17	0.23
Al_2O_3	15.08	0.06	24.42	0.09	12.20	0.07	0.21	0.02
FeO	3.94	0.17	2.55	0.18	4.32	0.21	4.01	0.02
MgO	20.08	0.16	23.69	0.36	16.10	0.21	54.26	0.17
CaO	12.98	0.09	6.55	0.48	16.46	0.45	0.35	0.01
total	98.39		100.15		99.21		100.00	
n	4		4		3		5	
Mg′	0.90		0.94		0.87		0.96	

Table 3-2 : continued

B797, d85+Ol, 1580°C, 30kb, 20hrs, liq+gt

	liq		gt	
wt%	$\bar{x}$	σ	$\bar{x}$	σ
SiO_2	45.95	0.30	43.54	0.20
Al_2O_3	18.12	0.14	24.47	0.23
FeO	4.64	0.23	3.55	0.13
MgO	21.90	0.33	25.22	0.37
CaO	8.19	0.05	3.60	0.54
total	98.80		100.38	
n	4		6	
Mg'	0.89		0.93	

B792, a85, 1620°C, 38kb, 20hrs, liq+gt+cp

	liq		gt		cp	
wt%	$\bar{x}$	σ	$\bar{x}$	σ	$\bar{x}$	σ
SiO_2	42.95	0.09	41.36	0.14	44.74	0.32
Al_2O_3	20.22	0.04	24.20	0.10	17.52	0.65
FeO	5.36	0.02	4.45	0.11	2.14	0.09
MgO	11.22	0.04	15.40	0.14	12.09	0.16
CaO	18.46	0.03	14.84	0.24	23.52	0.16
total	98.21		100.25		100.01	
n	3		5		4	
Mg'	0.79		0.86		0.91	

B809, c85, 1630°C, 40kb, 20hrs, liq+gt+cp

	liq		gt		cp	
wt%	$\bar{x}$	σ	$\bar{x}$	σ	$\bar{x}$	σ
SiO_2	48.20	0.63	42.91	0.41	51.47	0.23
Al_2O_3	14.74	0.24	24.72	0.14	7.88	0.34
FeO	7.12	0.28	5.67	0.22	3.42	0.06
MgO	16.29	0.49	20.52	0.79	18.38	0.22
CaO	13.89	0.19	6.63	0.81	18.18	0.29
total	100.24		100.45		99.30	
n	11		5		5	
Mg'	0.80		0.87		0.91	

Table 3–2 : continued

B807, d85, 1675°C, 40kb, 20hrs, liq+gt+op

	liq		gt		op	
wt%	$\bar{x}$	σ	$\bar{x}$	σ	$\bar{x}$	σ
SiO_2	50.28	0.88	43.96	0.27	55.42	0.17
Al_2O_3	13.96	0.55	25.15	0.19	5.45	0.06
FeO	7.99	0.64	5.36	0.12	5.48	0.08
MgO	16.88	1.00	22.14	0.47	31.39	0.17
CaO	10.66	0.36	3.75	0.43	2.18	0.22
total	99.77		100.33		99.92	
n	10		8		4	
Mg′	0.79		0.88		0.91	

B784, b85+S, 1600°C, 40kb, 20hrs, liq+gt+cp

	liq		gt		cp	
wt%	$\bar{x}$	σ	$\bar{x}$	σ	$\bar{x}$	σ
SiO_2	53.43	0.04	42.72	0.18	50.56	0.22
Al_2O_3	18.38	0.06	24.42	0.10	12.01	0.39
FeO	4.21	0.02	5.63	0.07	2.79	0.04
MgO	7.75	0.04	18.85	0.17	14.71	0.25
CaO	15.31	0.05	9.50	0.13	20.05	0.09
total	99.08		101.12		100.12	
n	5		5		5	
Mg′	0.77		0.86		0.90	

B811, d85+Ol, 1640°C, 40kb, 21hrs, liq+gt+op

	liq		gt		op	
wt%	$\bar{x}$	σ	$\bar{x}$	σ	$\bar{x}$	σ
SiO_2	49.85	0.37	43.45	0.36	54.60	0.14
Al_2O_3	12.28	0.34	24.35	0.40	4.48	0.24
FeO	2.22	0.13	3.22	0.58	2.99	0.30
MgO	27.78	0.16	25.12	0.39	34.66	0.45
CaO	5.45	0.10	3.46	0.33	1.71	0.21
total	97.58		99.60		98.44	
n	3		6		5	
Mg′	0.96		0.93		0.95	

d85, but the resultant assemblages were liq+gt (B797) and liq+gt+op (B811), and these phases had compositions within the plane CS-MS-A. Searches of the charges using backscattered electron imaging did not reveal any other phases to balance the results with the starting compositions.

The olivine-bearing results were also checked by calculating their olivine-liquid Mg/Fe partition coefficients and comparing them with the value of 0.30±0.002P (kb) (*e.g.* 0.36 at 30kb) of Takahashi & Kushiro (1983).

Projections in the CMAS system do not preserve information about the iron content of the phases so it was checked that this was consistent with the starting material for each experiment by a mass balance calculation using estimates of the proportions of the phases from the CMAS projections and from the charges themselves. The phases observed and analysed from experiments B776 and B777 were too poor in iron to represent their starting materials. Progressive grinding and polishing of these samples eventually revealed the presence of metallic iron globules to balance the iron budget. This shows that the reduction of ferrous iron to iron metal is possible for an experimental charge in a graphite capsule. It is unclear why only these two experiments were affected since the conditions under which they were performed were similar to experiments in which no reduction occurred. In experiment B777 the iron reduction probably took place towards the beginning of the experiment, which then re-equilibrated since the olivine-liquid Mg/Fe partition coefficient indicates that the olivine and liquid were in equilbrium.

Experiments B776, B777, B797 and B811 were considered suspect and excluded from the dataset used to derive mineral-melt equations in Chapter 4.

3.3. Quench crystallisation

In every experiment in this study, a fringe of quench crystals occured between the equilibrium crystals in the lower parts of the charges and the glasses in the upper parts. The habit and extent of the quench crystallisation was the same in 30kb and 40kb experiments. Figure 3-1 shows a typical example. Figure 3-2 shows two backscattered electron images of the same example. Elongate, branched and feathery quench crystals up to 50μm long can be seen with bright grain boundaries. Discrete bright spots, approximately 1μm across, also occur along the grain boundaries. Brightness in backscattered electron images is related to the average atomic number of the elements in the phases observed, so the bright spots and the bright grain boundaries are iron-rich compared to the quench crystals, although they are too small to analyse quantitatively.

Analyses of glasses and quench fringes from three experiments are given in Table 3-3 and plotted in Figure 3-3. Quench analyses were obtained from an area of approximately $50\mu m^2$ using a rastered electron beam. Glass and quench analyses are not significantly different. This suggests that the quench fringes grew iso-chemically, with material not incorporated into the lattice of the quench crystals, particularly iron, swept to the grain boundaries and trapped there, so that there was very little mass transfer between the remaining liquid and the growing quench fringe. This shows that, in contrast to the quench crystallisation from small liquid pools discussed in Section 2.4, the growth of a quench fringe into a relatively large volume of segregated liquid does not affect the direct determination of the equilibrium melt composition.

In most experiments, the liquid composition was determined by analysis of the glass, but in several experiments with extensive growth of quench crystals

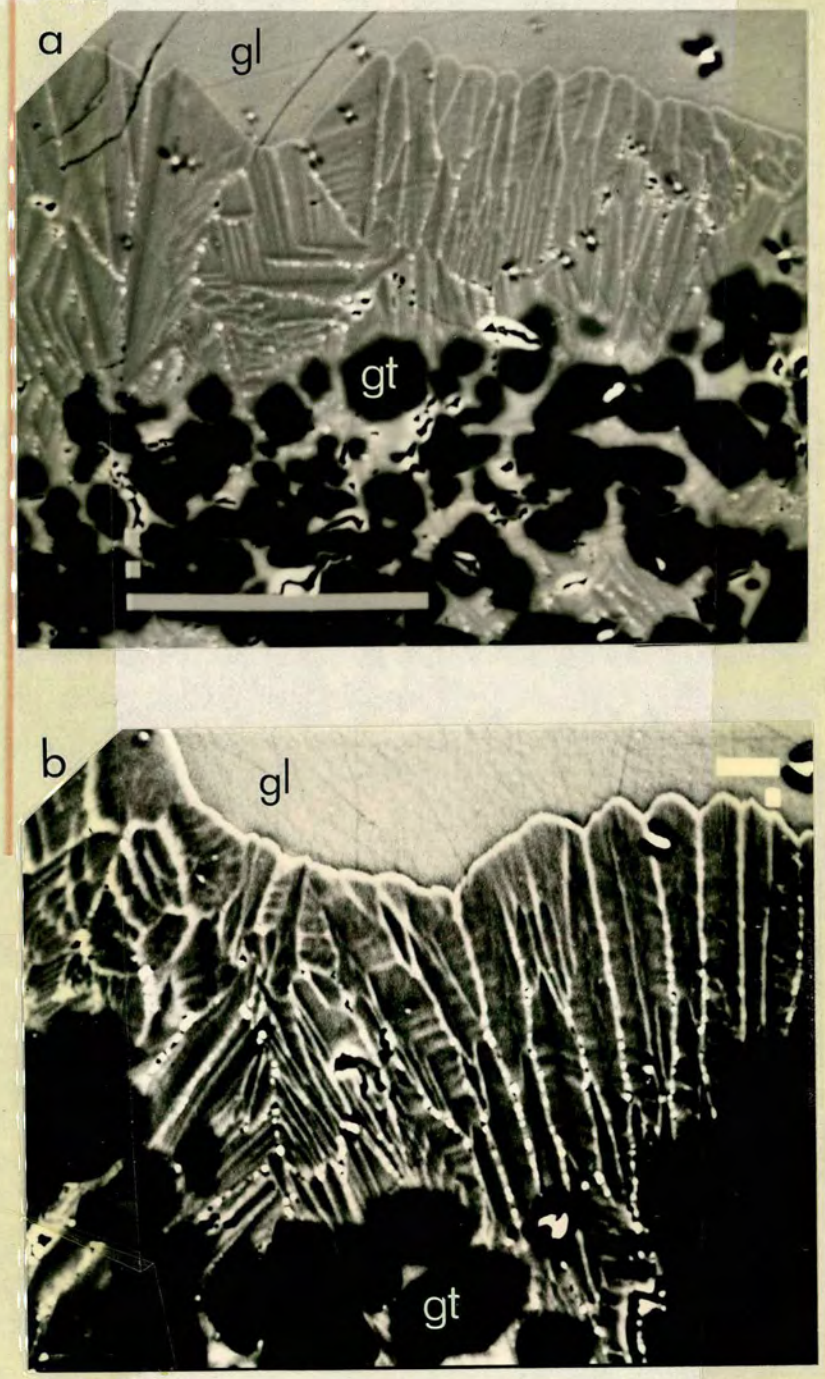

Figure 3–2 : Backscattered electron images showing the structure of the quench crystals. Scale bars are 100µm (a) and 10µm (b). In both images, garnet crystals (gt) and unmodified glass (gl) are also present. Bright grain boundaries between the quench crystals, and bright spots on these grain boundaries represent iron–rich areas.

Table 3-3 : Comparison of glass (gl) and quench (q) analyses. In each case the mean ($\bar{x}$) and standard deviation (σ) of n analyses is given.

	expt. B736				expt. B695			
	glass		quench		glass		quench	
wt%	$\bar{x}$	σ	$\bar{x}$	σ	$\bar{x}$	σ	$\bar{x}$	σ
SiO_2	44.84	0.31	44.54	0.21	47.24	0.17	46.69	0.13
Al_2O_3	17.44	0.26	17.36	0.19	16.93	0.08	16.37	0.14
FeO	7.43	0.33	7.12	0.19	7.42	0.06	7.51	0.02
MgO	14.66	0.32	14.73	0.05	17.78	0.14	17.55	0.18
CaO	15.11	0.19	15.24	0.18	10.10	0.04	10.17	0.04
total	99.58		98.99		99.47		98.29	
n	7		7		3		4	

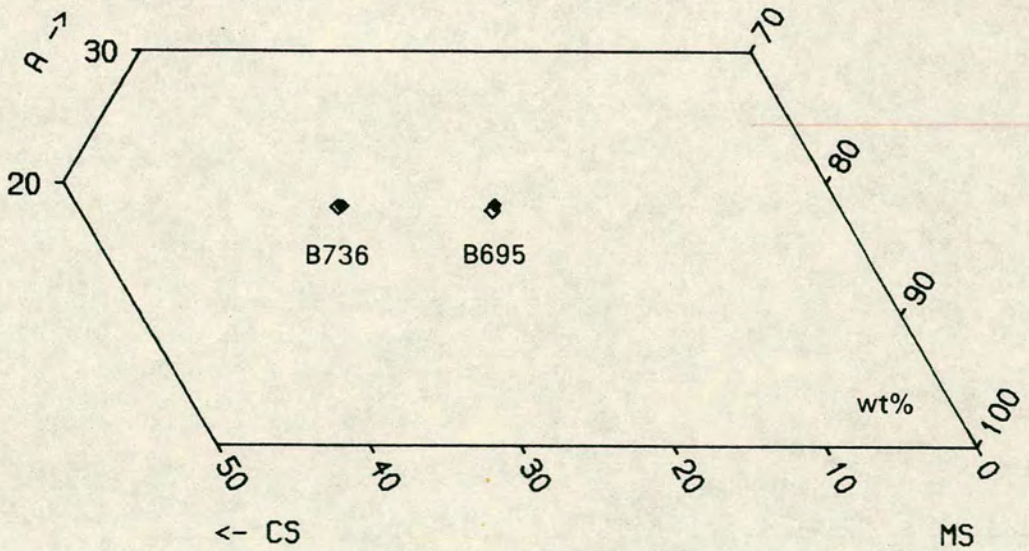

Figure 3-3 : Comparison of glass (filled symbols) and quench (open symbols) analyses for experiments B736 and B695. All analyses lie in the plane CS-MS-A.

and little or no remaining glass, rastered beam analysis of the quench was used. Analysis of areas of quench crystals to determine liquid compositions has been recently reported by Takahashi & Scarfe (1985) and Takahashi (1986).

Quench crystals were examined as a grain mount in transmitted light and showed moderate-high birefringence. One experiment (on starting composition d85) was conducted to yield only glass and quench. This was examined by X-ray diffraction and clinopyroxene peaks were identified by comparison of the diffraction pattern with the calculated patterns of diopside and clinoenstatite from Borg & Smith (1969) (Figure 3-4). The quench crystals are therefore believed to be clinopyroxene.

3.4. Phase chemistry

The ranges of chemical compositions of the liquids, garnets and pyroxenes of Table 3-2 (excluding experiments B776, B777, B797 and B811) are summarised in Table 3-4. The garnets are pyrope-grossular-almandine solid solutions and are plotted in Figures 3-5 and 3-6. The clinopyroxenes can be described in terms of the four components diopside, Ca-tschermak pyroxene, enstatite and ferrosilite and the orthopyroxenes by the four components enstatite, Mg-tschermak pyroxene, diopside and ferrosilite. Pyroxene compositions are plotted in Figures 3-7 and 3-8. Olivine was present in only three experiments and had the compositions Fo_{90}, Fo_{93} and Fo_{96}. Spinel was present in five experiments and had an essentially constant composition of $Mg_{0.9}\ Fe_{0.1}Al_2O_4$.

3.5. Phase relations

To choose the starting compositions of this study it was assumed that the melting relations of the plane CS-MS-A in the system $CaO-MgO-FeO-Al_2O_3-SiO_2$ were similar to those deduced in the system

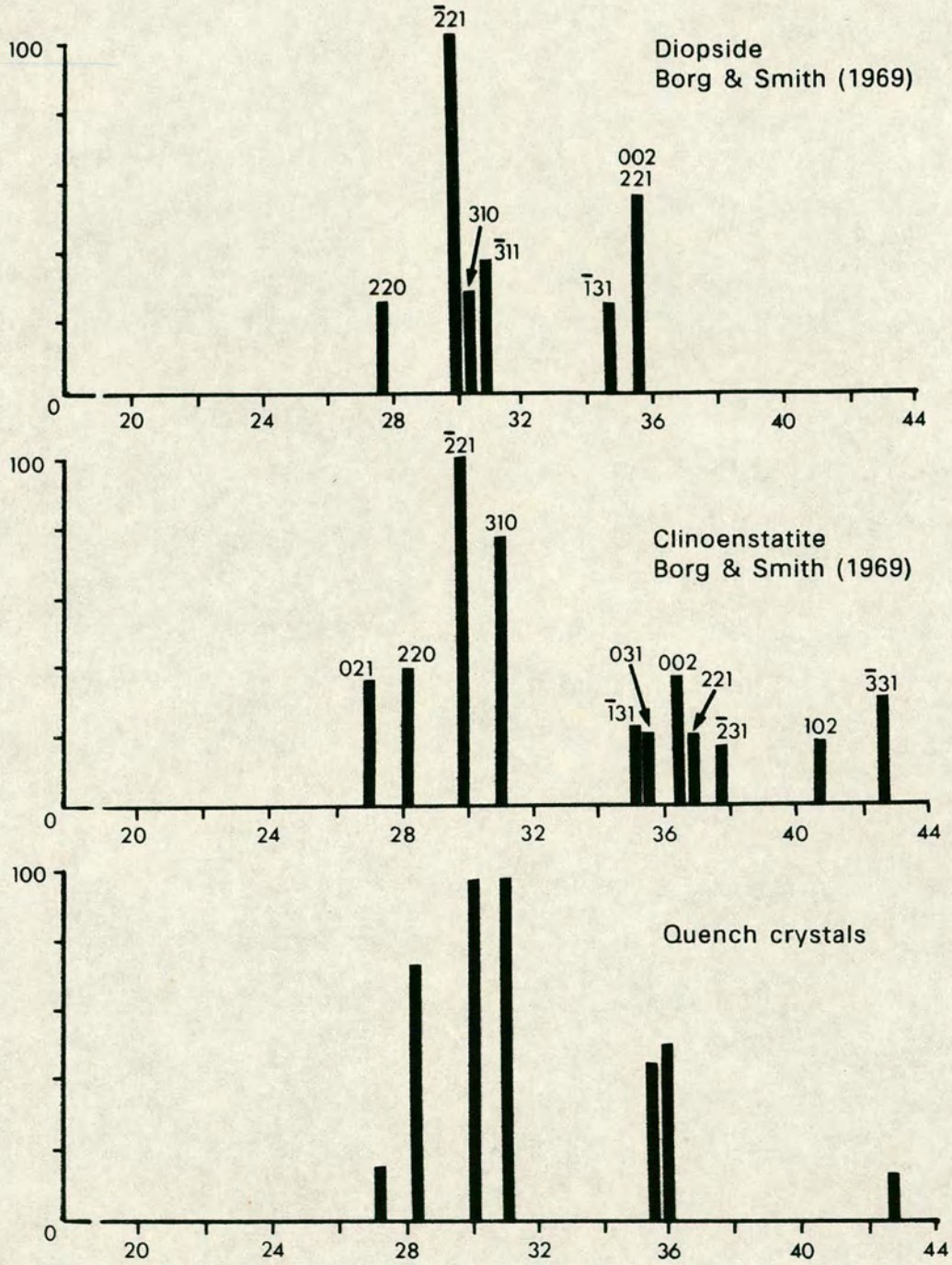

Figure 3-4 : Comparison of X-ray diffraction pattern of quench crystals with calculated patterns from Borg & Smith (1969). Ordinate - I/I_1, the peak intensity relative to the strongest peak. Abscissa - degrees 2θ

Table 3-4 : Compositional ranges of phases in Table 3-2.
(excluding experiments B776, B777, B797 and B811)

Liquids

	max.	min.
SiO_2	55.77	42.95
Al_2O_3	20.22	13.96
FeO	9.46	4.12
MgO	21.58	7.75
CaO	19.29	6.93

Garnets

	max.	min.
SiO_2	43.96	41.40
Al_2O_3	25.15	23.00
FeO	6.80	2.42
MgO	25.18	12.55
CaO	20.61	2.72

components ranges (mol%)
Pyrope ($Mg_3Al_2Si_3O_{12}$) Py_{45}-Py_{86}
Grossular ($Ca_3Al_2Si_3O_{12}$) Gr_7-Gr_{51}
Almandine ($Fe_3Al_2Si_3O_{12}$) Alm_5-Alm_{13}

Clinopyroxenes

	max.	min.
SiO_2	52.69	44.30
Al_2O_3	19.05	7.45
FeO	4.58	1.94
MgO	24.72	12.05
CaO	23.52	10.06

components ranges (mol%)
Diopside ($CaMgSi_2O_3$) Di_{23}-Di_{59}
Ca-Tschermak pyroxene ($CaAl_2SiO_6$) $CaTs_{15}$-$CaTs_{41}$
Enstatite ($MgSiO_3$) En_8-En_{53}
Ferrosilite ($FeSiO_3$) Fs_3-Fs_7

Orthopyroxenes

	max.	min.
SiO_2	55.42	52.25
Al_2O_3	10.09	5.45
FeO	6.25	4.68
MgO	32.24	30.76
CaO	2.49	1.40

components ranges (mol%)
Enstatite ($MgSiO_3$) En_{64}-En_{71}
Mg-Tschermak pyroxene ($MgAl_2SiO_6$) $MgTs_{11}$-$MgTs_{22}$
Diopside ($CaMgSi_2O_6$) Di_5-Di_9
Ferrosilite ($FeSiO_3$) Fs_6-Fs_9

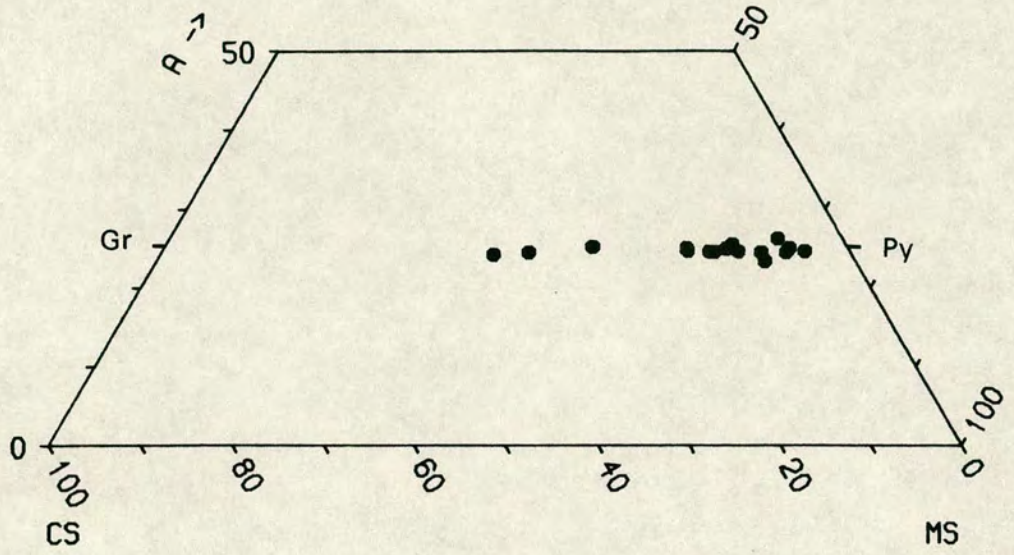

Figure 3-5 : Garnet compositions plotted in CS-MS-A (mol%).

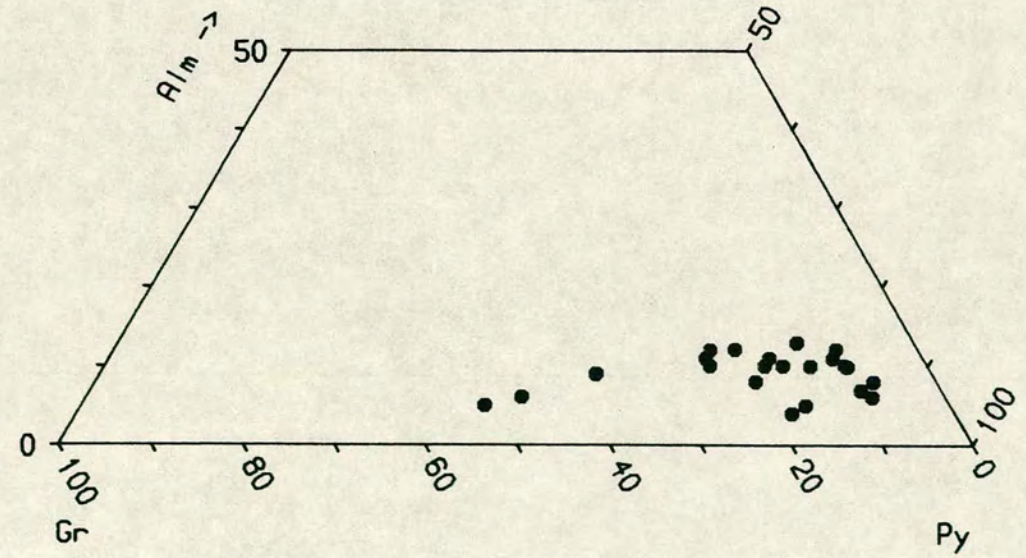

Figure 3-6 : Garnet compositions plotted in the plane pyrope-grossular-almandine (Py-Gr-Alm, mol%).

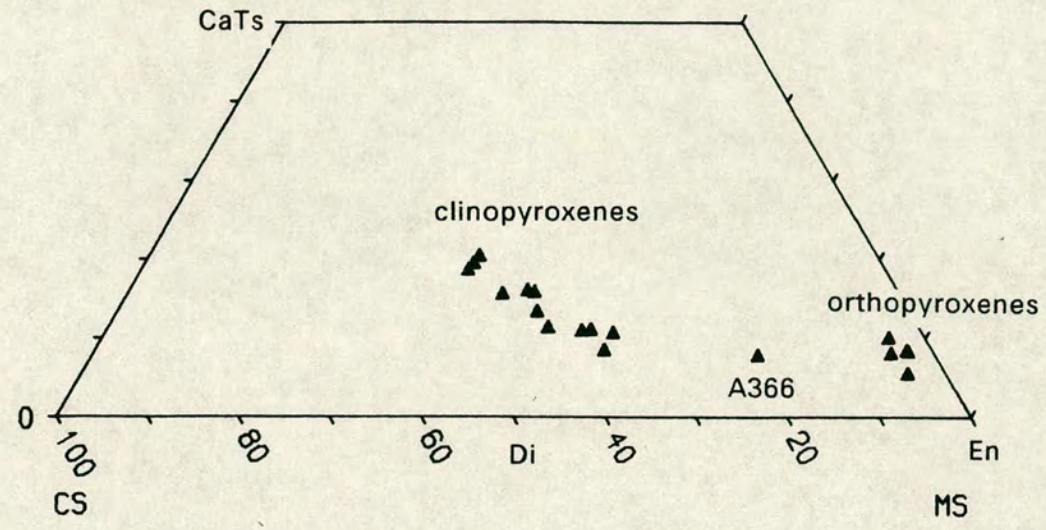

Figure 3-7 : Clinopyroxenes and orthopyroxenes plotted in CS-MS-A (mol%).

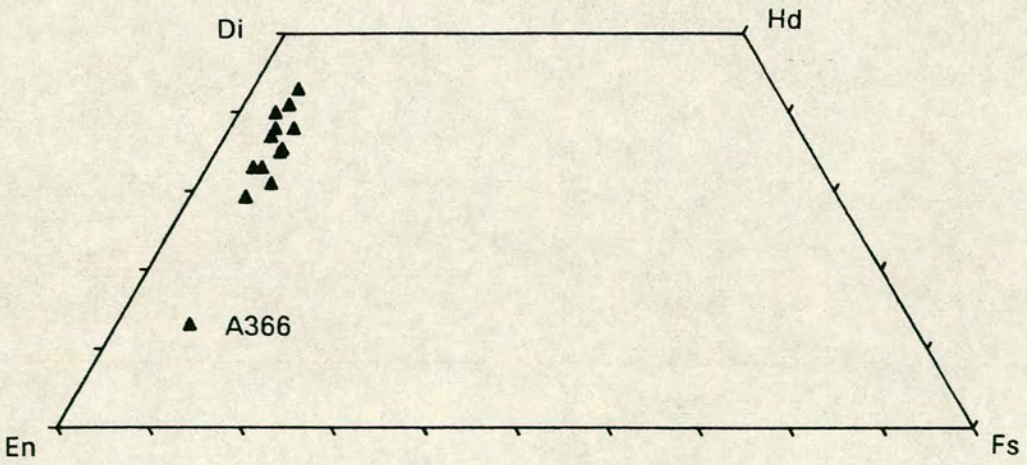

Figure 3-8 : Clinopyroxenes projected from Ca-tschermak pyroxene into the pyroxene quadrilateral (Di-En-Hd-Fs,mol%).

$CaSiO_3$-$MgSiO_3$-Al_2O_3 by Maaløe & Wyllie (1979). Figure 3-9 shows the phase relations in the plane CS-MS-A at 30kb as deduced from experiments of this study. The main features are a reaction orthopyroxene + liquid = clinopyroxene + garnet at the point R at approximately 1580°C and a minimum on the garnet-clinopyroxene cotectic, M, at approximately 1540°C. Both of these features are present in the Maaløe & Wyllie (1978) diagram (see Figure 2-2). The spinel field is larger than that of the iron-free system and intersects the garnet-clinopyroxene cotectic curve near the position of the minimum.

In Figure 3-9, all garnet , clinopyroxene and orthopyroxene compositions lie in the plane CS-MS-A which is thus a true ternary system outwith the spinel liquidus field, and constitutes a thermal barrier at 30kb. This is confirmed by the experiments on the starting materials removed from the plane, since these contain liquid at lower temperatures than experiments on starting materials in the plane. Figure 3-9 also shows the compositions of garnets and clinopyroxenes coexisting with the liquids. It can be seen that the enstatite content of the clinopyroxenes decreases with increasing Al_2O_3 content. The 40kb experiments show that the Al_2O_3 contents of both clinopyroxenes and orthopyroxenes decrease with increasing pressure.

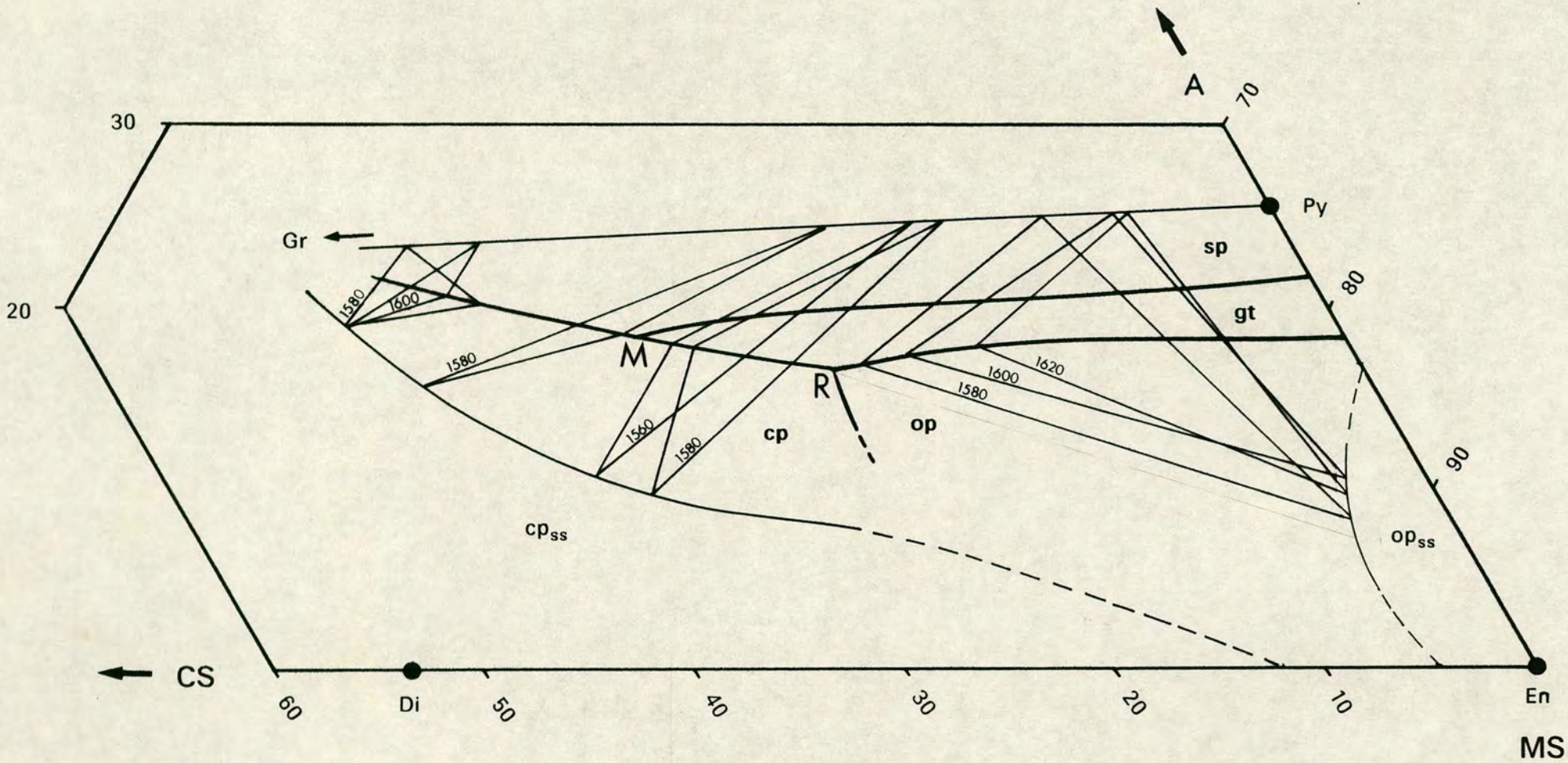

Figure 3–9 : Liquidus projection of part of the plane CS–MS–A (wt%) for experiments of this study. Data shown (three–phase triangles and temperatures in °C) are for 30kb experiments on in–plane starting compositions. Liquidus fields are labelled in bold type. R is a reaction point where liquid + orthopyroxene = garnet + clinopyroxene. M marks the approximate position of a minimum on the garnet–clinopyroxene cotectic. Clinopyroxene and orthopyroxene solid solution fields (cp_{ss} and op_{ss}) are extrapolated according to the experimental data of Davis & Boyd (1966) for the join diopside–enstatite, and Boyd & England (1964) for enstatite–pyrope.

CHAPTER 4

MINERAL–MELT EQUATIONS

4.1. Derivation of the basic form

For equilibrium between a crystalline phase (*e.g.* garnet) and a silicate liquid phase a reaction can be written for each component (*e.g.* pyrope):

$$Mg_3Al_2Si_3O_{12}^{gt} = Mg_3Al_2Si_3O_{12}^{liq} \qquad (4\text{–}1)$$

where the superscripts gt and liq denote the pyrope component in the garnet solid solution and the liquid respectively. For pure pyrope, taking the standard state to be the pure end-member at 1 bar and the temperature of interest, the standard free energy change (ΔG°) of reaction 4–1 can be written:

$$\Delta G^\circ = \Delta H^\circ - T\Delta S^\circ + (P-1)\Delta V^\circ \qquad (4\text{–}2)$$

where:
ΔH° – 1 bar enthalpy of fusion of pure pyrope
ΔS° – 1 bar entropy of fusion of pure pyrope
T – absolute temperature
ΔV° – volume change of fusion of pure pyrope
P – pressure in bars

For a garnet solution, the free energy change (ΔG) of reaction 4–1 is related to the standard free energy change by the equation:

$$\Delta G = \Delta G^\circ + RT\ln K \qquad (4\text{–}3)$$

$$\text{where } K = a_{Py}^{liq}/a_{Py}^{gt}$$

K is the equilibrium constant of the reaction, R is the gas constant, and a_{Py}^{liq} and

a^{gt}_{py} denote the activities of the pyrope component in the liquid and the garnet respectively. Thus for a multicomponent garnet in equilibrium with a silicate liquid, the reaction for each component i is :

$$\Delta G = 0 = \Delta H^\circ - T\Delta S^\circ + (P-1)\Delta V^\circ + RT\ln\left(a_i^{liq}/a_i^{gt}\right) \qquad (4\text{-}4)$$

The data presented in Chapter 3 consist of the compositions of coexisting crystals and liquids at known temperature and pressure conditions. In equation 4-4 the equilibrium constant is written in terms of component activities, so suitable relationships between phase compositions and component activities are required before these data can be used. The activity-composition relationships used in this study are discussed in Section 4.2. In order to demonstrate the general form of the mineral-melt equations it is sufficient to note that: $a_i^j = X_i^j\gamma_i^j$ where a_i^j is the activity of component i in phase j, X_i^j is the mole fraction of i in j and γ_i^j is the activity coefficient of i in j. Equation 4-4 can now be written:

$$\Delta G = 0 = \Delta H^\circ - T\Delta S^\circ + (P-1)\Delta V^\circ + RT\ln\left(X_i^{liq}\gamma_i^{liq}/X_i^{gt}\gamma_i^{gt}\right) \qquad (4\text{-}5)$$

which can be rearranged:

$$RT\ln\left(X_i^{gt}/X_i^{liq}\right) = \Delta H^\circ - T\Delta S^\circ + (P-1)\Delta V^\circ + RT\ln\gamma_i^{liq} - RT\ln\gamma_i^{gt} \qquad (4\text{-}6)$$

If the liquid and garnet phases both behave as ideal solutions, then γ_i^{liq} and γ_i^{gt} are unity and $RT\ln\gamma_i^{liq}$ and $RT\ln\gamma_i^{gt}$ are zero. If the liquid and garnet phases are not ideal then the activity coefficient terms may be written as functions of composition and various "interaction parameters". This is discussed in detail in Sections 4.2.3 and 4.5.2, but the general form of the mineral-melt equations

can now be written:

$$RT\ln\left(X_i^{gt}/X_i^{liq}\right) = \Delta H^o - T\Delta S^o + (P-1)\Delta V^o + \sum C_r X_r \qquad (4-7)$$

where each X_r is a compositional variable and each C_r is a compositionally-independent interaction parameter. Further rearrangement yields:

$$\ln\left(X_i^{gt}/X_i^{liq}\right) = C_o + C_1/T + C_2(P-1)/T + \sum C_r X_r/T \qquad (4-8)$$

where C_0, C_1 and C_2 are constants representing $-\Delta S^o/R$, $\Delta H^o/R$ and $\Delta V^o/R$ respectively.

Equation (4-8) now has the form of a multiple linear regression model with a dependent variable on the left-hand side, related to a number of independent variables on the right-hand side. In this chapter, equations of the form of 4-8 are fitted to the experimental data of Chapter 3 by the method of least squares, by which the partial regression coefficients C_0, C_1, C_2 and C_r are determined so as to minimise the sum of the squared differences between the observed values of $\ln(X_i^{xtal}/X_i^{liq})$ and the values estimated from the regression model. This yields mineral-melt eqations which describe single-component partition coefficients (X_i^{xtal}/X_i^{liq}) as functions of temperature, pressure and composition.

4.2. Activity-composition relationships

4.2.1. Garnets

Available calorimetric and experimental data on binary joins in Mg-Ca-Fe garnets (Hensen *et al.*, 1975; Haselton & Newton, 1980; Ganguly & Saxena, 1984) suggest that these garnets mix ideally at temperatures greater than

about 1400°C. This was assumed to be true in this study.

All of the garnets in this study are pyrope-grossular-almandine solid solutions and have the formula $(Mg,Ca,Fe)_3Al_2Si_3O_{12}$. Mixing only occurs on the cubic site. There are three cubic sites per formula unit and since the activity coefficients are unity for the case of ideal mixing, the acivities of the garnet end-member components in the garnet solid solution can be expressed:

$$a^{gt}_{Py} = X^{gt}_{Py}\gamma^{gt}_{Py} = X^{gt}_{Py} = \left(X^{cubic}_{Mg}\right)^3$$

$$a^{gt}_{Gr} = X^{gt}_{Gr} = \left(X^{cubic}_{Ca}\right)^3$$

$$a^{gt}_{Alm} = X^{gt}_{Alm} = \left(X^{cubic}_{Fe}\right)^3$$

where X^{cubic}_{Mg} = cation fraction of Mg on cubic site (= Mg/(Mg+Ca+Fe))

4.2.2. Clinopyroxenes

The clinopyroxenes in this study can be described in terms of the four components diopside (Di), enstatite (En), ferrosilite (Fs) and Ca-tschermak pyroxene (CaTs) (Section 3-4). In the absence of sufficient data on the mixing properties of these components, they were treated as mixing ideally. The general formula for the clinpyroxenes in this study is $(Ca,Mg,Fe)^{M2}(Mg,Fe,Al)^{M1}(Si,Al)^{T}_2O_6$, where M2, M1 and T denote the different cation sites. Site occupancies were calculated according to the following scheme based on a formula with 4 cations and 6 oxygens.

1. All Si assigned to T.
2. Half Al assigned to T, half Al assigned to M1.
3. All Ca assigned to M2.
4. Mg and Fe assigned to M1 and M2 with Mg/Fe ratio the same on both sites.

The thermodynamic mole fractions of the four pyroxene components were then written in terms of site occupancy and a local charge balance model. Thus the activities of the pyroxene end-member components were expressed:

$$a_{Di}^{cp} = X_{Di}^{cp}\gamma_{Di}^{cp} = X_{Di}^{cp} = X_{Ca}^{M2}X_{Mg}^{M1}$$

$$a_{En}^{cp} = X_{En}^{cp} = X_{Mg}^{M2}X_{Mg}^{M1}$$

$$a_{Fs}^{cp} = X_{Fs}^{cp} = X_{Fe}^{M2}X_{Fe}^{M1}$$

$$a_{CaTs}^{cp} = X_{CaTs}^{cp} = X_{Ca}^{M2}X_{Al}^{M1}$$

where X_{Ca}^{M2} = cation fraction of Ca on M2 site *etc.*

4.2.3. Liquids

In equation 4-8, X_i^{liq} denoted the mole fraction of a mineral end-member component (*e.g.* pyrope) in the liquid phase. Whereas site-occupancy models can be used to express mole fractions in crystalline solutions, they are not applicable to the liquid phase since liquids do not contain specific sites on which mixing takes place. The approach used in this study is to express each X_i^{liq} in terms of probability. For example:

$$X_{Py}^{liq} = \left(\tfrac{8}{3}X_{Mg}^{liq}\right)^3\left(4X_{Al}^{liq}\right)^2\left(\tfrac{8}{3}X_{Si}^{liq}\right)^3$$

where X_{Mg}^{liq} = cation fraction of Mg in the liquid
= Mg/(Mg+Ca+Fe+Al+Si)

This can be viewed as the probability that any 8 adjacent cations in the liquid will be 3Mg, 2Al and 3Si which, with appropriate oxygens, would constitute a

"pyrope unit" in the liquid. Stoichiometric factors of 8/3, 4 and 8/3 are required since a pure pyrope liquid ($X_{Py}^{liq}=1$) would have cation fractions $X_{Mg}^{liq}=3/8$, $X_{Al}^{liq}=2/8$ and $X_{Si}^{liq}=3/8$. For both garnet–liquid and clinopyroxene–liquid equations, a model was used in which the mineral end–member components mixed ideally in the liquid phase. In this case, their activities were expressed:

$$a_{Py}^{liq} = X_{Py}^{liq} = \left(\tfrac{8}{3}X_{Mg}^{liq}\right)^3\left(4X_{Al}^{liq}\right)^2\left(\tfrac{8}{3}X_{Si}^{liq}\right)^3$$

$$a_{Gr}^{liq} = X_{Gr}^{liq} = \left(\tfrac{8}{3}X_{Ca}^{liq}\right)^3\left(4X_{Al}^{liq}\right)^2\left(\tfrac{8}{3}X_{Si}^{liq}\right)^3$$

$$a_{Alm}^{liq} = X_{Alm}^{liq} = \left(\tfrac{8}{3}X_{Si}^{liq}\right)^3\left(4X_{Al}^{liq}\right)^2\left(\tfrac{8}{3}X_{Si}^{liq}\right)^3$$

$$a_{Di}^{liq} = X_{Di}^{liq} = 4X_{Ca}^{liq}\,4X_{Mg}^{liq}\left(2X_{Si}^{liq}\right)^2$$

$$a_{En}^{liq} = X_{En}^{liq} = \left(2X_{Mg}^{liq}\right)^2\left(2X_{Si}^{liq}\right)^2$$

$$a_{Fs}^{liq} = X_{Fs}^{liq} = \left(2X_{Fe}^{liq}\right)^2\left(2X_{Si}^{liq}\right)^2$$

$$a_{CaTs}^{liq} = X_{CaTs}^{liq} = 4X_{Ca}^{liq}\left(2X_{Al}^{liq}\right)^2 4X_{Si}^{liq}$$

Garnet–liquid equations with mixing in the liquid phase expressed as a regular solution model were also used. Their activity coefficients were expressed using the following formula derived from the generalised expression of Berman & Brown (1984):

$$RT\ln\gamma_i^{liq} = \sum_m \sum_{j=1}^{4} \sum_{k=j+1}^{5} n_m W_{jk}\left(Q_m X_j X_k / X_m - X_j X_k\right) \qquad (4\text{–}9)$$

where i is the mineral end–member component (*e.g.* pyrope) and m is, in turn, each of the cations of the mineral end–member component (*e.g.* Mg, Al and Si if i is pyrope). The subscripts j and k refer to the cations in the liquid in the order Si(1), Al(2), Fe(3), Mg(4), Ca(5). Each X_j, X_k and X_m is the cation fraction of the subscript cation in the liquid, and n_m is the number of m cations in the formula of the mineral end–member component (*e.g.* for pyrope $n_{Mg}=3$, $n_{Al}=2$, $n_{Si}=3$). The term Q_m is the number of subscripts j and k which are equal to m

(*e.g.* if m=Mg, Q_m=1 if either j=1 or k=1, otherwise Q_m=0). The term W_{jk} is the j-k interaction parameter (*e.g.* if j=1 and k=2, W_{12} is the Si-Al interaction parameter) and appears on the right hand side of equation 4-8 as one of the partial regression coefficients C_r.

4.3. Equations obtained by least-squares fitting

Equations were fitted to data consisting of coexisting crystal and liquid compositions at known conditions of temperature and pressure. The data from the experiments of this study are given in Table 3-2. Experiments B776, B777, B797 and B811 were excluded. Where available, high-pressure melting points of the pure end-member minerals were incorporated as this was found to improve the fits of the equations. The following data were used: 40kb melting point of pure pyrope (1790°C, from Boyd & England, 1962); 50kb melting point of pure pyrope (1850°C, from Ohtani & Irifune, 1986); liquid e_1 and coexisting grossular-rich garnet at 1525°C and 30kb extracted from Figure 1 of Maaloe & Wyllie (1979); 26kb melting point of pure almandine (1485°C, from Keesman *et al.*, 1971); 25kb melting point of pure diopside (1715°C, from Table 2-4 of this study). The equations were fitted to the datasets by a computer program originally written by Dr. C.E. Ford for olivine-liquid equilibria and modified by me for garnet-liquid and clinopyroxene-liquid equilibria. Table 4-1 shows the equations fitted and the partial regression coefficients obtained by the least-squares fitting procedure.

Two versions of the garnet-liquid equations using the regular liquid model were fitted to the data. In the first (equations 4, 5 and 6 of Table 4-1), all 13 partial regression coefficients (C_0, C_1, C_2 and the interaction parameters C_3-C_{12}) were assumed to be significant. In the second version (equations 7, 8 and 9 of Table 4-1), variables with partial regression coefficients with standard errors >100% were eliminated. To do this the variable with the least

Table 4-1 : Equations used and partial regression coefficients derived.

garnets- ideal mixing
liquids - ideal mixing

$$\ln\left(X_i^{gt}/X_i^{liq}\right) = C_0 + C_1/T + C_2P/T$$

Eq.no.	1		2		3	
	Py	s.e.	Gr	s.e.	Alm	s.e.
C_0	-1.650 E 1	18.11	-2.075 E 1	83.47	-2.317 E 1	29.93
C_1	2.820 E 4	16.52	3.470 E 4	81.79	3.499 E 4	33.08
C_2	1.417 E-1	27.43	2.855 E-2	538.72	2.110 E-1	32.50

garnets - ideal mixing
liquids - regular mixing
all variables retained - see text

$$\ln\left(X_i^{gt}/X_i^{liq}\right) = C_0 + C_1/T + C_2P/T + C_3X_3/T + \ldots + C_{12}X_{12}/T$$

Eq.no.	4		5		6	
	Py	s.e.	Gr	s.e.	Alm	s.e.
C_0	-9.370 E 0	80.81	2.010 E 1	143.63	-3.141 E 1	72.78
C_1	1.505 E 4	974.34	-5.805 E 5	98.06	1.051 E 6	63.49
C_2	6.786 E-2	109.82	-2.990 E-1	67.18	6.377 E-1	41.74
C_3	-7.961 E 3	1037.02	3.068 E 5	90.12	-4.110 E 5	73.22
C_4	-4.940 E 5	340.54	-1.328 E 5	734.89	-2.839 E 4	103.07
C_5	1.565 E 4	99.07	5.427 E 4	300.48	6.423 E 4	84.12
C_6	-2.056 E 4	111.38	3.759 E 4	294.13	-4.447 E 3	1078.64
C_7	1.643 E 4	228.30	1.653 E 5	608.57	-8.969 E 5	61.38
C_8	-1.340 E 4	866.52	1.858 E 5	145.89	-5.470 E 5	56.33
C_9	-7.243 E 4	178.26	3.763 E 5	124.72	-8.502 E 5	60.15
C_{10}	-1.470 E 5	140.31	-3.902 E 5	158.68	-4.475 E 4	69.30
C_{11}	-2.400 E 5	102.75	-2.468 E 5	185.30	-2.360 E 4	78.40
C_{12}	-1.075 E 4	41.65	-2.939 E 3	743.79	-7.657 E 4	48.26

Table 4–1 : continued

garnets – ideal mixing
liquids – regular mixing
selected variables – see text

equation as above

Eq.no.	7		8		9	
	Py	s.e.	Gr	s.e.	Alm	s.e.
C_0	-1.264 E 1	37.95	2.378 E 1	61.37	-3.220 E 1	61.05
C_1	2.258 E 4	36.80	-6.181 E 5	52.13	1.086 E 6	47.60
C_2	8.899 E-2	46.10	-3.124 E-1	42.01	6.520 E-1	30.84
C_3	–	–	2.386 E 5	71.17	-4.278 E 5	52.07
C_4	–	–	–	–	-2.837 E 4	95.57
C_5	–	–	–	–	6.482 E 4	76.68
C_6	-3.291 E 4	24.47	6.117 E 4	63.78	–	–
C_7	–	–	4.006 E 5	40.56	-9.242 E 5	46.65
C_8	–	–	2.042 E 5	82.06	-5.620 E 5	43.29
C_9	-2.676 E 4	37.80	4.508 E 5	52.35	-8.726 E 5	47.86
C_{10}	-3.862 E 4	43.69	-4.073 E 5	72.44	-4.614 E 4	54.54
C_{11}	-8.574 E 4	36.37	-2.843 E 5	78.91	-2.247 E 4	57.40
C_{12}	-9.634 E 3	22.93	–	–	-7.482 E 4	39.32

clinopyroxenes – ideal mixing
liquids – ideal mixing

$$\ln\left(X_i^{cp}/X_i^{liq}\right) = C_0 + C_1/T + C_2P/T$$

Eq.no.	10		11		12		13	
	Di	s.e.	En	s.e	Fs	s.e.	CaTs	s.e.
C_0	-5.327 E 0	15.69	-2.995 E 1	42.88	-1.244 E 1	57.72	1.180 E 1	46.08
C_1	9.453 E 3	16.60	5.059 E 4	43.62	1.687 E 4	73.16	-1.829 E 4	51.09
C_2	4.407 E-2	17.47	1.599 E-1	45.50	1.152 E-1	35.32	-9.035 E-2	34.09

i – mineral end-member component (Py, Di, *etc.*)
T – absolute temperature
P – pressure in bars
E – exponent notation (*e.g.* -1.650 E 1 = -1.650×10^1)
s.e. – standard error of each partial regression coefficient as a percentage. If standard error >100, then value of partial regression coefficient is not significantly different from zero.

significant partial regression coefficient (*i.e.* the highest standard error) was eliminated and the equation refitted. This procedure was repeated until all the remaining variables had partial regression coefficients with standard errors of less than 100%.

The clinopyroxene–liquid pair from experiment A366 was omitted from the dataset used to fit the clinopyroxene liquid equations (equations 10, 11, 12 and 13 of Table 4–1), because inclusion resulted in very much poorer fits. The clinopyroxene from experiment A366 is by far the most enstatite–rich encountered in this study (see Table 3–2 and Figures 3–7 and 3–8), so its exclusion from the dataset may only restrict the applicability of mineral–melt equations 10 to 13 of Table 4–1 to the compositional range which the majority of the clinopyroxenes occupy. A more complex clinopyroxene or liquid model may be able to accommodate compositions such as that from experiment A366, but this was not attempted due to the limited amount of data available.

4.4. Statistical testing of the fitted equations

The significance of each fitted equation was investigated by partitioning the sums of squares and performing an analysis of variance (see *e.g.* Freund & Minton, 1979, pp.64–68). The multiple correlation coefficient , R, was calculated as an indicator of the goodness of the fit of each equation. Results of these two statistical tests, and the formulae used to apply them, are given in Table 4–2.

Table 4–2 shows that equations 2, 6 and 11 of Table 4–1 failed the test for significance at the 0.10 confidence level. This means that the null hypothesis (that all the partial regression coefficients are equal to zero, *i.e.* the regression model does not fit the data) cannot be rejected at this confidence level. If the regression does not fit the data, then the expected F–value is near unity and R^2

Table 4-2 : Multiple correlation coefficients and significance of fits.

Eq.no.		F	sig.	R
1	Py	18.69	0.01	0.83
2	Gr	0.83	n.s.	0.31
3	Alm	6.00	0.05	0.65
4	Py	12.71	0.01	0.98
5	Gr	11.33	0.01	0.98
6	Alm	2.75	n.s.	0.94
7	Py	29.55	0.01	0.97
8	Gr	21.66	0.01	0.98
9	Alm	4.82	0.05	0.94
10	Di	39.62	0.01	0.94
11	En	2.03	n.s.	0.56
12	Fs	4.60	0.05	0.71
13	CaTs	4.35	0.05	0.70

F - value of the F-ratio.
sig. - confidence level at which result is significant.
n.s. - result is not significant at the 0.10 confidence level.
R - multiple regression coefficient.
Eq.no. - equation numbers refer to Table 4-1

$$R = \sqrt{(SSR/SST)}$$

$$F = (SSR/m)/(SSE/(n-m-1))$$

where:
SSR = regression sum of squares = $\Sigma(\hat{\mu}_x-\bar{y})^2$
SSE = residual sum of squares = $\Sigma(y-\hat{\mu}_x)^2$
y - a measured value of the dependent variable
$\bar{y}$ - the mean of the measured values (= $\Sigma y/n$)
$\hat{\mu}_x$ - value of the dependent variable estimated from the regression model
n - number of measured values of the dependent variable
m - number of independent variables in the regression model

is approximately m/n (Freund & Minton, 1979, p.71). For equation 2 of Table 4-1, F=0.83, R^2=0.096 and m/n=0.1, so it must be concluded that this mineral-melt equation is not statistically significant. Equations 6 and 11 have F-values which are definitely not near unity, and as they only just fail to be significant at the 0.10 confidence level, they are still considered to be valid.

4.5. Approaches tried and discarded

In addition to the mineral-melt equations derived and described above, several other approaches were tried but discarded as they offered no material improvement.

4.5.1. Regular solution model for liquids

A regular solution formalism was used in Section 4.2.3 to express $RT\ln\gamma_i^{liq}$ for mineral-melt equations 4 to 9 of Table 4-1 and the partial regression coefficients corresponding to the interaction parameters were derived by the least-squares fitting procedure. However, if the liquid were behaving as a true regular solution, the interaction parameters should be the same in each equation (*e.g.* W_{Si-Al} (partial regression coefficient C_3) in equation 4 should be the same as W_{Si-Al} in equation 5 etc.). Table 4-2 shows that this is not the case, thus equations 4 to 9 involve an approximation to a regular solution model for the liquid, some of the difference between the true behaviour of the liquid and the regular solution model being absorbed by the partial regression coefficients.

Versions of mineral melt equations 4, 5 and 6 of Table 4-1 were fitted in which the partial regression coefficients corresponding to the interaction parameters were constrained to be the same for all three equations. The resultant equations were poorer fits to the data than the original equations upon which this condition was not forced. The performance of the new

equations was similarly poorer when used to recover the dataset as described in Section 5.2 below. It was concluded that a regular solution model could not fully describe the silicate liquids encountered in this study, but that expressions based on a regular solution model could be used in mineral–melt equations fitted to experimental data over a given range of temperature, pressure and composition.

The performance of more complex solution models could not be investigated in this study because the number of interaction parameters required was too great to be fitted to the available data. (In order to be able to fit a multiple linear regression model with m independent variables to data consisting of n observations of the dependent variable, n must be greater than m).

4.5.2. Non–ideal mixing in garnets

In Section 4.2.1 it was noted that the available evidence suggested that pyrope–grossular–almandine garnets mixed ideally at temperatures greater than about 1400°C, and ideal behaviour was assumed for the garnets in equations 1 to 9 of Table 4–1. To verify this assumption, further equations were formulated and fitted to the data. These equations included an activity coefficient term for each garnet end–member component calculated according to an asymmetrical solution model and using interaction parameters taken from Ganguly & Saxena (1984). Inclusion of activity coefficient terms did not significantly improve or worsen any of the fits obtained to the garnet–liquid equations. It was concluded that, for the purposes of this study at least, Py–Gr–Alm garnets can be treated as ideal solutions at high temperatures.

4.5.3. Use of olivine-like components

Throughout this chapter the liquid phase has been described in terms of simple oxide components such that, for example:

$$X_{Py}^{liq} = \left(\tfrac{8}{3}X_{MgO}^{liq}\right)^3\left(4X_{AlO3/2}^{liq}\right)^2\left(\tfrac{8}{3}X_{SiO2}^{liq}\right)^3$$

However, the $CaO-MgO-FeO-Al_2O_3-SiO_2$ system of this study comprises a large compositional space and it is possible that the local shape of the Gibbs free energy of mixing (G_{mix}) surface in the region of the experimental data may be better described by a set of multi-oxide components. Why this might be so is illustrated in Figure 4-1. To test this hypothesis, mineral end-member components in the liquid phase were expressed in terms of Mg_2SiO_4, Ca_2SiO_4, Fe_2SiO_4, $AlO_{3/2}$ and SiO_2. These multi-oxide components can still represent the compositions of all the experimental phases without recourse to negative components, but the compositional space which they span is restricted compared to the simple oxides. Using the multi-oxide components, the mole fractions of the mineral end-member components were expressed, for example:

$$X_{Py}^{liq} = \left(\tfrac{10}{3}X_{Mg2SiO4}^{liq}\right)^{3/2}\left(\tfrac{5}{2}X_{AlO3/2}^{liq}\right)^2\left(\tfrac{10}{3}X_{SiO2}^{liq}\right)^{3/2}$$

since pyrope, $Mg_3Al_2Si_3O_{12}$ = 3/2 Mg_2SiO_4 + 2 $AlO_{3/2}$ + 3/2 SiO_2. The fractions 10/3, 5/2 and 10/3 are stoichiometric factors as explained in Section 4.2.3.

Mineral-melt equations in which the mineral end-member components in the liquid phase were expressed in this way were fitted to the data. The fits obtained were not significantly better or worse than those in which the simple oxides had been used. This approach was not pursued further.

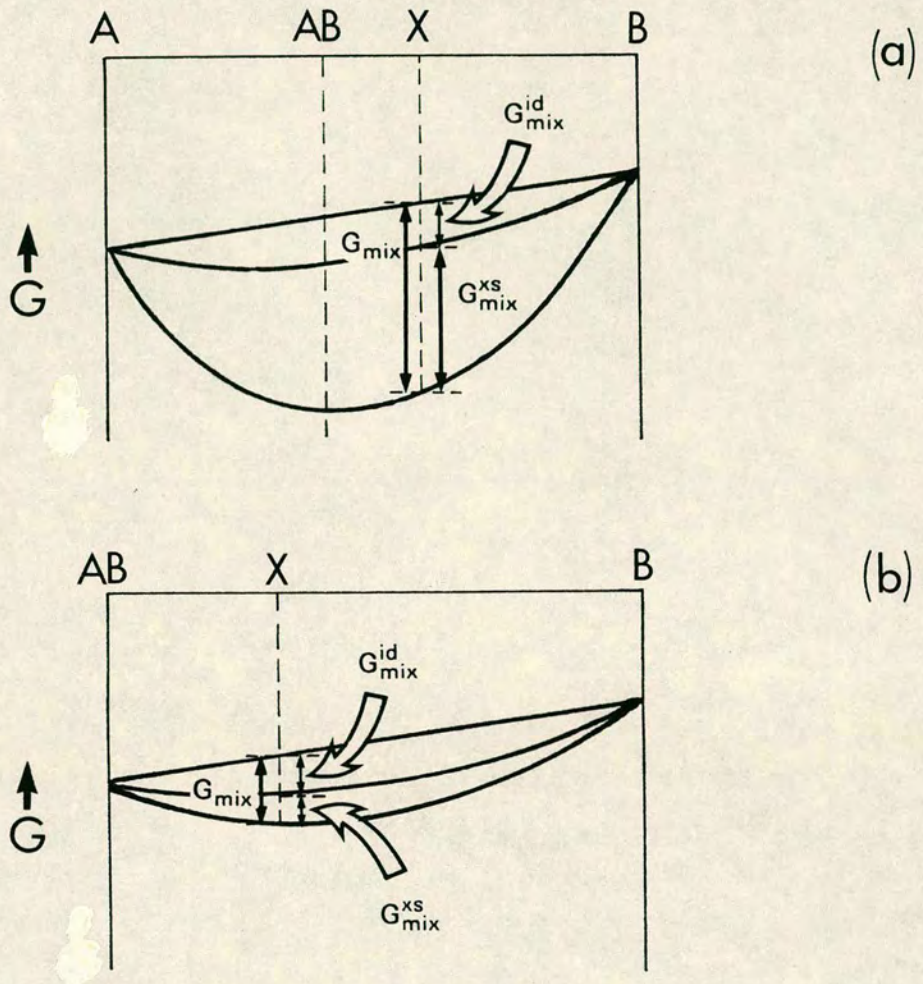

Figure 4–1 : In the system A–B, the free energy of mixing (G_{mix}) of composition X is the sum of an ideal contribution (G^{id}_{mix}) and an excess contribution (G^{xs}_{mix}). If composition X is described in terms of components A and B (a), then G^{xs}_{mix} is large compared to G^{id}_{mix} and the activity of A or B in X will be poorly expressed by a ideal solution model. If composition X is described in terms of components AB and B (b), then G^{xs}_{mix} is smaller than in (a) and the activities of AB and B in X will be more nearly described by a ideal solution model.

CHAPTER 5

APPLICATION OF MINERAL-MELT EQUATIONS

5.1. Principle

The mineral-melt equations derived in Chapter 4 are now used to calculate the equilibrium temperature and the composition of the coexisting crystalline phase for any given liquid in equilibrium with garnet and/or clinopyroxene at a given pressure. The procedure followed is:

1. A value for the equilibrium temperature is assumed.

2. The mole fraction of each mineral end-member component in the crystalline phase is calculated using the appropriate mineral-melt equation, the given liquid composition and pressure, and the assumed temperature.

3. The sum of the mole fractions is calculated. If crystal and liquid are in equilibrium at the assumed temperature, this sum will be equal to 1. If the temperature is too high, the sum will be less than 1, and if the temperature is too low, the sum will be greater than 1.

4. If the sum of the mole fractions is not 1, the temperature is raised or lowered slightly and the mole fractions recalculated. This is repeated until the sum of the mole fractions becomes equal to 1.

Computer programs to perform these calculations for olivine-liquid equilibria were written by Dr. C.E. Ford, and have been modified by me for garnet-liquid and clinopyroxene-liquid equilibria.

5.2. Recovery of original dataset

Each set of mineral-melt equations was tested to see how well they could reproduce the experimental data. The liquid composition and pressure of each experiment was used to calculate the coexisting crystal composition and the equilibrium temperature as detailed in Section 5.1. The calculated values were then compared with the measured values from the experiments. Results are summarised in Table 5-1 and plotted in Figures 5-1 to 5-17.

5.2.1. Ideal solution models

Figures 5-1 to 5-4 show that, using mineral-melt equations 1, 2 and 3 of Table 4-1 (garnets - ideal mixing; liquids - ideal mixing) the greatest discrepancies between the measured and calculated values of temperature and garnet composition occur for experiments B739, B740 and B792, which contain the most grossular-rich garnets and the most calcic liquids of the study. That the ideal model is insufficient for calcic compositions is further shown by the large discrepancy between the measured and calculated composition of the grossular-rich garnet taken from Maaløe & Wyllie (Figure 5-3). For experiments other than B739, B740 and B792, and for pure pyrope and pure almandine, the agreement between measured values and calculated values produced by the ideal model is good.

For clinopyroxenes, the use of mineral-melt equations 10, 11, 12 and 13 of Table 4-1 (clinopyroxenes - ideal mixing; liquids - ideal mixing) produces good agreement between measured and calculated values for all experiments (Figures 5-12 to 5-17).

For those experiments with both garnet and clinopyroxene in equilibrium with liquid, temperatures calculated according to the garnet-liquid equations and to the clinopyroxene-liquid equations are in good agreement (Table 5-2).

Table 5–1 : Analysis of the unsigned differences between measured values of temperature and crystal composition, and values calculated by mineral–melt equations. For each equation, the maximum difference and the mean differences are given, and also 2 standard deviations about the mean (2σ), and the number of values.

Eq.no.		maximum difference	mean difference	2σ	number of values
garnets – ideal mixing					
liquids – ideal mixing					
1	Py	16.6 mol%	4.3 mol%	9.2 mol%	20
2	Gr	32.7 mol%	6.5 mol%	17.2 mol%	19
3	Alm	4.0 mol%	1.5 mol%	1.8 mol%	19
	Temp	40°C	12.2°C	17.0°C	22
garnets – ideal mixing					
liquids – regular mixing					
all variables retained					
4	Py *	9.5 mol%	2.1 mol%	4.4 mol%	19
5	Gr *	12.7 mol%	2.4 mol%	6.8 mol%	18
6	Alm *	4.3 mol%	1.0 mol%	2.2 mol%	18
	Temp *	96°C	16.3°C	45.4°C	21
garnets – ideal mixing					
liquids – regular mixing					
selected variables					
7	Py *	6.8 mol%	1.9 mol%	3.4 mol%	19
8	Gr *	8.7 mol%	2.3 mol%	5.2 mol%	18
9	Alm *	2.9 mol%	0.9 mol%	1.6 mol%	18
	Temp *	60°C	14.6°C	29.4°C	21
clinopyroxenes – ideal mixing					
liquids – ideal mixing					
10	Di	5.9 mol%	2.3 mol%	3.8 mol%	13
11	En	7.0 mol%	2.7 mol%	4.6 mol%	12
12	Fs	1.4 mol%	0.5 mol%	0.8 mol%	12
13	CaTs	4.8 mol%	1.8 mol%	3.0 mol%	12
	Temp	20°C	8.5°C	11.8°C	13

* – Figures from experiment B768 excluded because the calculated mole fractions of the garnet components fail to sum to 1 – see text.

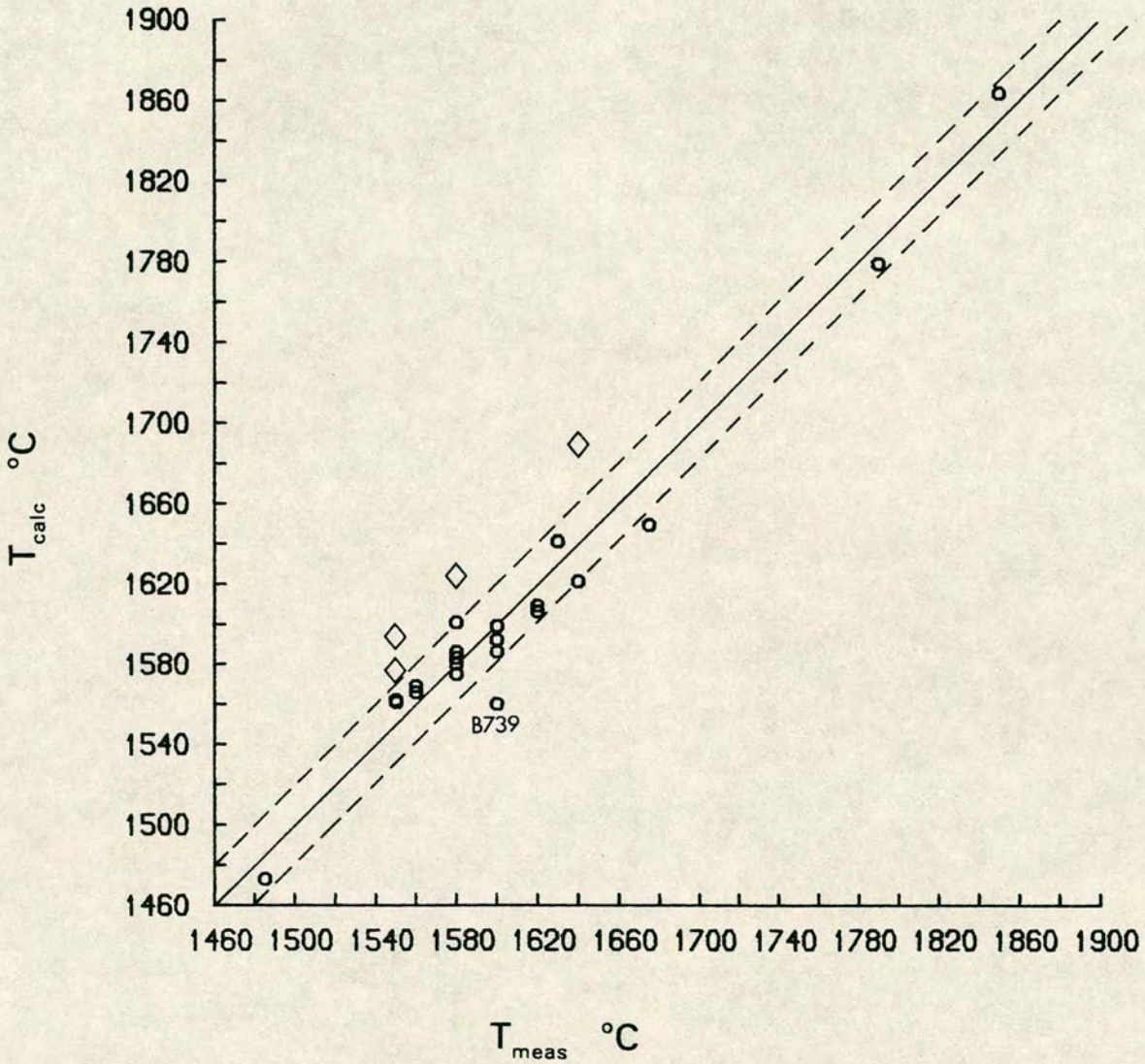

Figure 5-1 : Calculated *vs.* measured temperatures. Equations 1, 2 and 3 of Table 4-1 (garnets - ideal mixing; liquids - ideal mixing). Solid line represents the 1:1 relation, dashed lines represent ±20°C. Diamond symbols are rejected experiments.

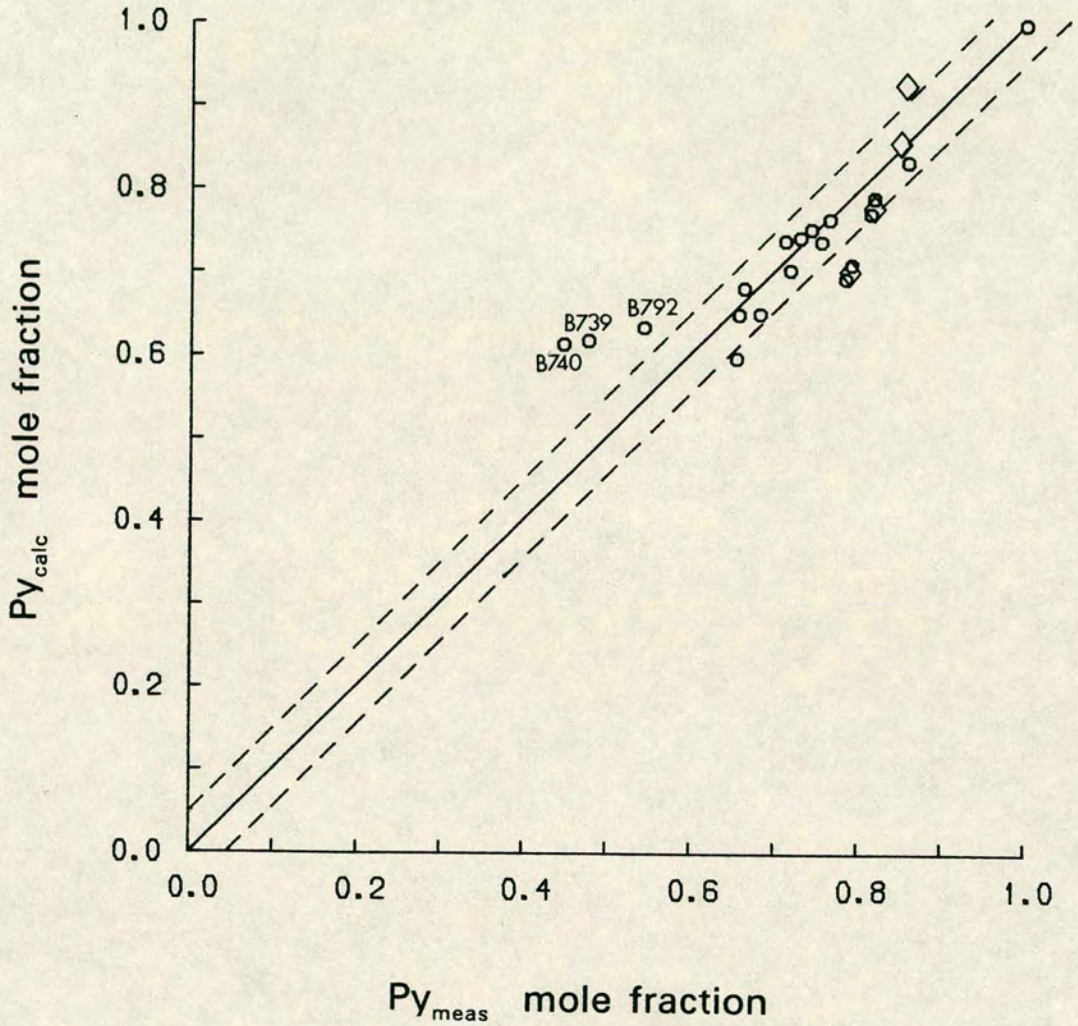

Figure 5–2 : Calculated *vs.* measured pyrope content of garnet. Equations 1, 2 and 3 of Table 4–1 (garnets – ideal mixing; liquids – ideal mixing). Solid line represents 1:1 relation, dashed lines represent ±5 mol%. Diamond symbols represent rejected experiments.

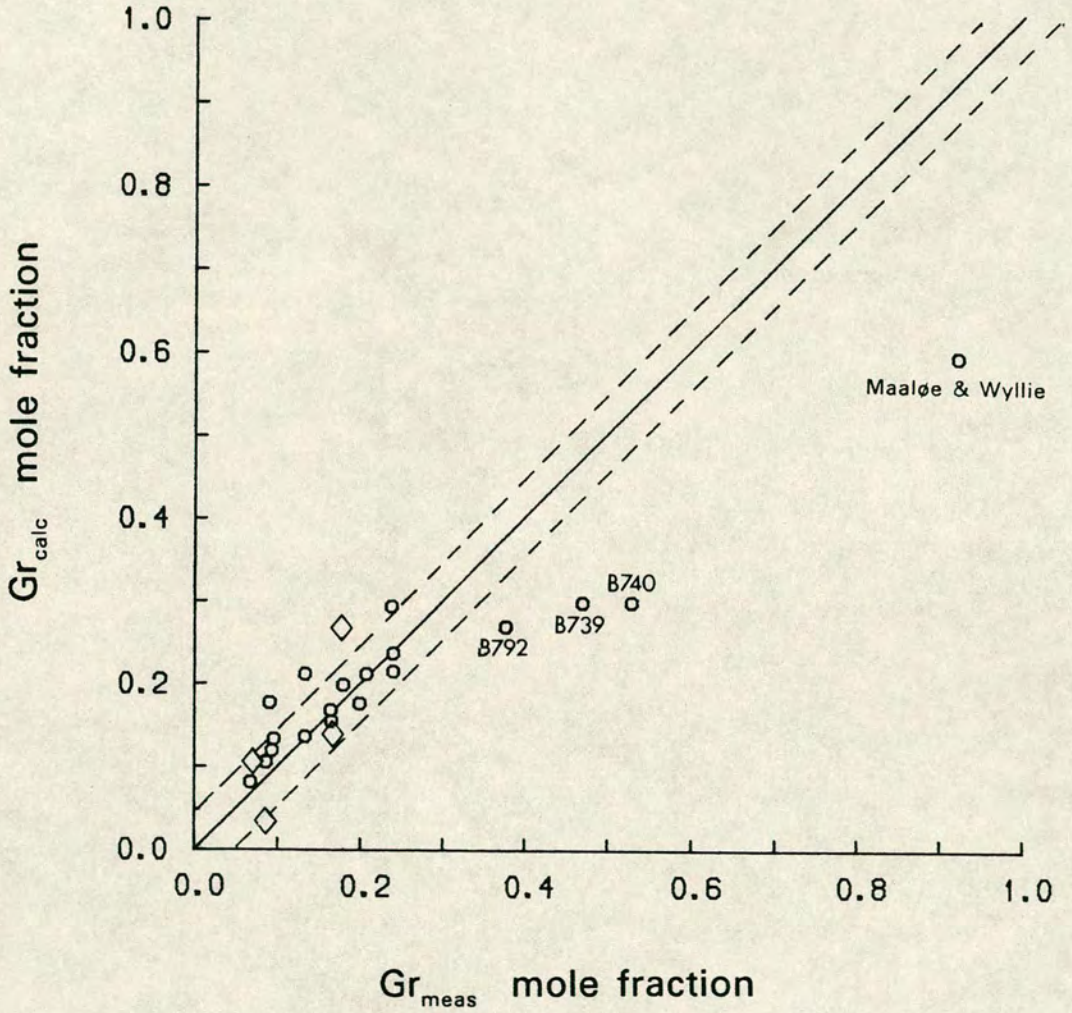

Figure 5–3 : Calculated *vs.* measured grossular content of garnet. Equations 1, 2 and 3 of Table 4–1 (garnets – ideal mixing; liquids – ideal mixing). Solid line represents the 1:1 relation, dashed lines represent ± 5 mol%. Diamond symbols represent rejected experiments.

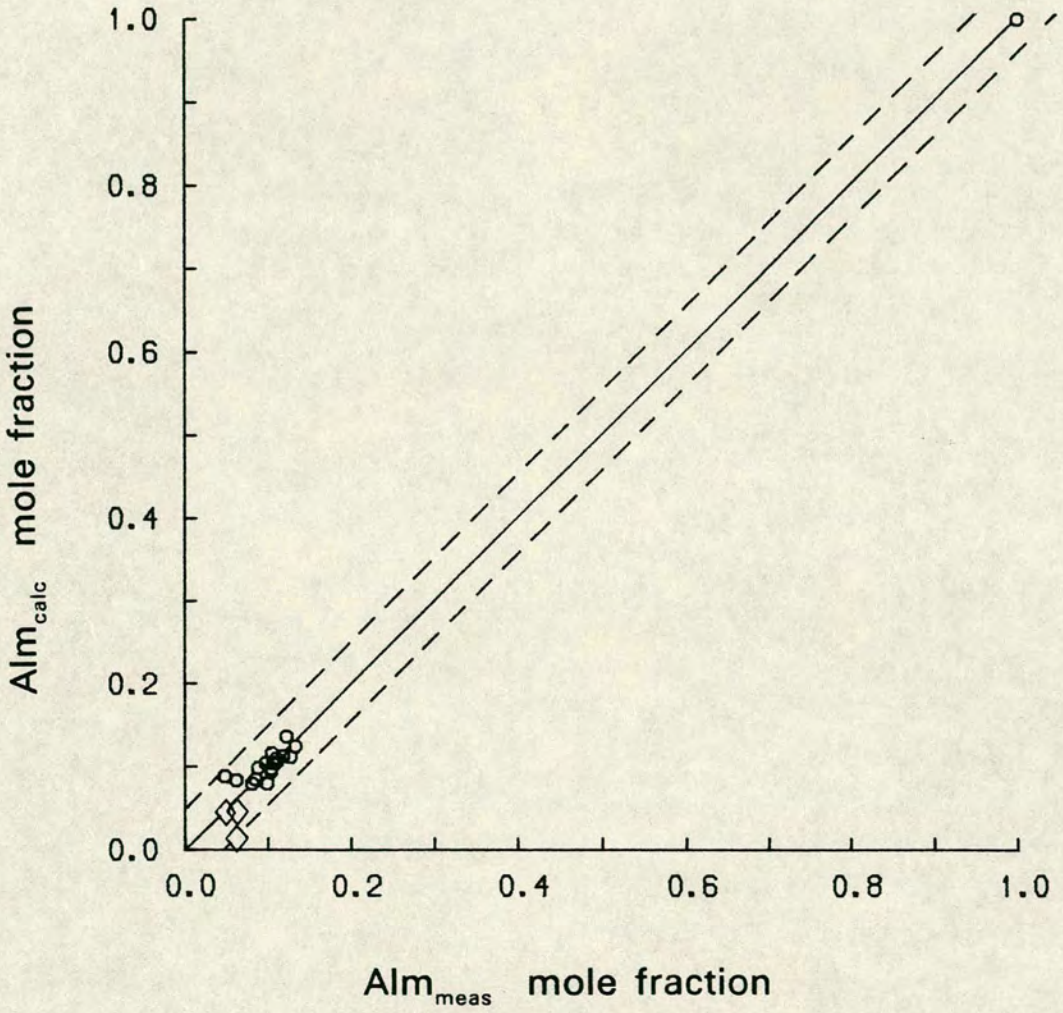

Figure 5-4 : Calculated *vs.* measured almandine content of garnet. Equations 1, 2 and 3 of Table 4-1 (garnets - ideal mixing; liquids - ideal mixing). Solid line represents 1:1 relation, dashed lines represent ± 5 mol%. Diamond symbols represent rejected experiments.

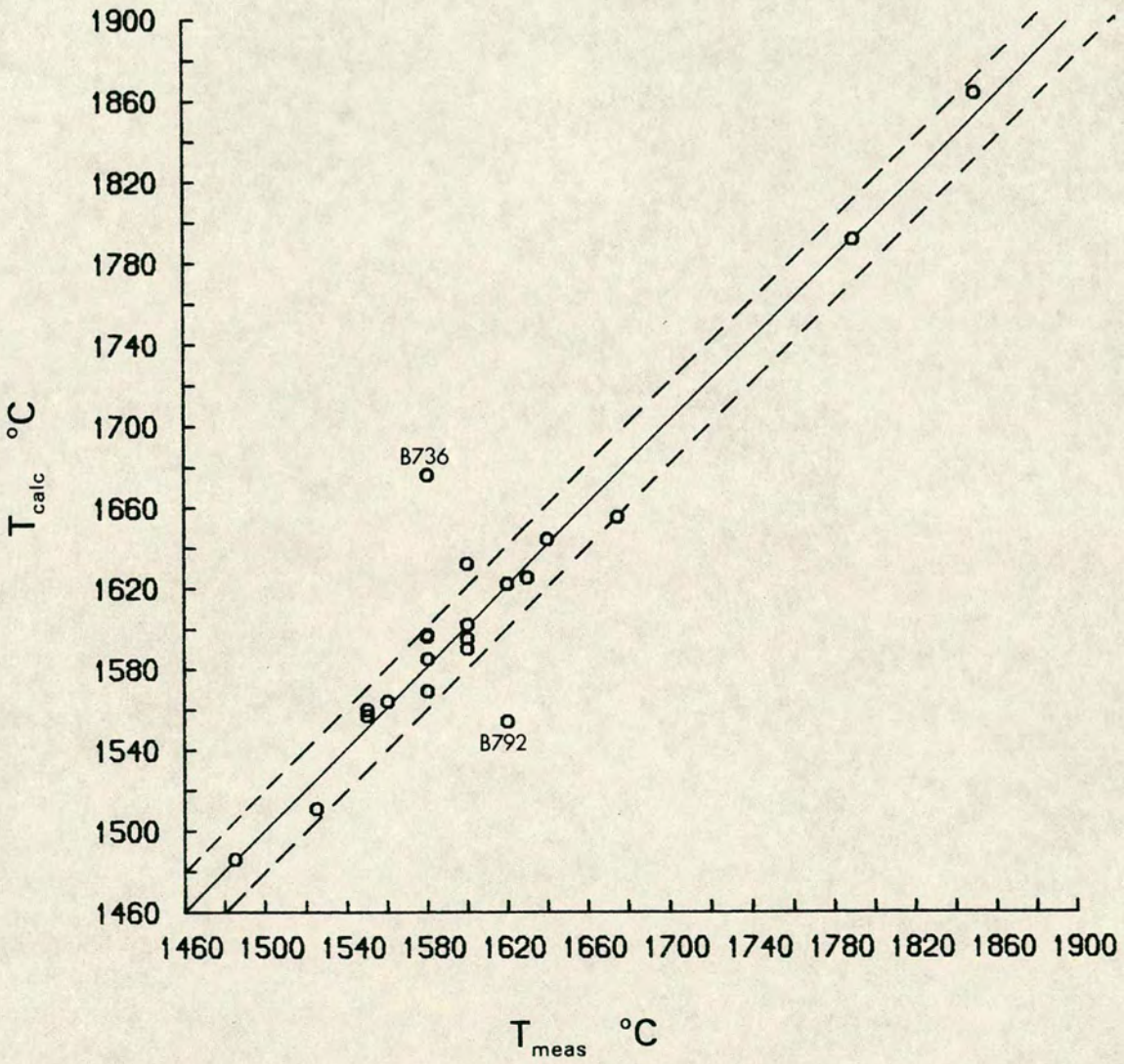

Figure 5–5 : Calculated *vs.* measured temperatures. Equations 4, 5 and 6 of Table 4–1 (garnets – ideal mixing; liquids – regular mixing, all variables retained). Solid line represents 1:1 relation, dashed lines represent ± 20°C.

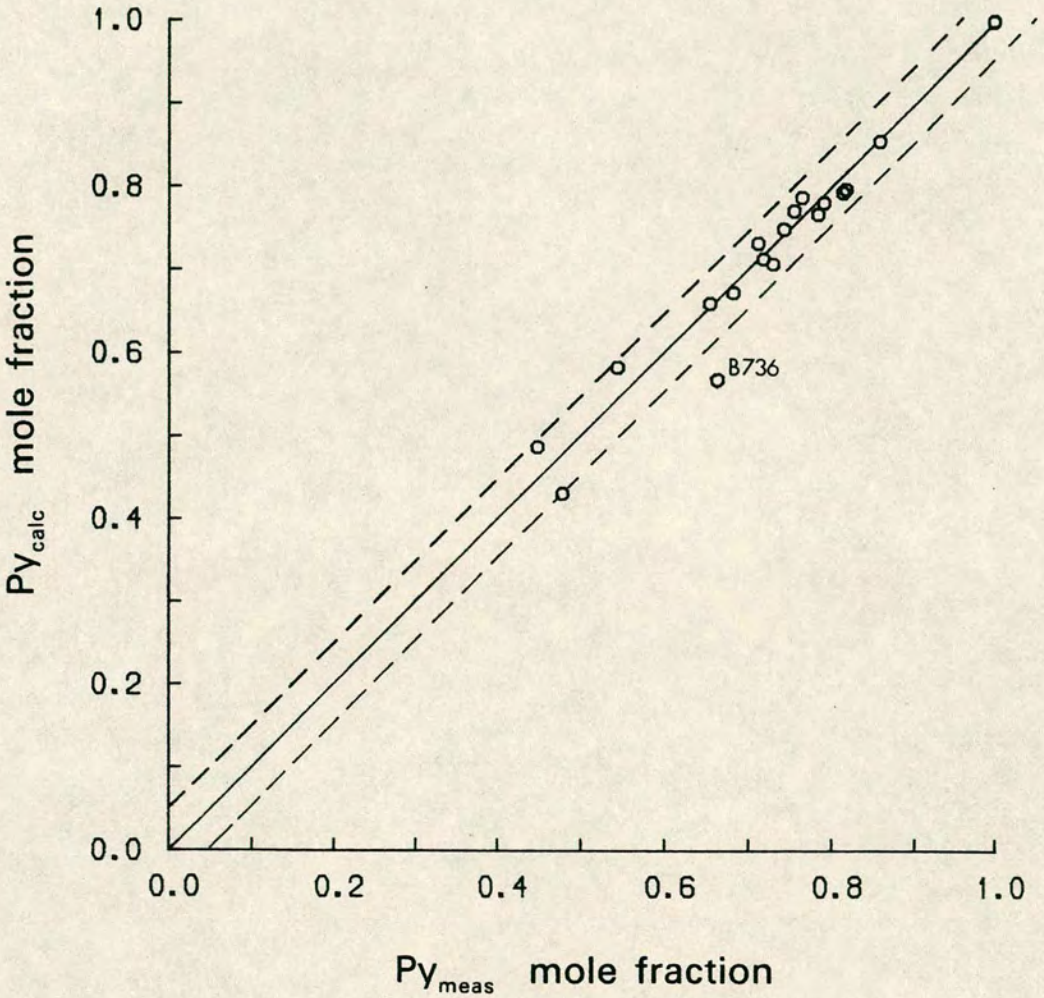

Figure 5-6 : Calculated *vs.* measured pyrope content of garnet. Equations 4, 5 and 6 of Table 4-1 (garnets - ideal mixing; liquids - regular mixing, all variables retained). Solid line represents the 1:1 relation, dashed lines represent ± 5 mol%.

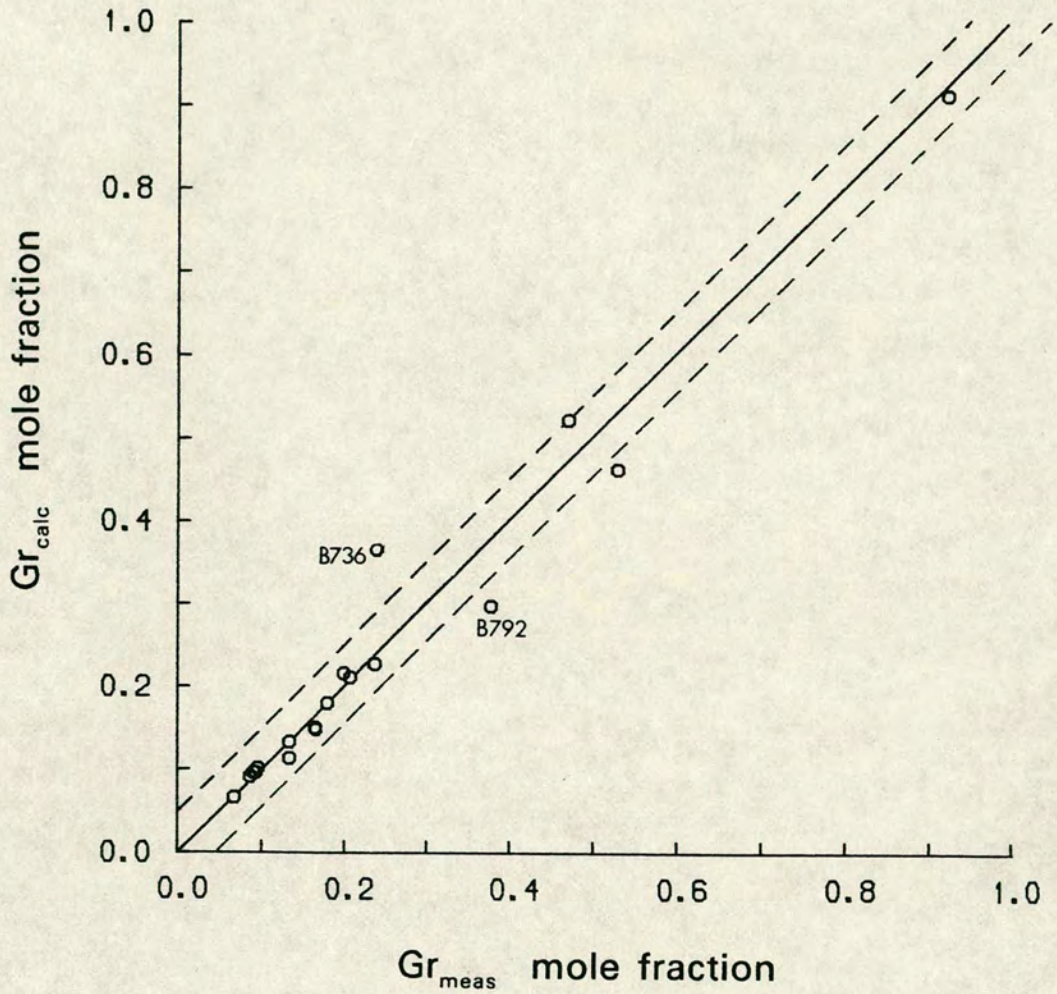

Figure 5–7 : Calculated *vs.* measured grossular content of garnet. Equations 4, 5 and 6 of Table 4–1 (garnets – ideal mixing; liquids – regular mixing, all variables retained). Solid line represents the 1:1 relation, dashed lines represent ± 5 mol%.

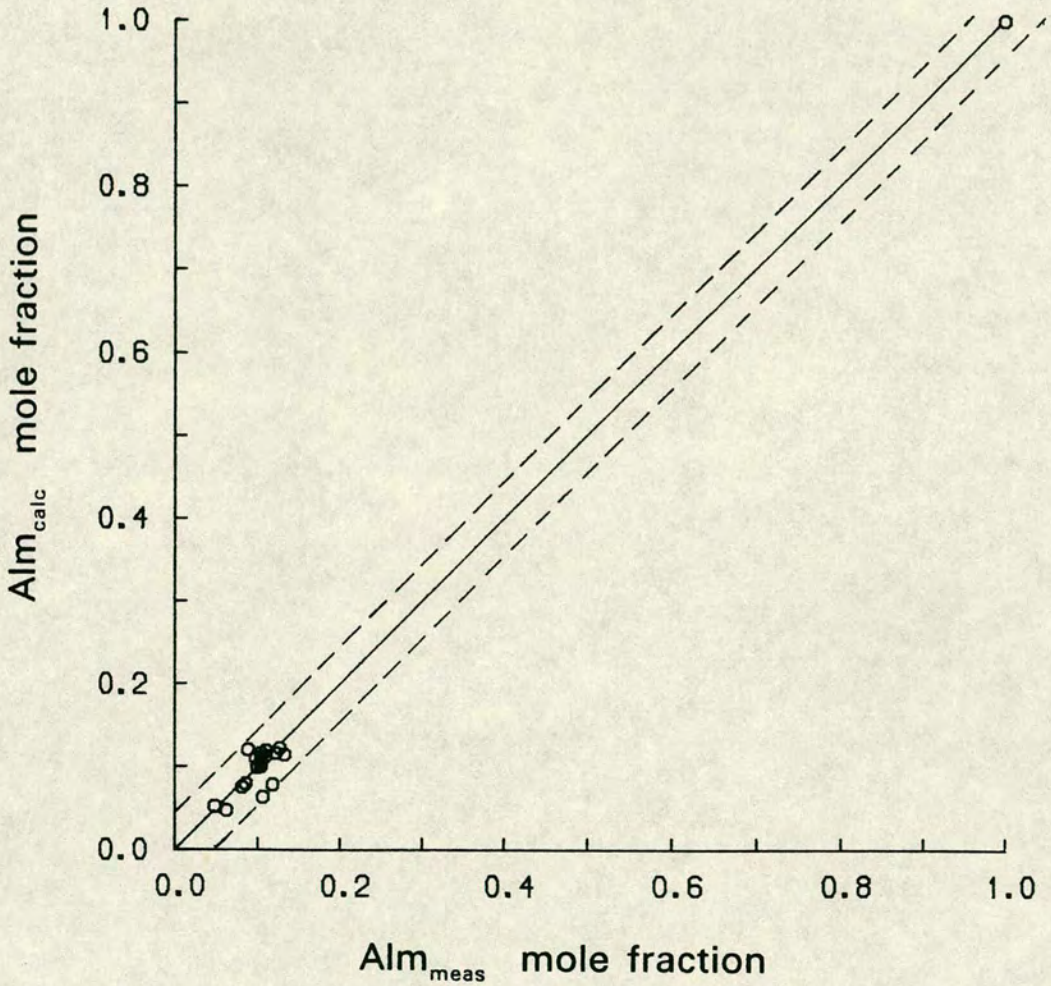

Figure 5-8 : Calculated *vs.* measured almandine content of garnet. Equations 4, 5 and 6 of Table 4-1 (garnets - ideal mixing; liquids - regular mixing, all variables retained). Solid line represents the 1:1 relation, dashed lines represent ± 5 mol%.

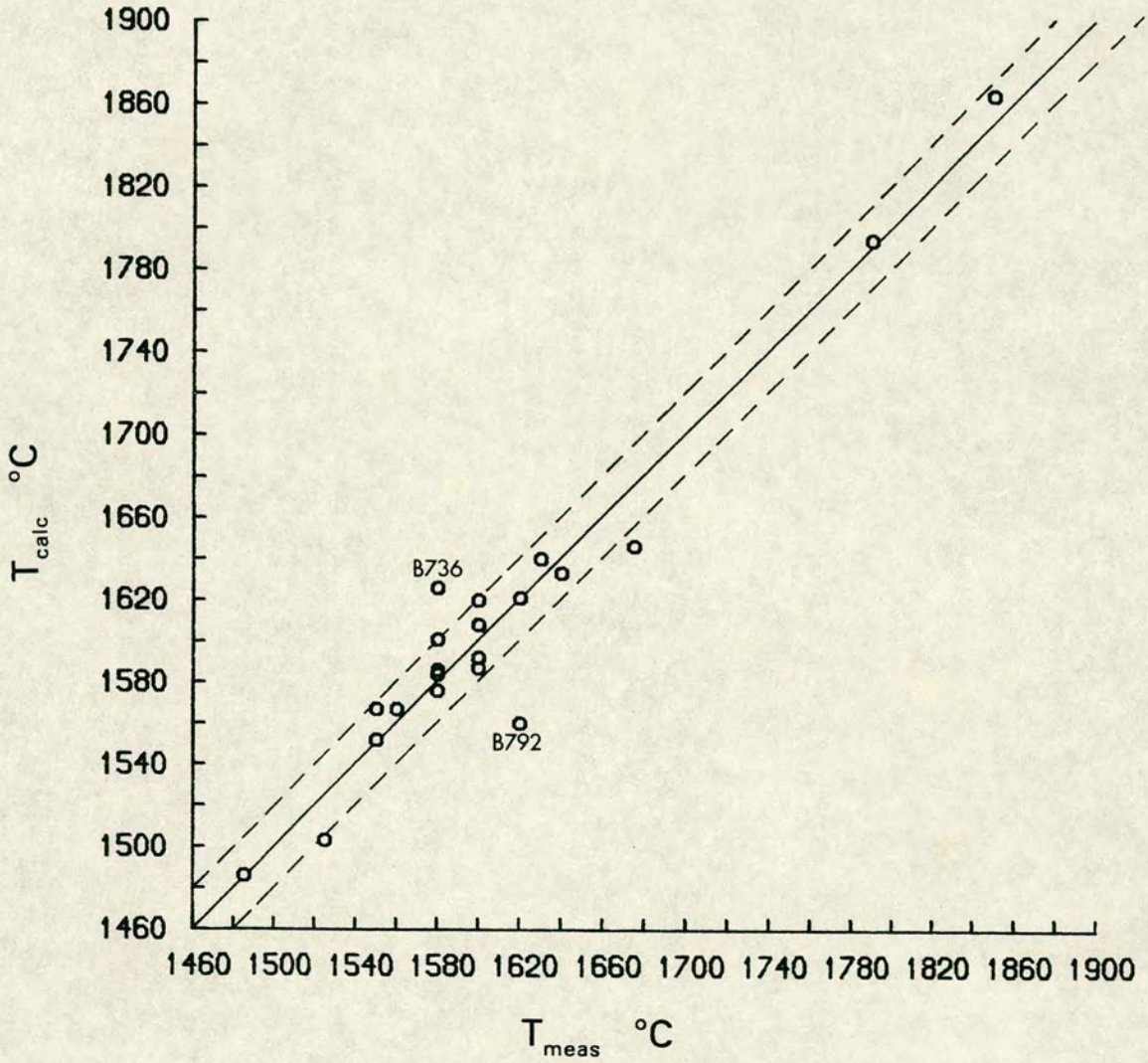

Figure 5-9 : Calculated *vs.* measured temperatures. Equations 7, 8 and 9 of Table 4-1 (garnets - ideal mixing; liquids - regular mixing, selected variables). Solid line represents the 1:1 relation, dashed lines represent ± 20°C.

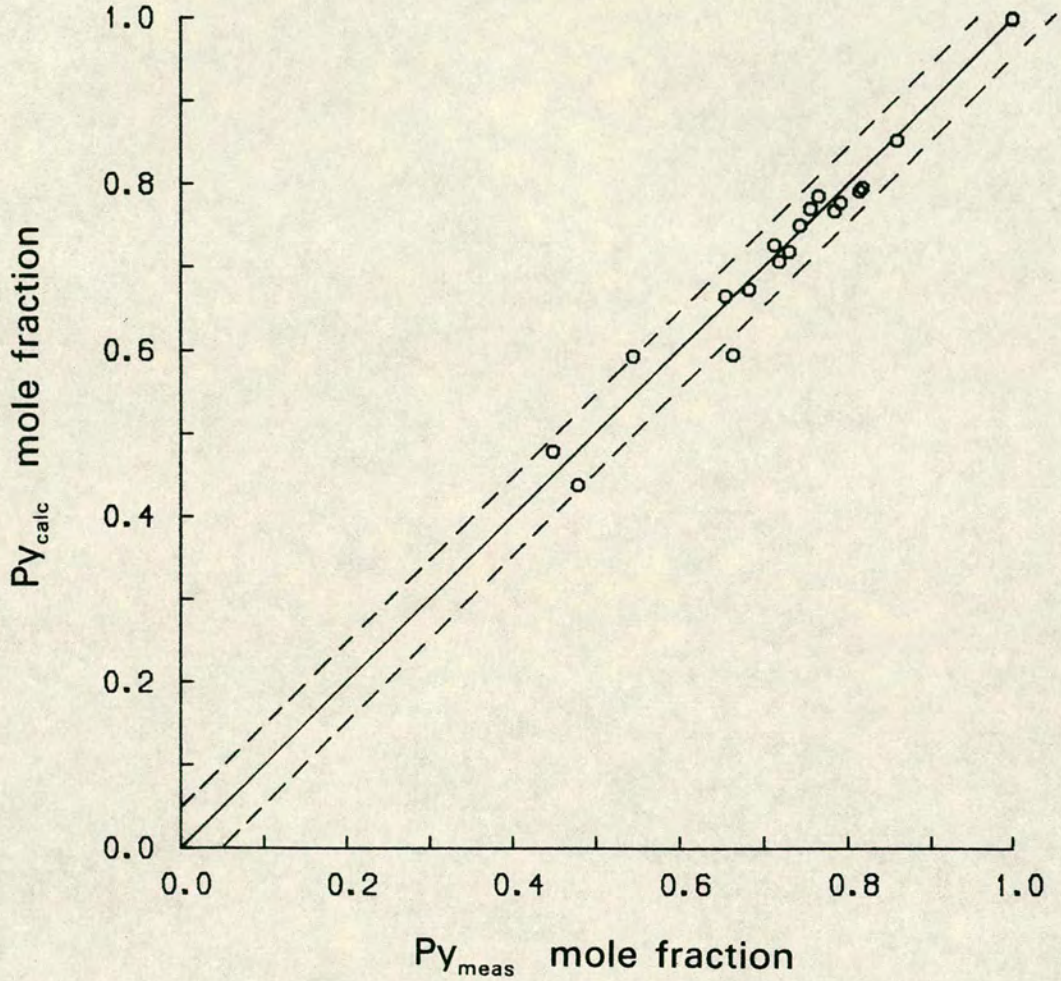

Figure 5–10 : Calculated *vs.* measured pyrope content of garnet. Equations 7, 8 and 9 of Table 4–1 (garnets – ideal mixing; liquids – regular mixing, selected variables). Solid line represents the 1:1 relation, dashed lines represent ± 5 mol%.

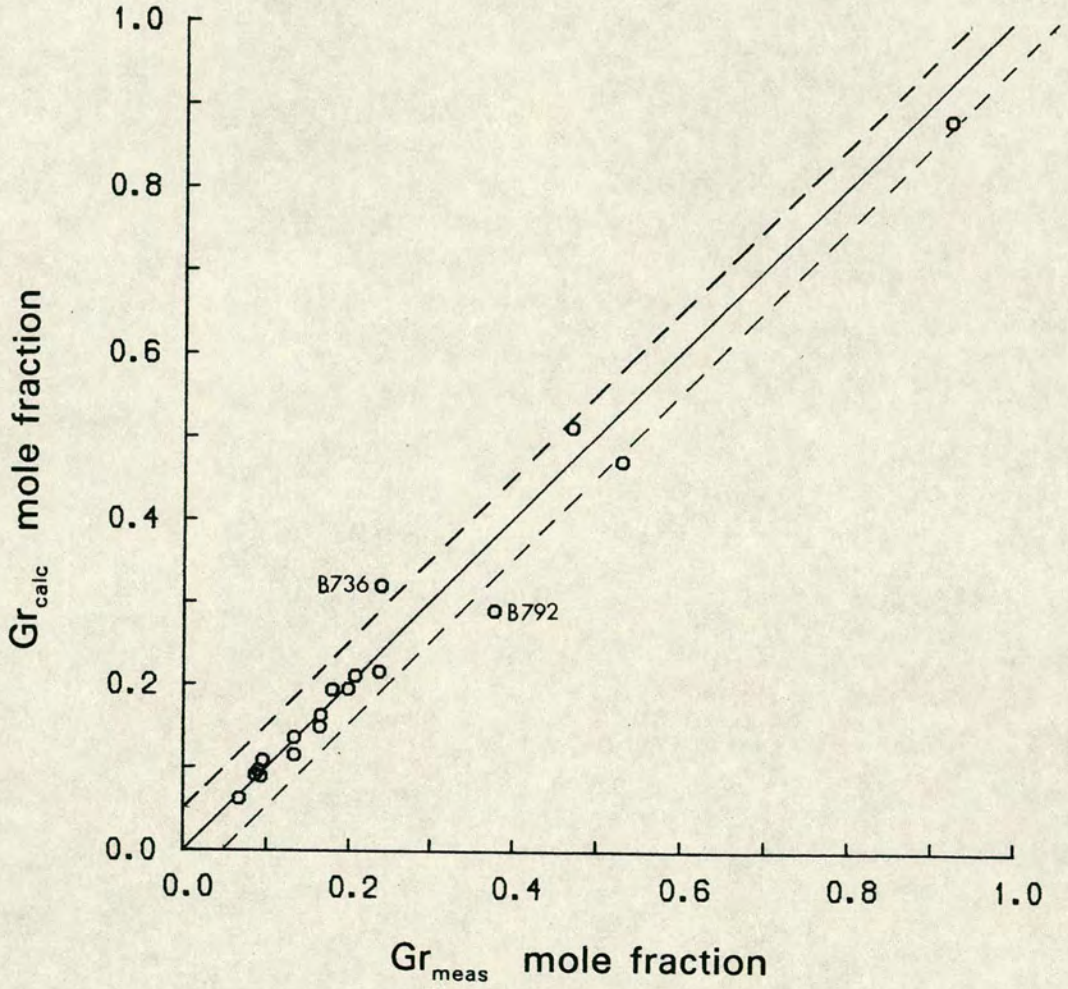

Figure 5–11 : Calculated *vs.* measured grossular content of garnet. Equations 7, 8 and 9 of Table 4–1 (garnets – ideal mixing; liquids – regular mixing, selected variables). Solid line represents the 1:1 relation, dashed lines represent ± 5 mol%.

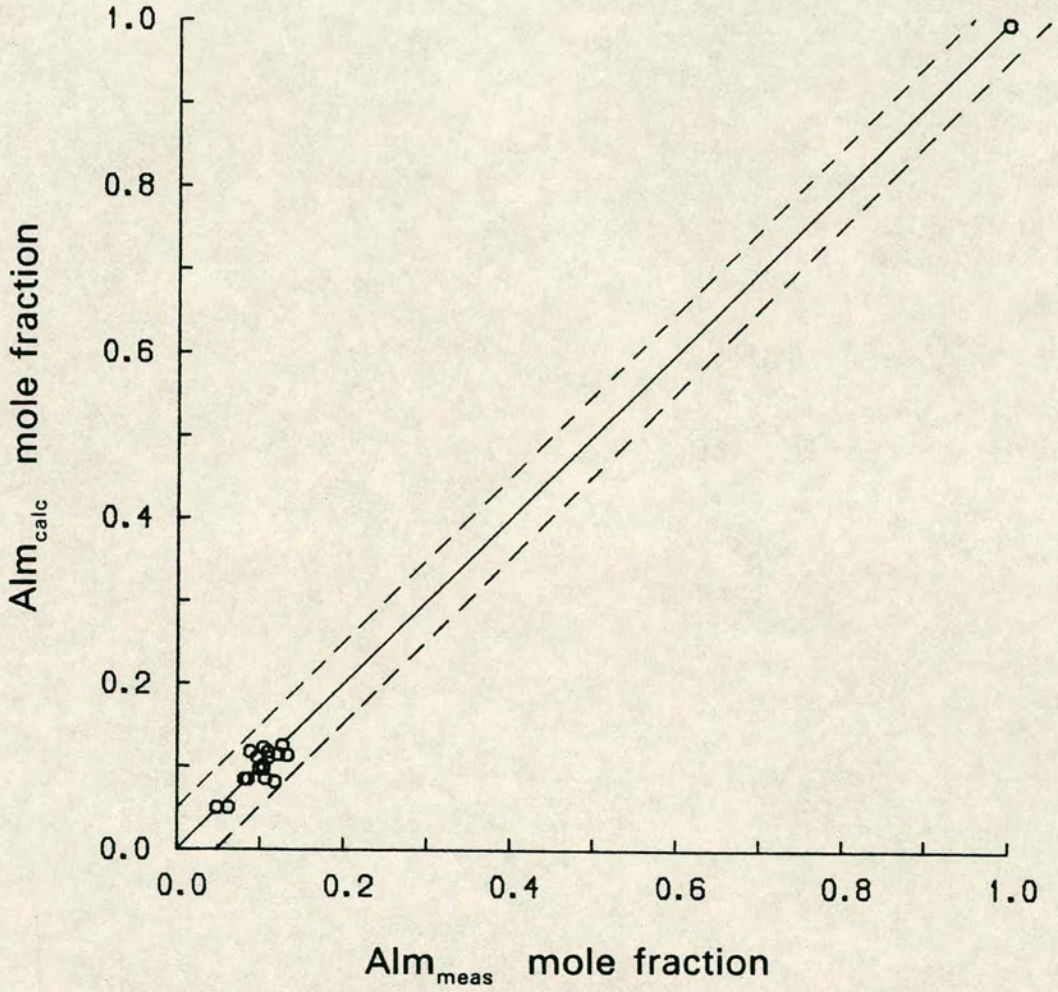

Figure 5–12 : Calculated *vs.* measured almandine content of garnet. Equations 7, 8 and 9 of Table 4–1 (garnets – ideal mixing; liquids – regular mixing, selected variables). Solid line represents the 1:1 relation, dashed lines represent ± 5 mol%.

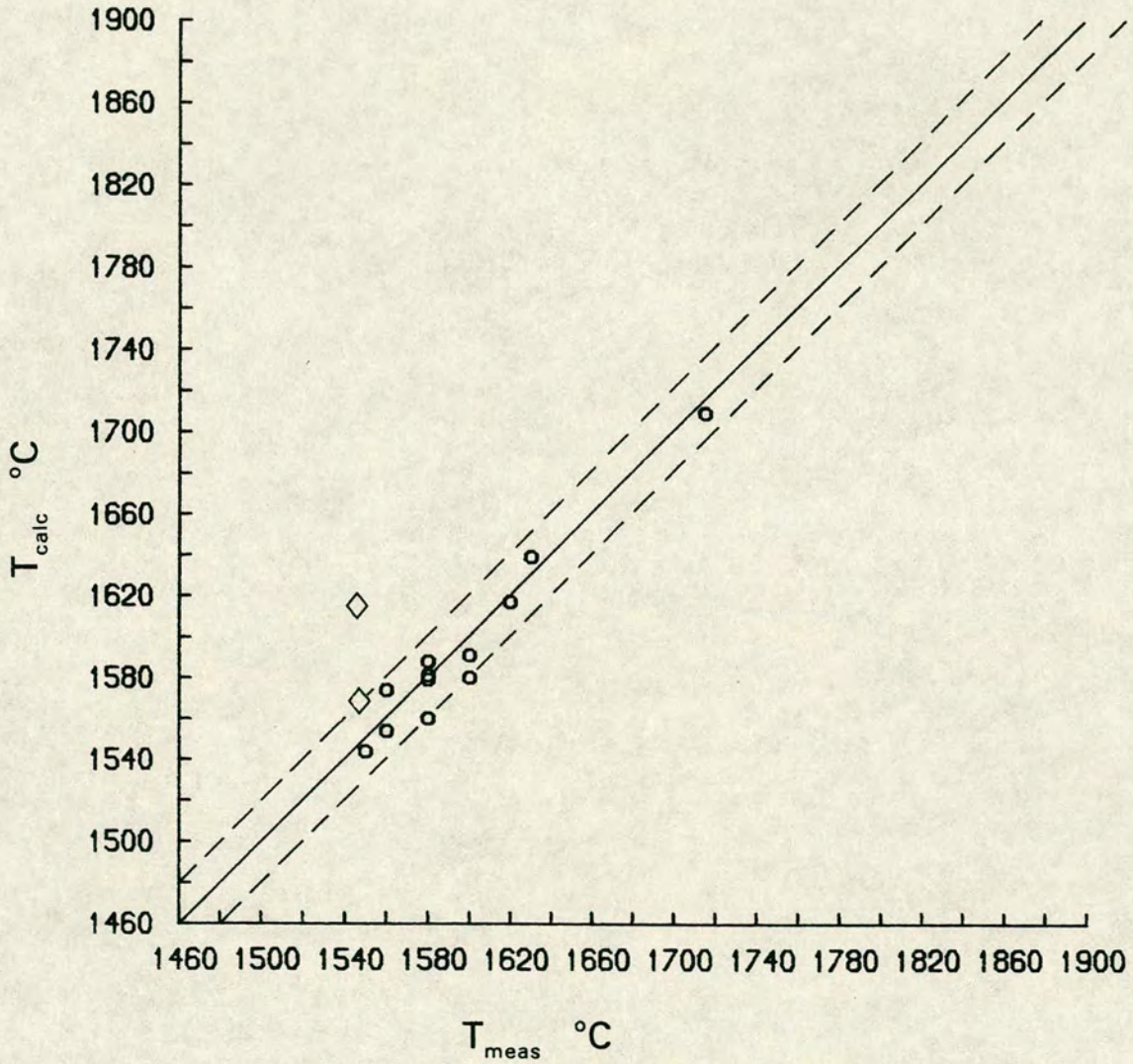

Figure 5–13 : Calculated *vs.* measured temperatures. Equations 10, 11, 12 and 13 of Table 4–1 (clinopyroxenes – ideal mixing; liquids – ideal mixing). Solid line represents the 1:1 relation, dashed lines represent ± 20°C. Diamond symbols represent rejected experiments.

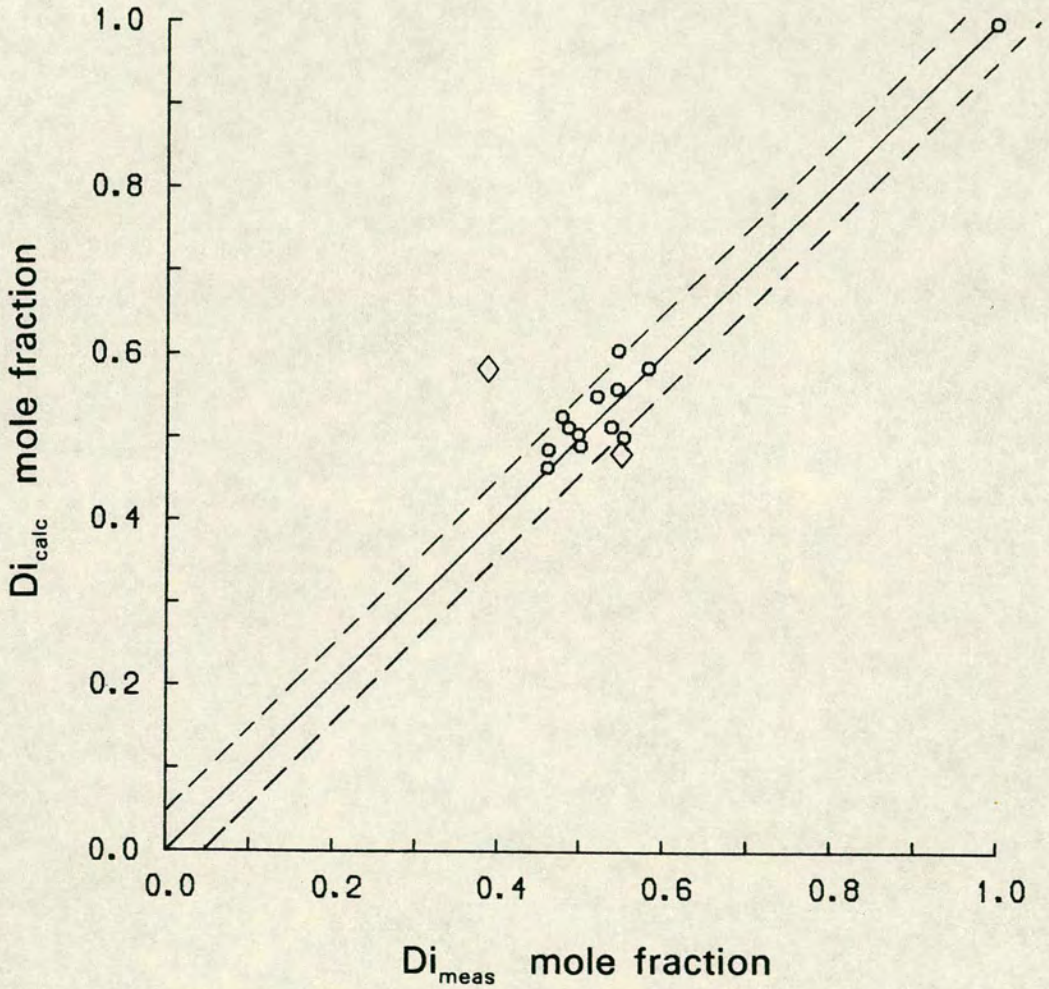

Figure 5–14 : Calculated *vs.* measured diopside content of clinopyroxene. Equations 10, 11, 12 and 13 of Table 4–1 (clinopyroxenes – ideal mixing; liquids – ideal mixing). Solid line represents the 1:1 relation, dashed lines represent ± 20°C. Diamond symbols represent rejected experiments.

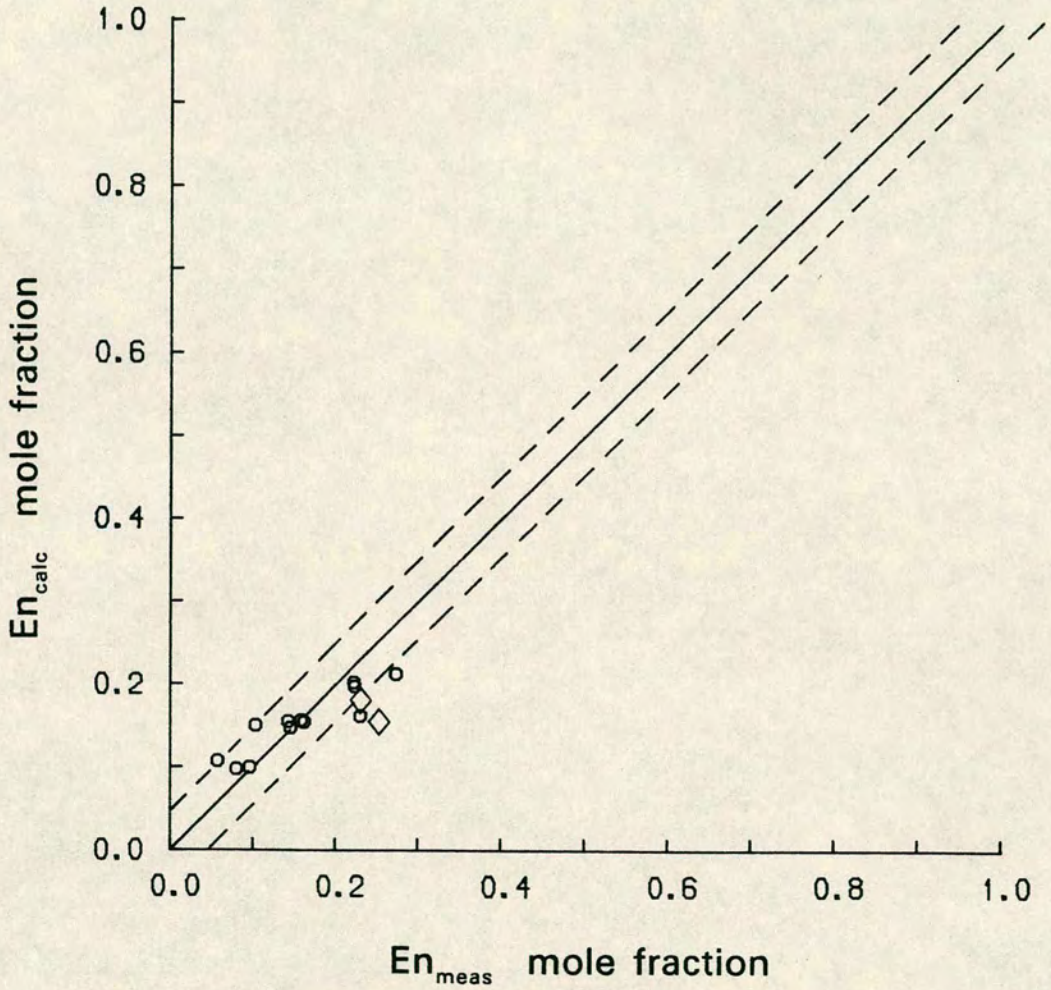

Figure 5–15 : Calculated *vs.* measured enstatite content of clinopyroxene. Equations 10, 11, 12 and 13 of Table 4–1 (clinopyroxenes – ideal mixing; liquids – ideal mixing). Solid line represents the 1:1 relation, dashed lines represent ± 20°C. Diamond symbols represent rejected experiments.

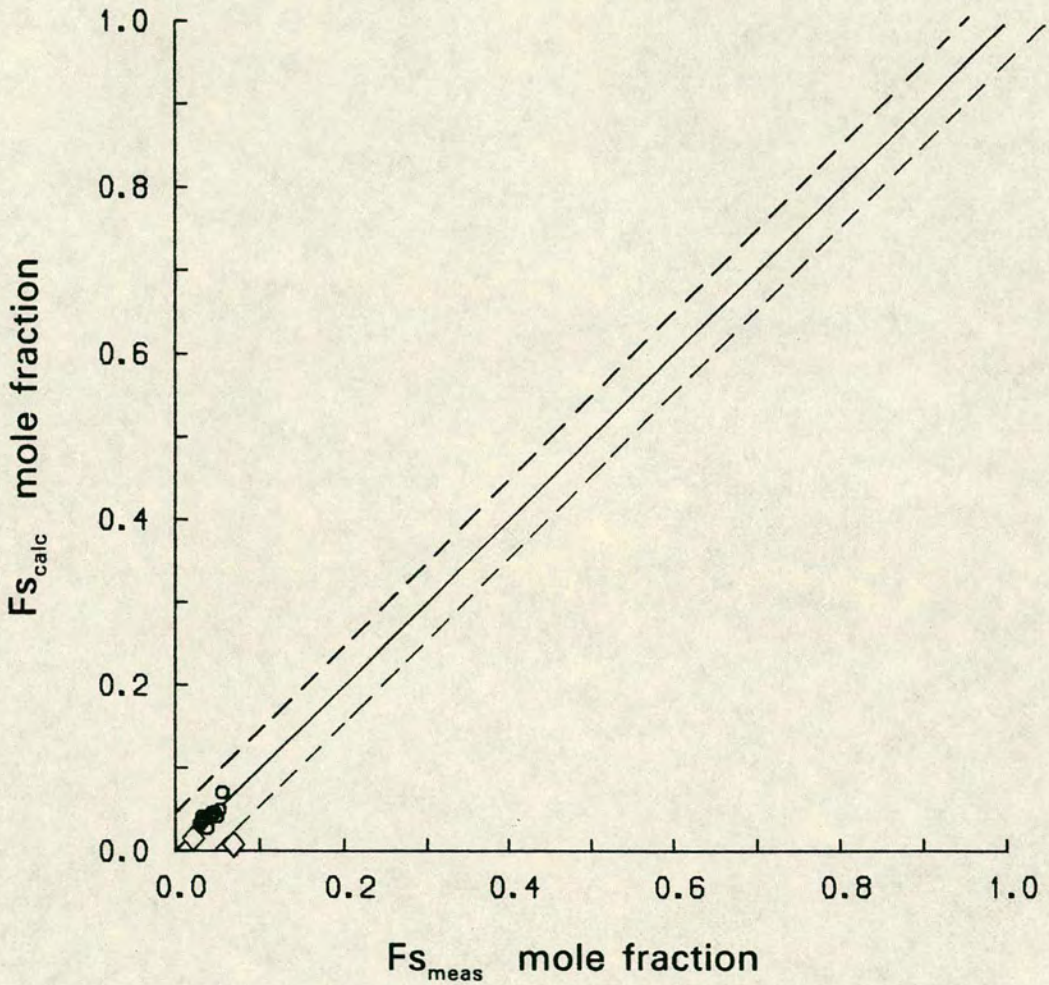

Figure 5–16 : Calculated *vs.* measured ferrosilite content of clinopyroxene. Equations 10, 11, 12 and 13 of Table 4–1 (clinopyroxenes – ideal mixing; liquids – ideal mixing). Solid line represents the 1:1 relation, dashed lines represent ± 20°C. Diamond symbols represent rejected experiments.

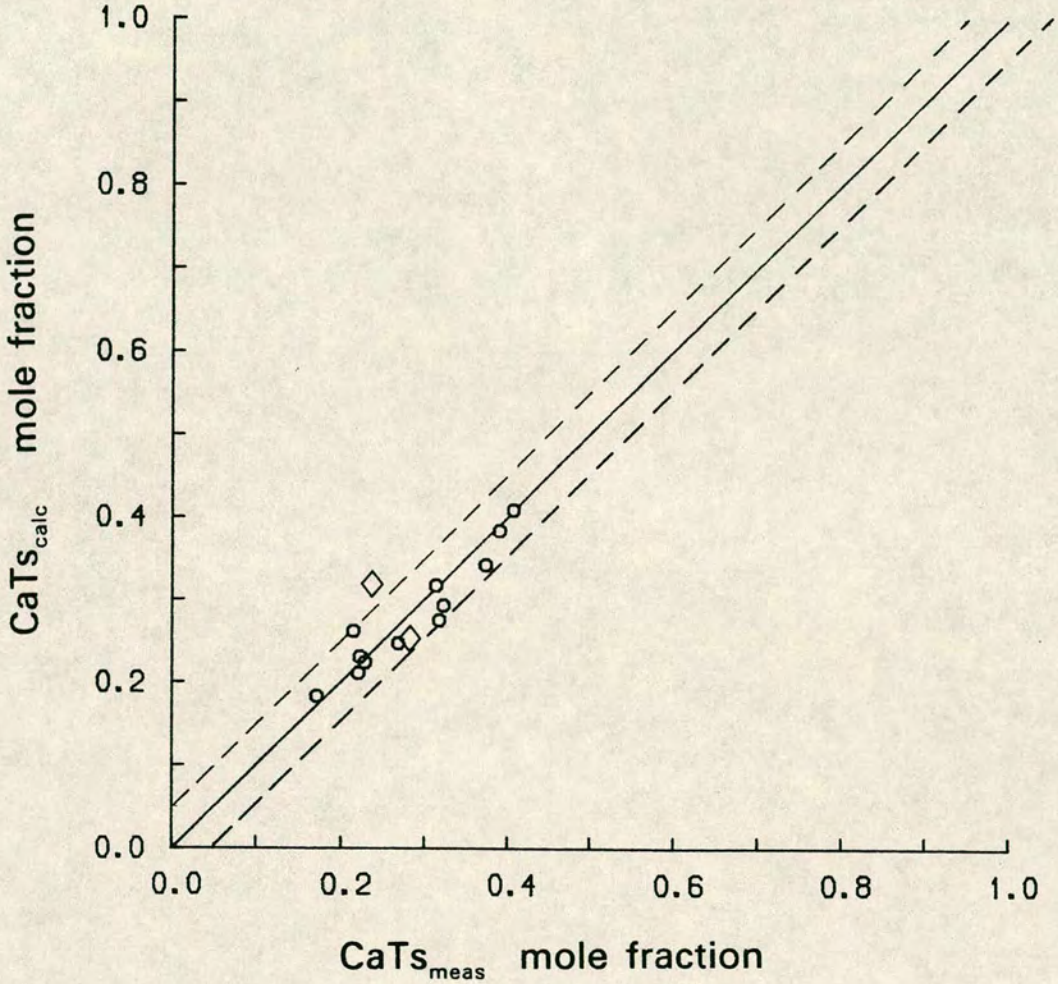

Figure 5–17 : Calculated *vs.* measured Ca-tschermak content of clinopyroxene. Equations 10, 11, 12 and 13 of Table 4-1 (clinopyroxenes – ideal mixing; liquids – ideal mixing). Solid line represents the 1:1 relation, dashed lines represent ± 20°C. Diamond symbols represent rejected experiments.

Table 5-2 : Comparison of calculated temperatures from garnet-liquid and clinopyroxene-liquid equations.

expt.	T_{gt}	T_{cp}	T_{meas}
B739	1560	1591	1600
B740	1561	1588	1580
B736	1575	1581	1580
B768	1569	1574	1560
B727	1580	1560	1580
A364	1566	1554	1560
B781	1583	1579	1580
B792	1609	1617	1620
B784	1586	1580	1600
B809	1641	1639	1630

T_{gt} - temperature calculated by equations 1, 2 and 3 of Table 4-1.
T_{cp} - temperature calculated by equations 10, 11, 12 and 13 of Table 4-1.
T_{meas} - measured temperature of experiment.

5.2.2. Non-ideal solution models

The existence of a minimum on the garnet-clinopyroxene cotectic curve in Figure 3-9 suggests that an ideal mixing model will not be sufficient to describe garnet-liquid and clinopyroxene-liquid equilibria over the whole range of the experiments of this study. Results from mineral-melt equations incorporating regular mixing in the liquid (equations 4 to 9 of Table 4-1) are summarised in Figures 5-5 to 5-12. Agreement between measured and calculated values of temperature and garnet composition are generally good, but there are large discrepancies for experiments B736 and B792. For experiment B768, the mole fractions of garnet components did not sum to 1 for any temperature between 1200°C and 2000°C (the range of temperatures tried). Reasons for this behaviour are discussed in Section 5.6.

5.3. Predicted equilibria for rejected experiments

Calculated and measured temperatures and crystal compsitions for experiments B776, B777, B797 and B811, rejected from the dataset (Section 4.3) are also plotted on Figures 5-1 to 5-4 and 5-13 to 5-17. Discrepancies between their calculated and measured values are generally greater than for the experiments of the dataset, justifying their exclusion and suggesting that they do not represent equilibrium assemblages.

For these four experiments, mineral-melt equations 4 to 9 of Table 4-1 (incorporating regular mixing in the liquid) gave calculated garnet mole fractions that did not sum to 1 for any temperature between 1200°C and 2000°C (the range of temperature tried). Reasons for this behaviour are discussed in Section 5.6.

5.4. Predicted equilibria for literature data

The experimental and analytical problems which have affected many published studies involving high-pressure crystal-liquid equilibria were discussed in Section 1.1.2. Three recent studies have avoided these problems by careful experimental design and have reported compositions of coexisting crystals and liquids in natural systems at high pressures. The five oxides of the system of this study (CaO, MgO, FeO, Al_2O_3, SiO_2) comprise over 96wt% of each phase of each result. The remaining oxides were treated as ideal dilutants - cation fractions were calulated from the full analysis (*e.g.* $X_{Mg} = X_{Mg}/X_{Mg}+X_{Fe}+X_{Ca}+X_{Si}+X_{Al}+X_{Na}+X_{Ti}+$ *etc.*) but no extra terms were added to the mineral-melt equations. Table 5-3 shows the reported measured values of temperature and crystal composition and the calculated values obtained from the mineral-melt equations. Agreement between the measured values and values calculated using equations with the ideal liquid model are fairly good, with the exception of the clinopyroxene composition for Takahashi (1986) experiment #43. The mineral-melt equations incorporating regular mixing in the liquid give poorer results.

5.5. Calculating garnet-liquid equilibria in CS-MS-A

Equilibrium temperatures and coexisting crystal compositions were calculated for a large number of liquid compositions in the plane CS-MS-A to produce partial phase diagrams contoured in temperature and garnet composition.

Figure 5-18 shows part of the plane CS-MS-A, with the experimentally determined phase relations from Figure 3-9. A large number of points in this part of the plane were chosen to form a grid. The iron-magnesium ratio for each of these compositions was set at Mg'=85. Taking each point as a liquid composition, the coexisting garnet composition and equilibrium temperature

Table 5-3 : Comparison of measured (M) and predicted (P) values of temperature (°C) and garnet and clinopyroxene compositions (mole fractions of components) for literature data.

	Py		Gr		Alm		Temp.	
	M	P	M	P	M	P	M	P
garnets – ideal mixing								
liquids – ideal mixing								
E&S#164	0.63	0.71	0.23	0.16	0.19	0.13	1470	1518
T#43	0.84	0.76	0.13	0.15	0.09	0.10	1550	1531
garnets – ideal mixing								
liquids – regular mixing								
all variables retained								
E&S#164	0.63	0.61	0.23	0.03	0.19	0.36	1470	1514
T#43	0.84	0.72	0.13	0.02	0.09	0.25	1550	1436
garnets – ideal mixing								
liquids – regular mixing								
selected variables								
E&S#164	0.63	0.64	0.23	0.03	0.19	0.32	1470	1538
T#43	0.84	0.79	0.13	0.02	0.09	0.21	1550	1475

	Di		En		Fs		CaTs		Temp.	
	M	P	M	P	M	P	M	P	M	P
clinopyroxenes – ideal mixing										
liquids – ideal mixing										
T&K#43	0.43	0.45	0.30	0.34	0.11	0.03	0.17	0.17	1400	1480
E&S#309	0.17	0.23	0.59	0.49	0.12	0.04	0.13	0.24	1375	1428
E&S#164	0.48	0.50	0.27	0.32	0.09	0.04	0.16	0.14	1470	1521
T#43	0.23	0.53	0.57	0.25	0.07	0.03	0.13	0.18	1550	1572

T&K#43 - Takahashi & Kushiro (1983) experiment no. 43
20kb, 1375°C, liq+ol+op+cp

E&S#309 - Elthon & Scarfe (1984) experiment no. 309
20kb, 1400°C, liq+ol+op+cp

E&S#164 - Elthon & Scarfe (1984) experiment no. 164
25kb, 1470°C, liq+ol+op+cp+gt

T#43 - Takahashi (1986) experiment no. 43
30kb, 1550°C, liq+ol+op+cp+gt

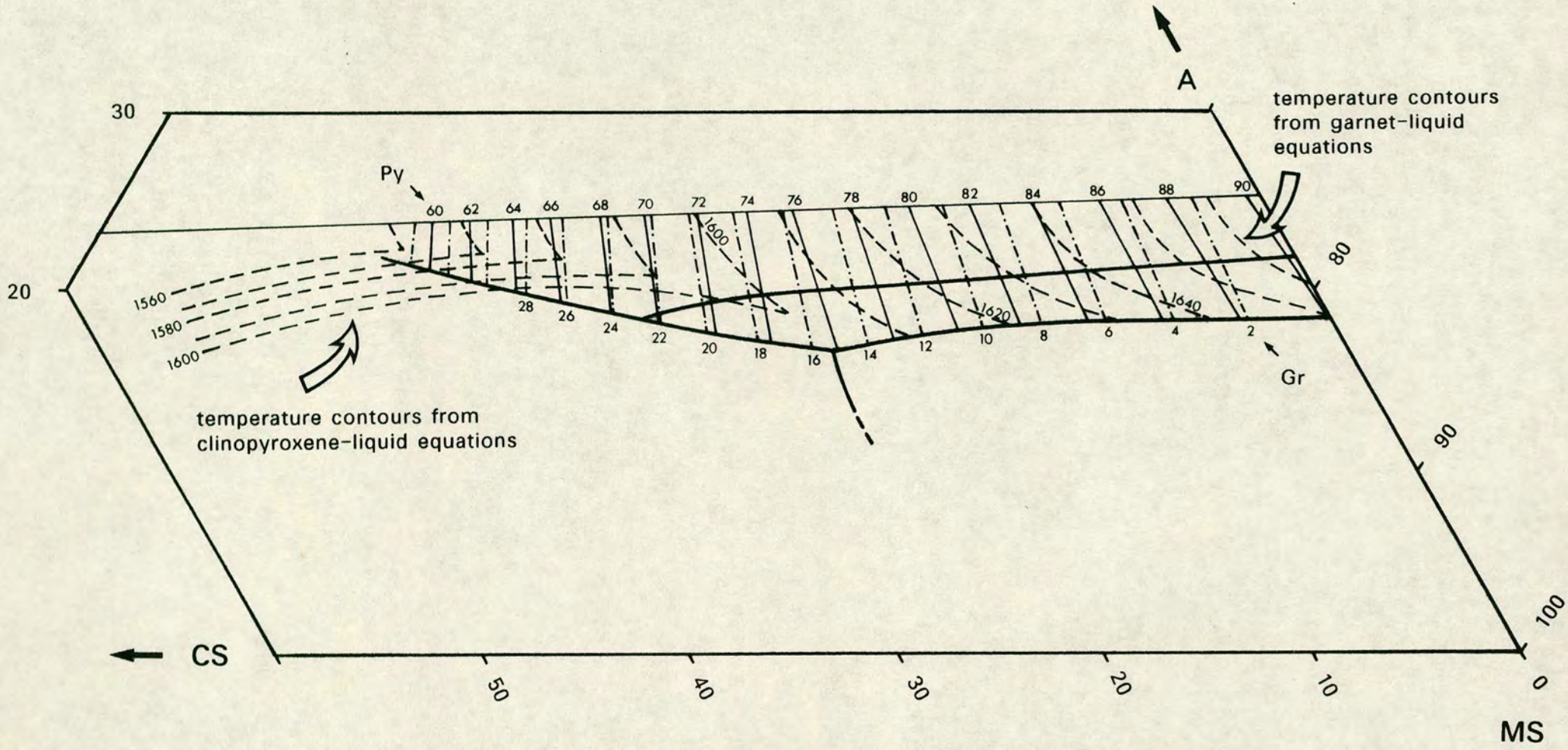

Figure 5-18 : Diagram of part of the plane CS-MS-A. Heavy lines are 30kb phase relations for in-plane starting compositions (see Figure 3-9). Temperature contours (°C) are calculated from both garnet-liquid and clinopyroxene-liquid equations (see text). The intersections of the two sets of temperature contours define the predicted position of the garnet-clinopyroxene cotectic. Note that the contours apply to liquids with Mg'=85 (see text), whereas the experimental liquids have Mg'=72-84 (Table 3-2). Composition contours of pyrope (Py, unbroken line) and grossular (Gr, broken line) wt% in garnet enable the composition of the garnet in equilibrium with any liquid to be determined. (The almandine content of any garnet is (100-Py-Gr) wt%).

were calculated using mineral-melt equations 1, 2 and 3 of Table 4-1 (taking the pressure to be 30kb). Mineral-melt equations 10, 11, 12 and 13 were used to obtain the coexisting clinopyroxene composition and equilibrium temperature for each point. Figure 5-18 was then contoured for temperature and garnet composition. Intersections between temperature contours produced by the garnet-liquid and the clinopyroxene-liquid equations define the predicted position of the garnet-clinopyroxene cotectic.

As noted in Section 5-2, mineral-melt equations using an ideal mixing model for the liquid cannot reproduce the temperature minimum observed in the experimental data. Accordingly, an attempt was made to repeat the contouring exercise with temperature and composition values calculated from the mineral-melt equations incorporating the regular mixing model. This was not possible because calculated values from mineral-melt equations 4 to 9 (Table 4-1) were not meaningful. Some adjacent liquid points had calculated temperatures several hundred degrees different, and for many of the liquid composition points, the mole fractions of the garnet components did not sum to 1 for any temperature between 1200°C and 2000°C (the range of temperatures tried). Reasons for this behaviour are discussed in Section 5.6.

For any liquid in equilibrium with garnet in Figure 5-18, the composition of the garnet and the temperature of the equilibrium can be read from the contours. Further diagrams could be generated for liquids with different Mg' values. In Figure 5-18, predicted temperatures and garnet compositions for liquids more calcic than the reaction point R, are of poorer quality to those for liquids elsewhere in the figure. This is because the non-ideal behaviour which results in a minimum on the garnet-clinopyroxene cotectic is not accounted for by the mineral-melt equations used to generate the figure.

Figure 5-19 shows a similar diagram, contoured with calculated temperature and garnet composition values for part of the system $CaSiO_3$-$MgSiO_3$-Al_2O_3. The experimentally determined phase relations of Maaløe & Wyllie (1979) for this system are also shown. Agreement between the calculated position of the garnet-clinopyroxene cotectic and the experimentally determined position is good. The temperatures and garnet compositions predicted for liquids lying on the pyrope-grossular join can be compared to the experimental results of Maaløe & Wyllie (1979). Comparisons for three bulk compositions are: (compositions in wt%)

bulk comp.	Py_{70}		Py_{80}		Py_{90}	
Maaløe & Wyllie	1625°C	Py_{79}	1670°C	Py_{87}	1690°C	Py_{94}
predicted	1615°C	Py_{74}	1640°C	Py_{87}	1670°C	Py_{94}

Agreement between predicted and experimentally determined values is good. In addition, Maaløe and Wyllie (1979) reported that, at 30kb, pure pyrope melted incongruently to spinel + liquid at 1705°C. Neither Figure 5-18 nor Figure 5-19 includes calculated temperatures or compositions for spinel equilibria because no mineral-melt equations were formulated for this phase due to insufficient data (in this respect it should be noted that these figures are not liquidus diagrams). However, the predicted values for a pure pyrope liquid are that it would be in equilibrium with a pure pyrope garnet at a temperature of 1694°C - a result in good agreement with the known incongruent melting point.

5.6. Numerical instability in mineral-melt equations with a regular mixing liquid

In Section 5.2, mineral-melt equations 4 to 9 (Table 4-1), which incorporate a regular mixing model for the liquid, gave calculated temperature and garnet composition values in good agreement with measured values for most of the experiments of the dataset. For a few experiments however, these equations

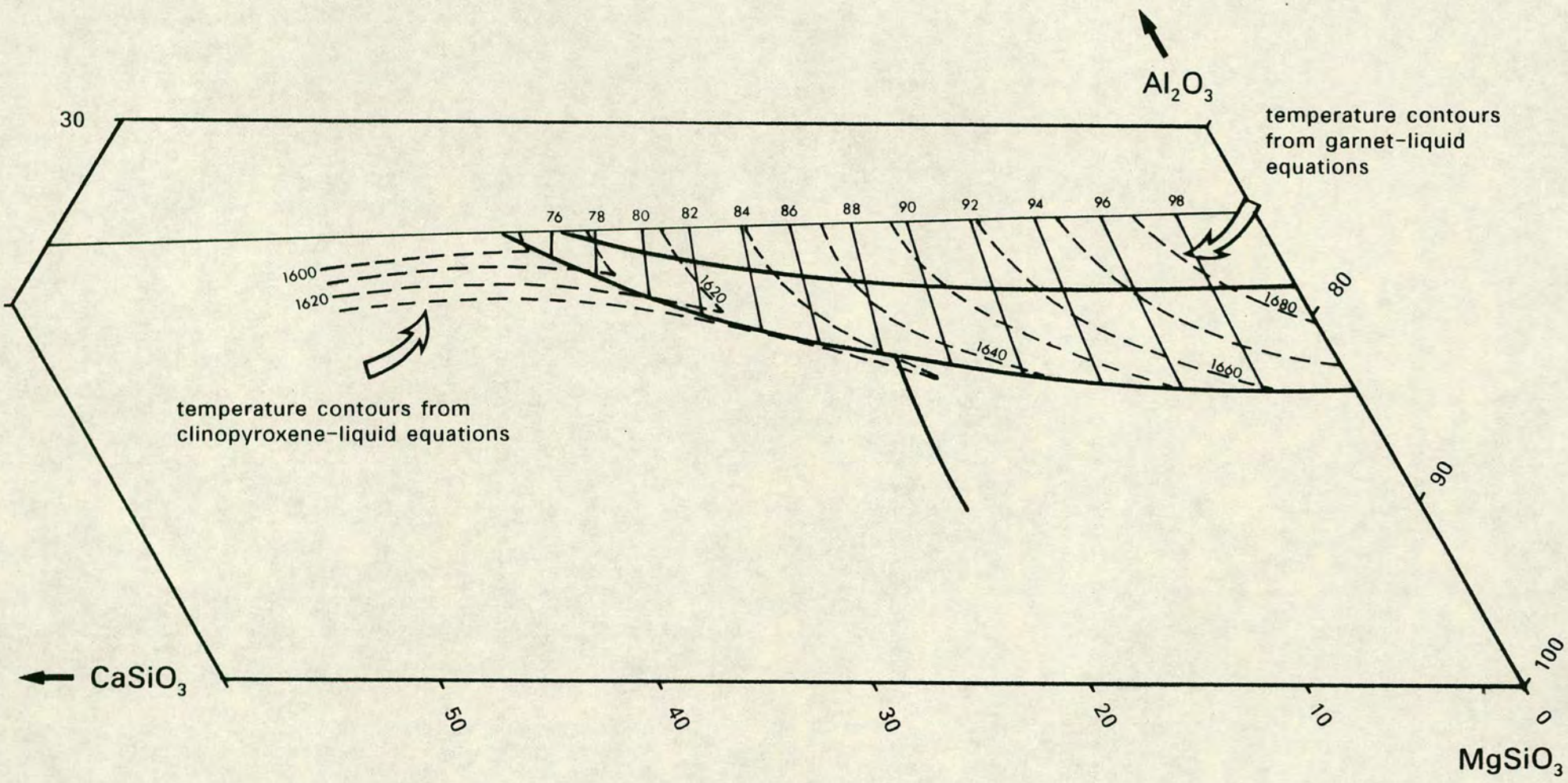

Figure 5-19 : Diagram of part of the system $CaSiO_3$-$MgSiO_3$-Al_2O_3 Heavy lines are 30kb phase relations (see Figure 2-2) from Maaløe & Wyllie (1979). Temperature contours (°C) are calculated by both garnet-liquid and clinopyroxene-liquid equations. The intersections of the two sets of temperature contours define the predicted position of the garnet-clinopyroxene cotectic. Composition contours are of wt% pyrope component in the garnet and since all garnets in this system are pyrope-grossular solid solutions, the grossular content is (100-Py)wt%.

gave calculated values with large discrepancies from the measured values. Sections 5.3 and 5.4 involved using the equations to predict values for data points not included in the original dataset to which the equations were fitted. Results from mineral–melt equations 4 to 9 were extremely poor, with often no temperature being found for which the mole fractions of the garnet components summed to 1. This behaviour may be due to multicollinearity – the existence of linear relationships between the nominally independant variables of the multiple regression model.

In equation 4–8 of Section 4.1, each C_r is a partial regression coefficient representing a binary interaction parameter (*e.g.* W_{SiAl}). Associated with each C_r is an X_r, a composite compositional variable calculated according to the expression in equation 4–9 in Section 4.2.3. Each X_r involves the cation fractions of the species of the associated interaction parameter. For example, to express the activity coefficient of the pyrope mineral end–member component, the compositional variable associated with the partial regression coefficient representing W_{SiAl} is $2X_{Si}+3X_{Al}-8X_{Si}X_{Al}$. Thus two binary interaction parameters with a common species (*e.g.* W_{SiAl} and W_{SiMg}) will be associated with compositional terms which are interrelated (*e.g.* $2X_{Si}+3X_{Al}-8X_{Si}X_{Al}$ and $2X_{Si}+3X_{Mg}-8X_{Si}X_{Al}$ for W_{SiAl} and W_{SiMg}). The nominally independent compositional variables are interrelated because a change in, say, X_{Si}, produces a change in the values of both variables.

It is clear that multicollinearity is a problem with mineral–melt equations incorporating a regular mixing model for the liquid because the compositional terms of the regular mixing model are interrelated. In multiple linear regression, a partial regression coefficient shows the change in the dependent variable associated with a unit change in the corresponding independent variable, all other variables remaining constant. If the independent variables

are interrelated, it is impossible for one to vary while the others remain at constant levels. Freund & Minton (1979) suggest that this dilemma is reflected by partial regression coefficients having large variances if multicollinearity is present. The large standard errors of the partial regression coefficients of mineral–melt equations 4 to 9 in Table 4–1 agree with this.

One way to avoid the multicollinearity problem is to avoid interrelated variables. This is not possible in this case because of the form of the regular solution model. Under these circumstances, data fitting procedures other than simple least–squares fitting may give better results. Ghiorso *et al.* (1983) used a method of least–squares fitting which allowed for uncertainties in the data and computed both the partial regression coefficients and their linear dependence on each other. Berman & Brown (1984) and Berman *et al.* (1986) have rejected multiple linear regression in favour of linear programming. This technique also incorporates uncertainties in the experimental conditions and analysed compositions. Neither of these approaches was attempted in this study because of a lack of the necessary mathematical expertise.

If the multicollinearity problem was overcome by the use of an appropriate mathematical technique, there would remain the problem of how well the true mixing surface was described by the regular mixing model. If the regular mixing model was insufficient to describe mixing in the liquid phase, then the mineral–melt equations incorporating that model would still perform poorly in prediction (*i.e.* interpolation and extrapolation). Alternatively, if the regular mixing model were sufficient to describe mixing in the experimental liquids, the mineral–melt equations might perform well at interpolation, but rapidly break down if used to extrapolate beyond the experimental dataset. Without eliminating the multicollinearity problem, it is not possible to comment further on how appropriate or useful the regular mixing model is.

5.7. Correlation of distribution coefficients with temperature

Mineral–melt equations 1 to 3 (garnets – ideal mixing; liquids – ideal mixing) and 10 to 13 of Table 4–1 (clinopyroxenes – ideal mixing; liquids – ideal mixing) have been used to predict the relationships between the mineral end-member component partition coefficients (*e.g.* X^{gt}_{Py}/X^{liq}_{Py}) and temperature and pressure. Results are shown in Figures 5–20 to 5–26. Experimental and pure end-member mineral data are also plotted. The general agreement between predicted and measured values is good, the exceptions being those experiments, discussed in Section 5.2, for which the ideal liquid model is insufficient.

Figures 5–20 to 5–26 show that, as temperature increases, X_i^{xtal}/X_i^{liq} decreases for Py, Gr, Alm, Di, En and Fs, but the opposite behaviour is shown by CaTs.

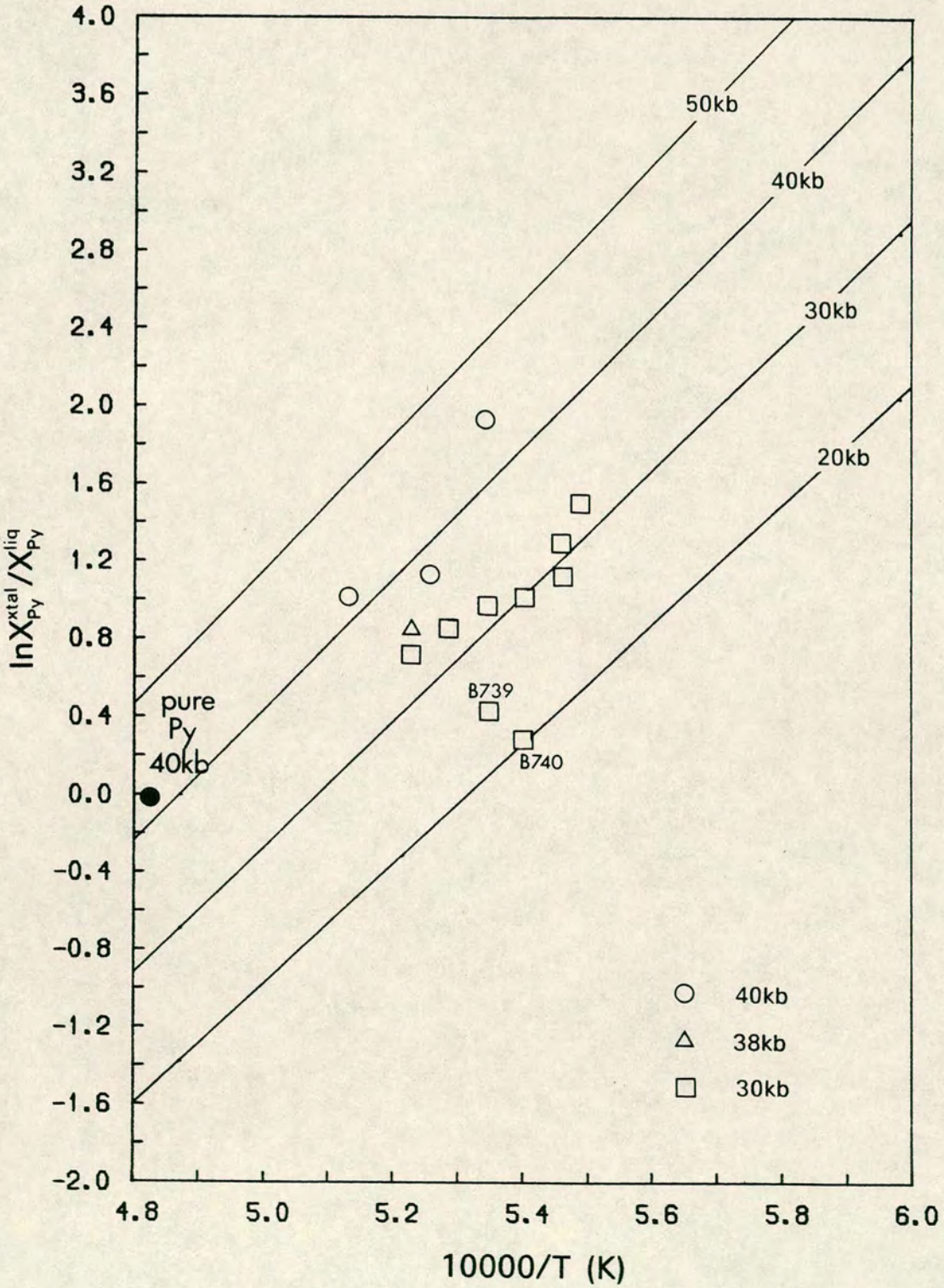

Figure 5-20 : Relationship of $\ln K_{Py}$ to 1/T for four pressures, predicted by equations 1, 2 and 3 of Table 4-1 (garnets - ideal mixing; liquids - ideal mixing). Values from experimental data are plotted as symbols.

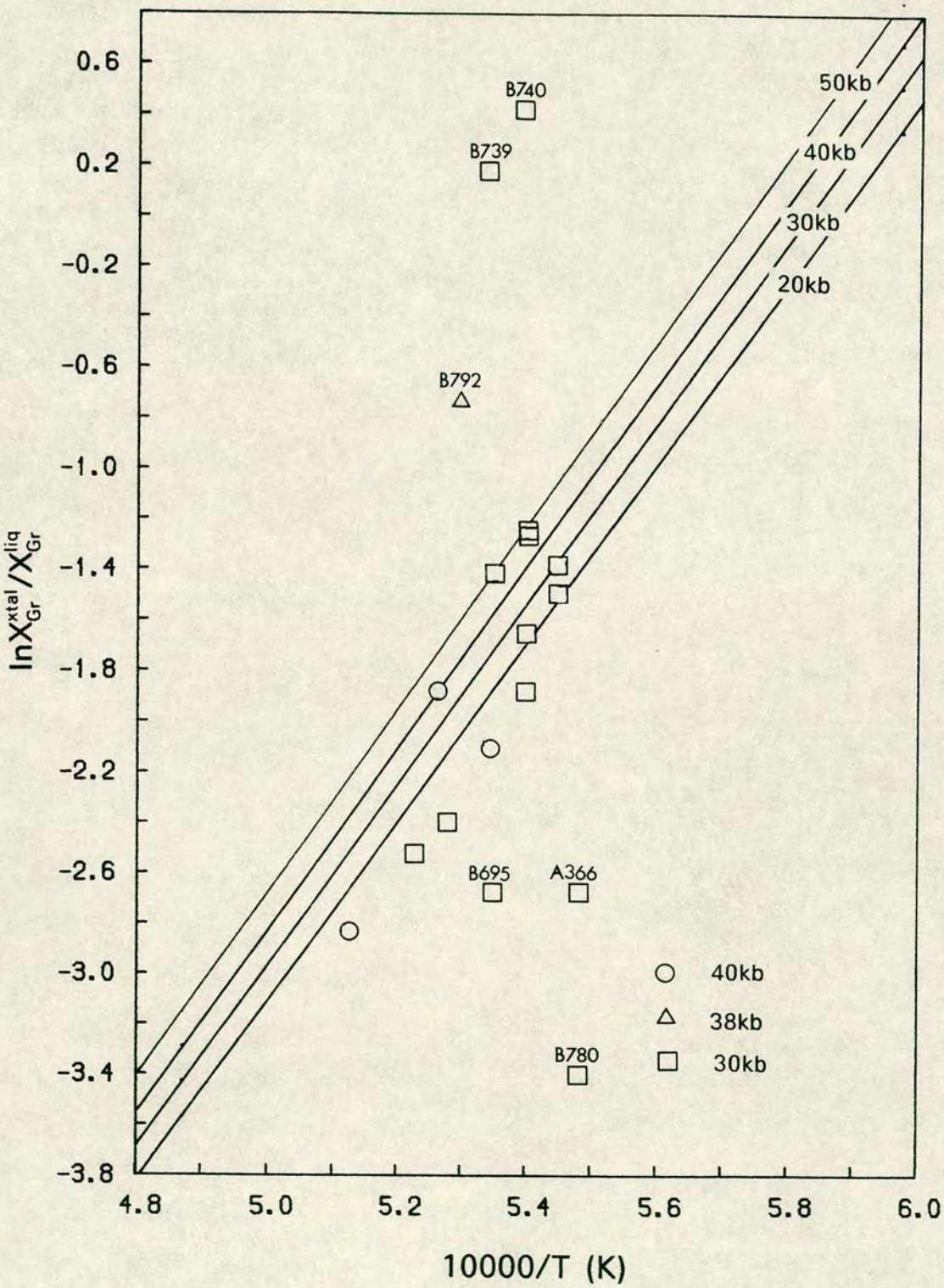

Figure 5-21 : Relationship of $\ln K_{Gr}$ to 1/T for four pressures, predicted by equations 1, 2 and 3 of Table 4-1 (garnets - ideal mixing; liquids - ideal mixing). Values from experimental data are plotted as symbols.

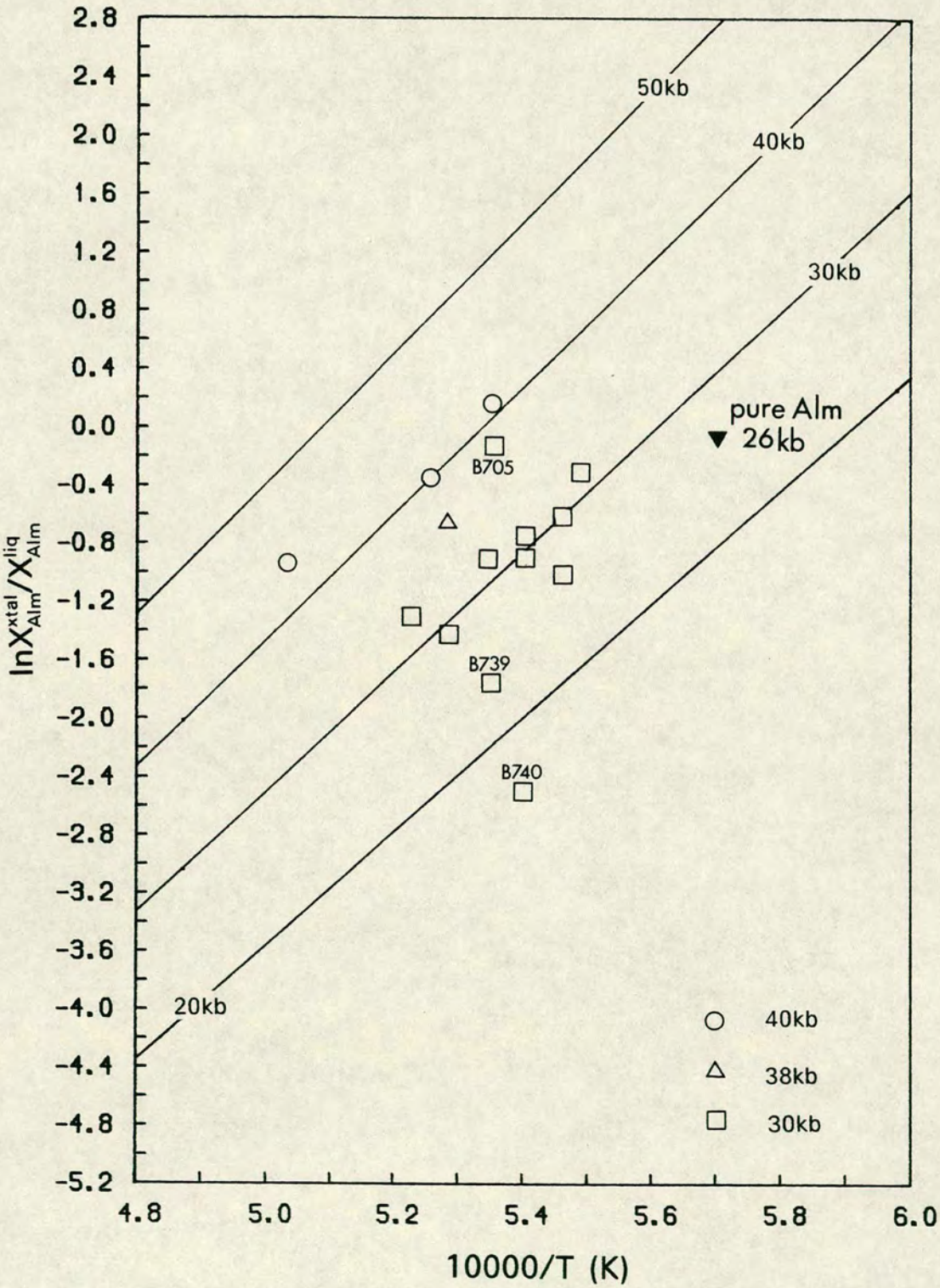

Figure 5–22 : Relationship of $\ln K_{Alm}$ to 1/T for four pressures, predicted by equations 1, 2 and 3 of Table 4–1 (garnets – ideal mixing; liquids – ideal mixing). Values from experimental data are plotted as symbols.

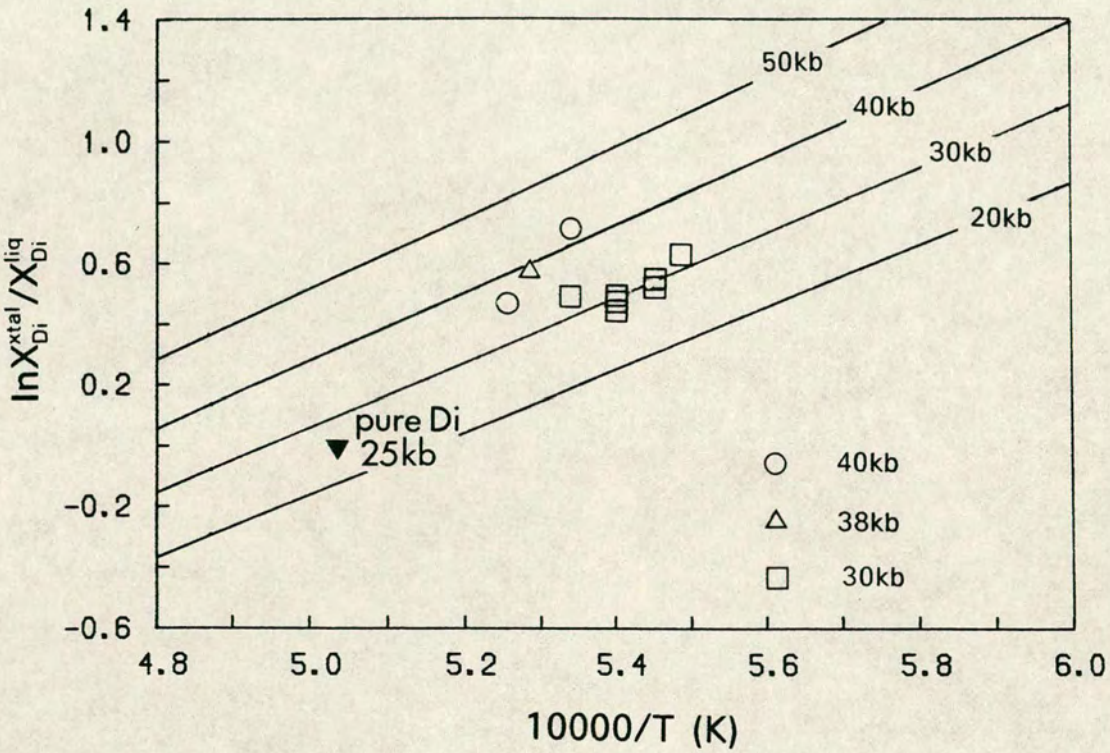

Figure 5-23 : Relationship of $\ln K_{Di}$ to 1/T for four pressures, predicted by equations 10, 11, 12 and 13 of Table 4-1 (clinopyroxenes - ideal mixing; liquids - ideal mixing). Values from experimental data are plotted as symbols.

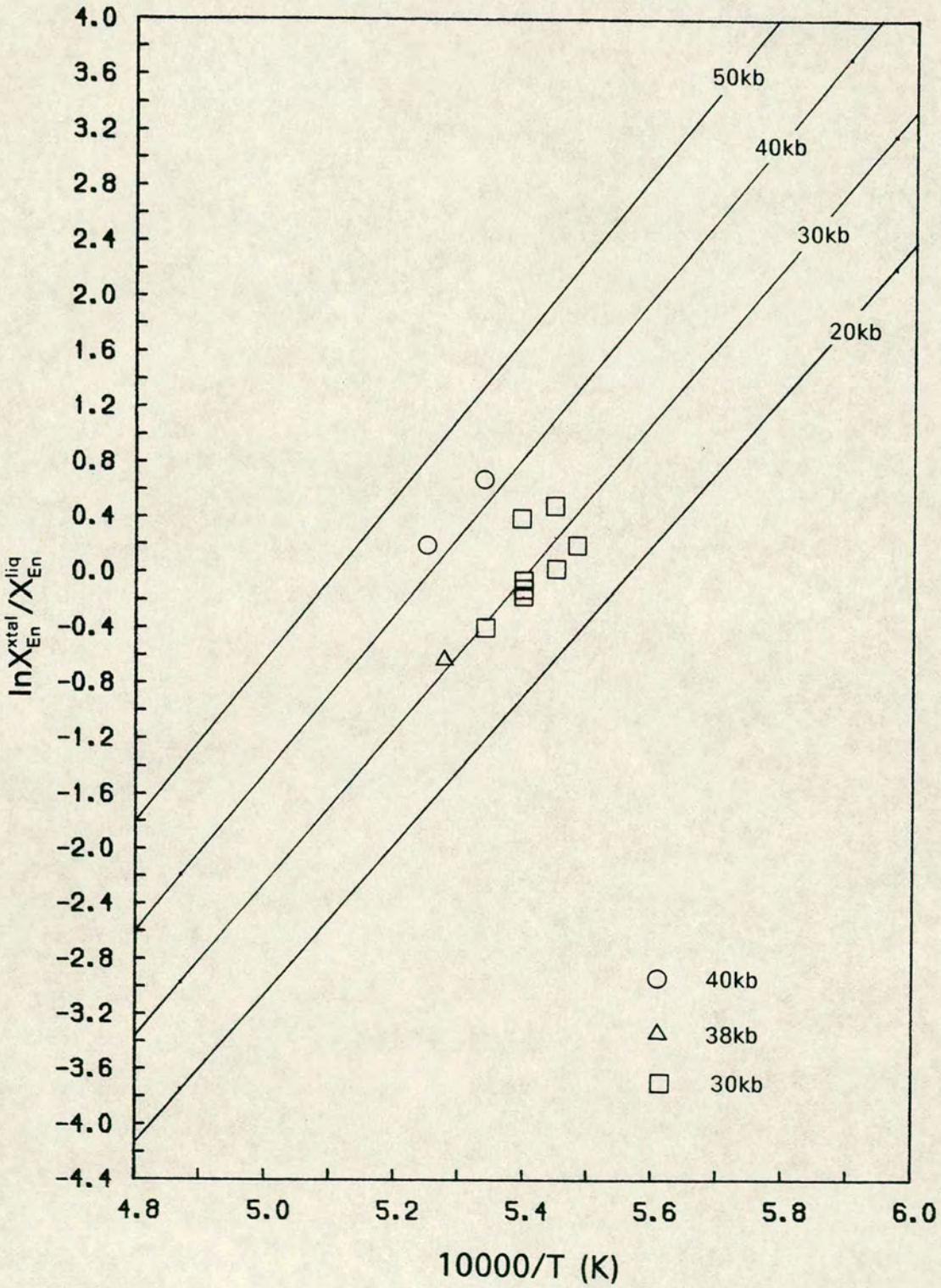

Figure 5-24 : Relationship of $\ln K_{En}$ to 1/T for four pressures, predicted by equations 10, 11, 12 and 13 of Table 4-1 (clinopyroxenes - ideal mixing; liquids - ideal mixing). Values from experimental data are plotted as symbols.

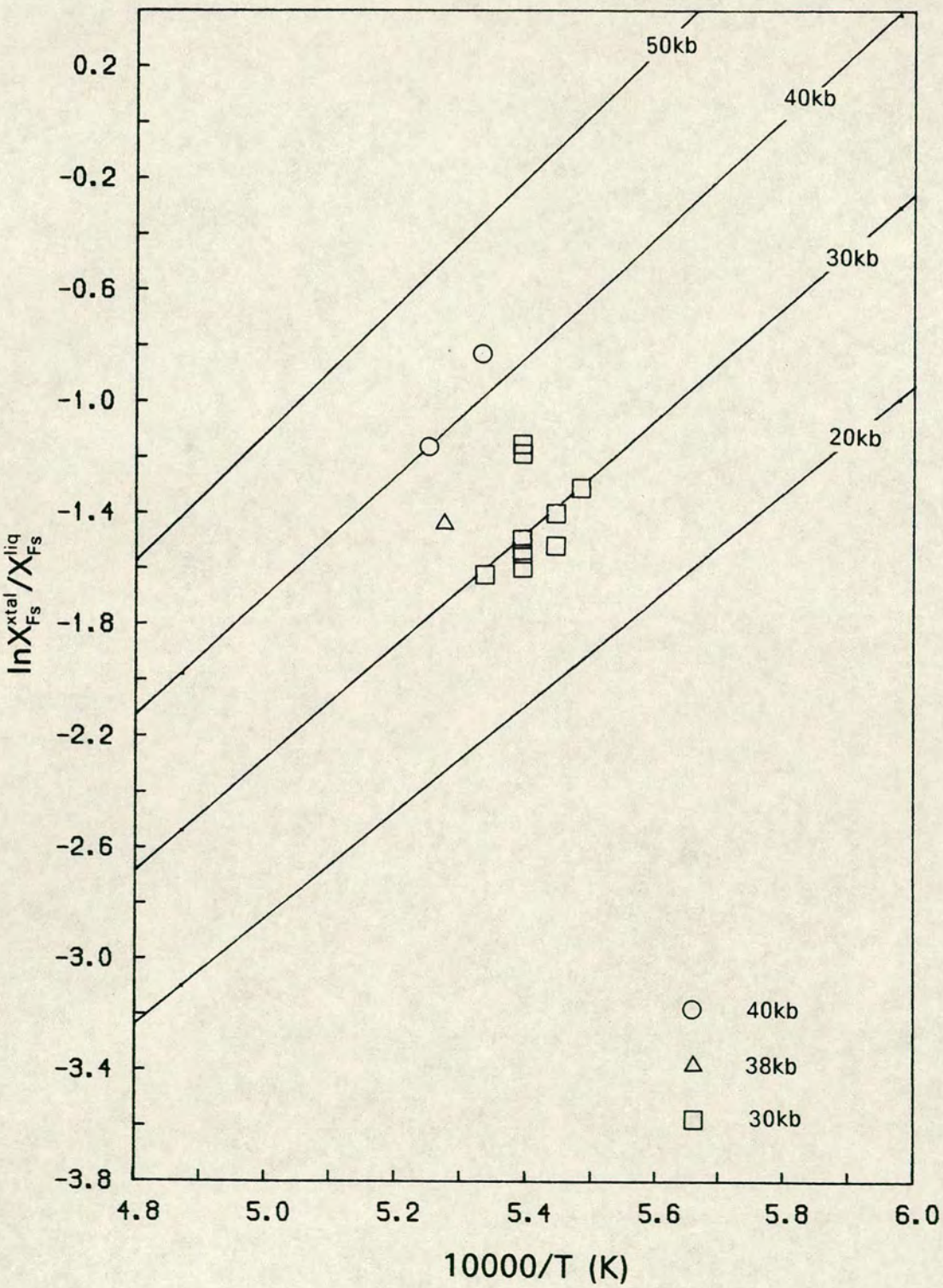

Figure 5-25 : Relationship of $\ln K_{Fs}$ to 1/T for four pressures, predicted by equations 10, 11, 12 and 13 of Table 4-1 (clinopyroxenes - ideal mixing; liquids - ideal mixing). Values from experimental data are plotted as symbols.

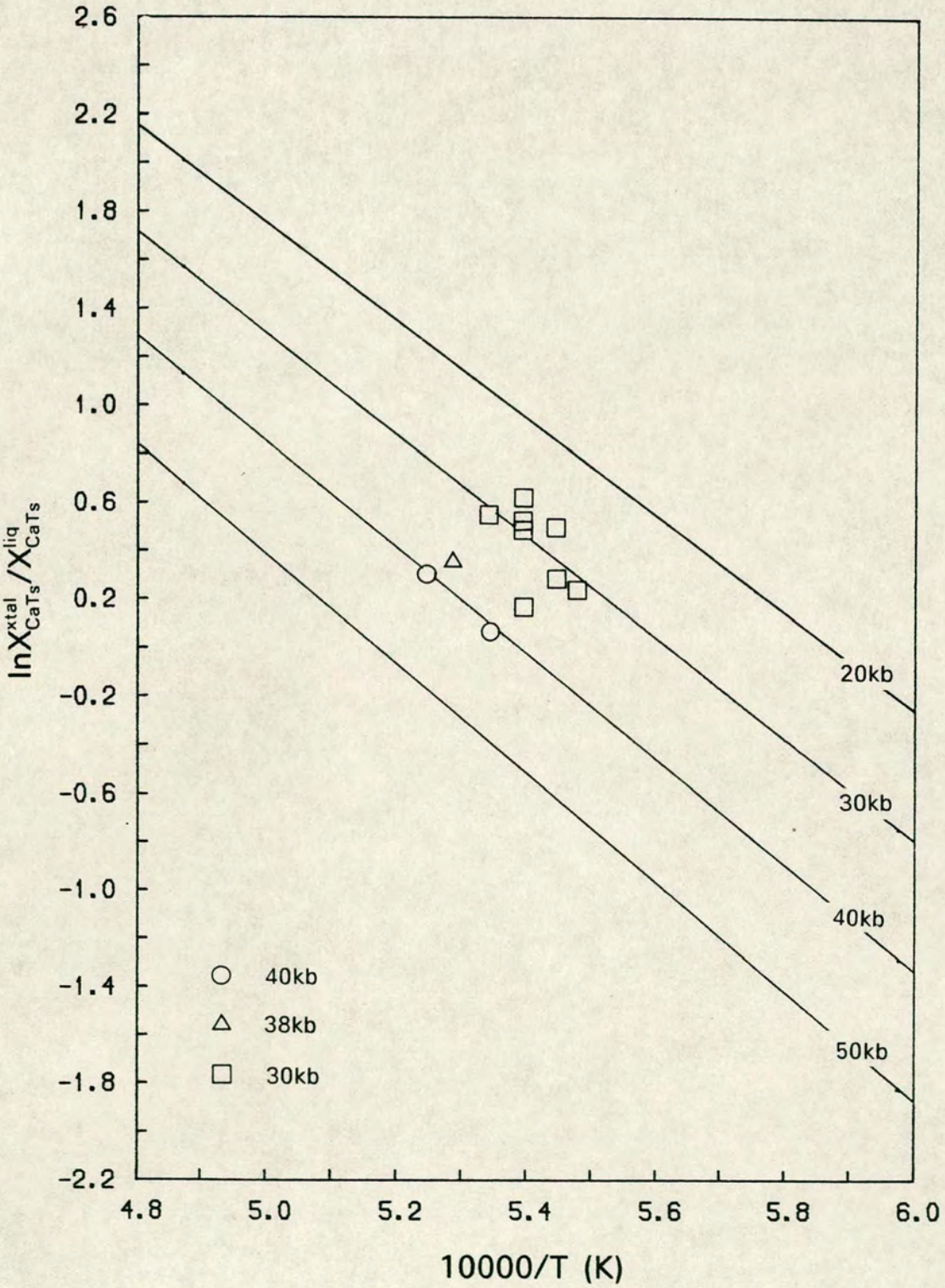

Figure 5-26 : Relationship of $\ln K_{CaTs}$ to 1/T for four pressures, predicted by equations 10, 11, 12 and 13 of Table 4-1 (clinopyroxenes - ideal mixing; liquids - ideal mixing). Values from experimental data are plotted as symbols.

CHAPTER 6

CONCLUSIONS

This study shows that the description and modelling of crystal–liquid equilibria by thermodynamically based relationships derived by fitting equations to an experimental dataset, already applied at low to moderate pressure (Ford *et al.*, 1983; Ghiorso *et al.*, 1983; Berman & Brown, 1984) can be extended to higher pressures.

6.1. Experiments

The use of graphite capsules and the choice of starting materials to yield a large liquid fraction enabled the experimental problems of iron–loss and melt–modification by quench crystallisation to be avoided. Quench crystals were seen in all experiments, but they were shown to grow iso–chemically and to have no effect on the composition of the remaining glass. The habit and extent of quench crystallisation was the same in 30kb and 40kb experiments. In some experiments all the liquid was preserved as quench crystals and analyses were taken using a rastered microprobe beam. Experiments were conducted on 12 different starting compositions to yield a range of compositions of coexisting crystals and liquids.

6.2. Mineral–melt equations

Garnet–liquid and clinopyroxene–liquid equations were derived which expressed the distribution coefficents of mineral end–member components between crystal and liquid phases as functions of temperature, pressure and liquid composition using an ideal mixing liquid model and a regular mixing liquid model. Garnet and clinopyroxene solid solutions were treated as ideal. The mineral–melt equations were each written in the form of a multiple linear regression model and were fitted to the experimental dataset by the method of

least squares.

For any liquid in equilibrium with garnet and/or clinopyroxene it is possible to use the mineral-melt equations to predict the temperature of the equilibrium and the composition of the coexisting crystal phase or phases, provided that the temperature, pressure and liquid composition are known.

Mineral-melt equations with the ideal liquid model recovered the datset to within 17°C, 9.2mol% Py, 17.2mol% Gr and 1.8mol% Alm (all 2σ). The greatest discrepancies between predicted and measured values were for grossular-rich garnets and calcic liquids (up to 40°C, 16.6mol% Py, 32.7mol% Gr and 4.0mol% Alm). The existence of a minimum on the garnet-clinopyroxene cotectic in the 30kb phase relations of the experiments of this study (Figure 3-9) shows that the ideal mixing liquid model is not appropriate for these compositions. Temperature and composition values predicted for the pyrope-rich ($>Py_{70}$) part of the iron-free join pyrope-grossular agree to within 30°C and 5wt% Py with the experimentally determined values of Maaløe & Wyllie (1979).

Garnet-liquid equations incorporating a regular mixing model for the liquid phase recovered the dataset to within 29.4°C, 3.4mol% Py, 5.2mol% Gr and 1.6mol% Alm (all 2σ), but were unable to predict values for liquids other than those of the datset due to the numerical instability of their derived partial regression coefficients. This is believed to be due to the existence of interrelationships amongst the compositional variables, which are assumed to be independent by the regression model.

Partial phase diagrams were constructed for part of the plane CS-MS-A involving garnet- and clinopyroxene-liquid equilibria. Predicted temperature and garnet composition values from the mineral-melt equations (ideal liquid model) were used to contour the diagrams. Predicted positions of the

garnet–clinopyroxene cotectic agree well with expeimentally determined positions. These diagrams, constructed for liquids with Mg'=85 and Mg'=100, can be read to obtain the composition of the garnet coexisting with any liquid and the equilibrium temperature.

6.3. Suggestions for future work

The mineral–melt equations using an ideal mixing liquid model perform well at predicting garnet–liquid and clinopyroxene–liquid equilibria for a restricted range of crystal and liquid compositions. Equations incorporating a regular solution model for the liquid recover the dataset more accurately, but cannot be used for prediction. Two lines of further research should be pursued to improve this situation. 1) Experiments are required which extend the temperature, pressure, and compositional ranges of the dataset. This could be achieved by using starting compositions containing additional components (*e.g.* Na, K, Cr, Ti). Such compositions would be expected to melt at lower temperatures than those in this study. 2) Investigation is required to find the most appropriate technique for fitting equations where many of the variables are interrelated. Mathematical programming (Berman *et al.*, 1986) may provide a basis for this.

Given suitable high–pressure data on orthopyroxene–liquid equilibria, the data of this study on garnet and clinopyroxene and the data of Ford *et al.* (1983) and Ford (1984) on olivine could be used to develop a predictive model of the melting behaviour of a gt+cp+op+ol upper mantle, and of the high–pressure crystallisation of its partial melts.

CHAPTER 7

APPENDIX

Whole-rock analyses of garnet-lherzolites as mantle-derived nodules in kimberlites and other volcanic rocks were collected from the literature. No distinction was made between granular and sheared garnet-lherzolites. The following mean oxide values were calculated. Oxides not shown below (H_2O^+, H_2O^-, P_2O_5 *etc.*) were not reported in all cases and so were not averaged. For the 161 analyses, the mean sum of the oxides CaO, MgO, FeO, Fe_2O_3 (where this was reported separately), Al_2O_3 and SiO_2 is 97.2wt%.

wt%	1	2
SiO_2	44.61	44.28
TiO_2	0.18	0.13
Al_2O_3	2.01	1.38
Cr_2O_3	0.33	0.39
Fe_2O_3	2.53	-
FeO	5.15	8.06
MnO	0.12	0.12
NiO	0.23	0.23
MgO	41.81	42.61
CaO	1.57	1.07
Na_2O	0.11	0.14
K_2O	0.13	0.09
$Fe^{2+}/Fe^{2+}+Fe^{3+}$	0.81	-
Mg' x	0.93	0.92
min	0.85	0.87

1 - mean oxides of 90 analyses with FeO and Fe_2O_3 reported separately
2 - mean oxides of 71 analyses with total iron reported as FeO

Mean (x) and minimum (min) Mg' values calculated:
Mg' = $Mg/Mg+Fe^{2+}$ for analyses with FeO and Fe_2O_3 reported
Mg' = $Mg/Mg+0.81\Sigma Fe$ for analyses with total iron as FeO

Analyses were taken from the following sources:

Aoki & Shiba (1973)

Chen (1971)

Carswell *et al.* (1979)

Carswell & Dawson (1970)

Boyd & Nixon (1973)

Cox *et al.* (1973)

Danchin (1979)

Ehrenberg (1982)

Ito & Kennedy (1967)

Jackson & Wright (1970)

Kushiro *et al.* (1972)

Mysen & Boettcher (1975a)

Rhodes & Dawson (1975)

CHAPTER 8

ACKNOWLEDGEMENTS

I am very grateful to Cliff Ford for his supervision and help throughout this project. I thank Pete Hill and Douglas Russell of the Edinburgh Microprobe Unit for their guidance and help with microprobe analysis, and Bill Tullis and Bob Brown of the workshop of the Experimental Petrology Unit for maintenance of the solid-media apparatus and manufacture of capsules and furnace parts. Gordon Biggar and Mark Welch kindly provided material for the diopside calibrations. Computer programs wriiten by Cliff Ford and by Andy Walker helped greatly with data handling and graph plotting. I acknowledge receipt of a NERC Research Studentship.

CHAPTER 9

REFERENCES

Aoki, K. & Shiba, I., (1973). Pyroxenes from lherzolite inclusions of Itinome-gata, Japan. Lithos **6**, 41-51.

Berman, R.G. & Brown, T.H., (1984). A thermodynamic model for multicomponent melts, with application to the system $CaO-Al_2O_3-SiO_2$. Geochim. Cosmochim. Acta **48**, 661-678.

Berman, R.G., Engi, M., Greenwood, H.J. & Brown, T.H., (1986). Derivation of internally-consistent thermodynamic data by the technique of mathematical programming: a review with application to the system $MgO-SiO_2-H_2O$. J. Petrol. **27**, 1331-1364.

Bickle, M.J., (1978). Magnesiowustite as O_2 calibrant in solid-media experiments. Prog. Exptl. Petrol., **4**, NERC, 122-125.

Bickle, M.J., Ford, C.E. & Nisbet, E.G., (1977). The petrogenesis of peridotitic komatiites: evidence from high-pressure melting experiments. Earth Planet. Sci. Lett. **37**, 97-106.

Biggar, G.M., (1977). Some disadvantages of $Pt_{95}Au_5$ as a container for molten silicates. Mineral. Mag. **41**, 555-556.

Biggar, G.M. & O'Hara, M.J., (1969). A comparison of gel and glass starting materials for phase equilibrium studies. Mineral. Mag. **37**, 198-205.

Bottinga, Y. & Weill, D.F., (1972). The viscosity of magmatic silicate liquid, a model for calculation. Amer. J. Sci. **272**, 438-475.

Borg, I.Y. & Smith, D.K., (1969). Calculated X-ray powder patterns for silicate minerals. Geol. Soc. Amer. Memoir **122**.

Boyd, F.R., (1970). The system $CaSiO_3-MgSiO_3-Al_2O_3$. Carnegie Inst. Wash. Yearbk. **68**, 214-221.

Boyd, F.R. & England, J.L., (1958). Development of high-pressure apparatus. Carnegie Inst. Wash. Yearbk. **57**, 170-173.

Boyd, F.R. & England, J.L., (1960). Apparatus for phase equilibrium experiments at pressures up to 50 kilobars and temperatures up to 1750°C. J. Geophys. Res. **65**, 741-748.

Boyd, F.R. & England, J.L., (1962). Effect of pressure on melting of pyrope. Carnegie Inst. Wash. Yearbk. **61**, 109-112.

Boyd, F.R. & England, J.L., (1963). Effect of pressure on the melting of diopside, $CaMgSi_2O_6$ and albite, $NaAlSi_3O_8$in the range up to 50kb. J. Geophys. Res. **68**, 311-323.

Boyd, F.R. & England, J.L., (1964). The system enstatite-pyrope. Carnegie Inst. Wash. Yearbk. **63**, 157-161.

Boyd, F.R. & Nixon, P.H., (1973). Structure of the upper mantle bemeath Lesotho. Carnegie Inst. Wash. Yearbk. **72**, 431–449.

Burnham, W.C., (1975). Water and magmas, a mixing model. Geochim. Cosmochim. Acta **39**, 1077–1084.

Burnham, W.C., (1979). The importance of volatile constituents. In "The Evolution of the Igneous Rocks: Fiftieth Anniversary Perspectives", H.S. Yoder (ed.), Princeton University Press, 439–482.

Burnham, W.C., (1981). The nature of multicomponent aluminosilicate melts. In "Chemistry and geochemistry of solutions at high temperatures and pressures", D.T. Rickard & F.E. Wickman (ed.). Phys. Chem. Earth **13,14**, 197–229.

Carswell, D.A., Clarke, D.B. & Mitchell, R.H., (1979). The petrology and geochemistry of ultramafic nodules from Pipe 200, Northern Lesotho. In "The Mantle Sample: Inclusions in Kimberlites and other volcanics", F.R. Boyd & H.O.A. Meyer (ed.). Amer. Geophys. Un., Washington, 127–144.

Carswell, D.A. & Dawson, J.B., (1970). Garnet peridotite xenoliths in South African kimberlite pipes and their petrogenesis. Contrib. Mineral. Petrol. **25**, 163–184.

Cawthorn, R.G., Ford, C.E., Biggar, G.M., Bravo, M.S. & Clarke, D.B., (1973). Determination of the liquid composition in experimental samples: discrepancies between microprobe analyses and other methods. Earth Planet. Sci. **21**, 1–5.

Chen, J., (1971). Petrology and chemistry of garnet lherzolite nodules from South Africa. Amer. Mineral. **56**, 2098–2110.

Cohen, L.H., Ito, K. & Kennedy, G.C., (1967). Melting and phase relations in an anhydrous basalt to 40 kilobars. Amer. J. Sci. **265**, 475–518.

Cox, K.G., Gurney, J.J. & Harte, B., (1973). Xenoliths from the Matsoku pipe. In "Lesotho Kimberlites", P.H. Nixon (ed.). Lesotho National Development Corporation, Maseru, 76–100.

Danchin, R.V., (1979). Mineralogy and bulk chemistry of garnet lherzolite and garnet harzburgite xenoliths from the Premier Mine, South Africa. In " The Mantle Sample: Inclusions in Kimberlites and other volcanics", F.R. Boyd & H.O.A. Meyer (ed.). Amer. Geophys. Un., Washington, 104–126.

Davis, B.T.C., (1964). The system diopside–forsterite–pyrope at 40 kilobars. Carnegie Inst. Wash. Yearbk. **63**, 165–171.

Davis, B.T.C. & Boyd, F.R., (1966). The join $Mg_2Si_2O_6$–$CaMgSi_2O_6$ at 30 kilobars pressure and its application to pyroxenes from kimberlites. J. Geophys. Res. **71**, 3567–3576.

Davis, B.T.C. & Schairer, J.F., (1965). Melting relations in the join diopside–forsterite–pyrope at 40 kilobars and at one atmosphere. Carnegie Inst. Wash. Yearbk. **64**, 123–126.

Dawson, J.B., Powell, D.G. & Reid, A.M., (1970). Ultrabasic xenoliths and lava from the Lashaine volcano, northern Tanzania. J. Petrol. **11**, 519–548.

Ehrenberg, S.N., (1982). Petrogenesis of garnet lherzolite and megacrystalline nodules from The Thumb, Navajo volcanic field. J. Petrol. **23**, 507–547.

Elthon, D. & Scarfe, C.M., (1984). High pressure phase equilibria of a high–magnesia basalt and the genesis of primary oceanic basalts. Amer. Mineral. **69**, 1–15.

Ford, C.E., (1984). Numerical modelling of phase composition changes during crystallisation of dry basic magmas. Prog. Exp. Petrol. **6**, NERC, 105–114.

Ford, C.E., Russell, D.G., Craven, J.A. & Fisk, M.R., (1983). Olivine–liquid equilibria : temperature, pressure and compositional dependence of the crystal/liquid cation partition coefficients for Mg, Fe^{2+}, Ca and Mn. J. Petrol. **24**, 256–265.

Freund, R.J. & Minton, P.D., (1979). Regression methods. Marcel Dekker, New York.

Ganguly, J. & Saxena, S.K., (1984). Mixing properties of aluminosilicate garnets: constraints from natural and experimental data, and applications to geothermo–barometry. Amer. Mineral. **69**, 88–97.

Ghiorso, M.S. & Carmichael, I.S.E., (1983). A regular solution model for met–aluminous silicate liquids: applications to geothermometry, immiscibility, and the source regions of basic magma. Contrib. Mineral. Petrol. **71**, 323–342.

Ghiorso, M.S., Carmichael, I.S.E., Rivers, M.L. & Sack, R.O., (1980). The Gibbs free energy of mixing of natural silicate liquids: an expanded regular solution approximation for the calculation of magmatic intensive variables. Contrib. Mineral. Petrol. **84**, 107–145.

Green, D.H. & Ringwood, A.E., (1967). The stability fields of aluminous pyroxene peridotite and garnet peridotite and their relevance in upper mantle structure. Earth Planet. Sci. Lett. **3**, 151–160.

Grover, J., (1976). Chemical mixing in multicomponent solutions: an introduction to the use of Margules and other thermodynamic excess functions to represent non–ideal behaviour. In "Thermodynamics in Geology", D.G. Fraser (ed.). Dordrecht–Holland, Reidel, 67–97.

Haselton, H.T. & Newton, R.C., (1980). Thermodynamics of pyrope–grossular garnets and their stabilities at high temperatures and high pressures. J. Geophys. Res. **85**, 6973–6982.

Hensen, B.J., Schmid, R. & Wood, B.J., (1975). Activity–composition relationships for pyrope–grossular garnet. Contrib. Mineral. Petrol. **52**, 161–166.

Hess, P.C., (1979). Polymerisation model for silicate melts. In "Physics of Magmatic Processes", R.B. Hargreaves (ed.). Princeton University Press, 3–48.

Howells, S., (1975). Experiments on eclogites and peridotites relevant to magma generation and temperature distribution in the upper mantle. Unpub. Ph.D. thesis, University of Edinburgh.

Ito, K. & Kennedy, G.C., (1967). Melting and phase relations in a natural peridotite to 40 kilobars. Amer. J. Sci. **265**, 519–538.

Jackson, E.D. & Wright, T.L., (1970). Xenoliths in the Honolulu Volcanic Series, Hawaii. J. Petrol. **11**, 405–430.

Jaques, A.L. & Green, D.H., (1979). Determination of liquid composition in high pressure melting of peridotite. Amer. Mineral. **64**, 1312–1321.

Johannes, W. & Bode, B., (1978). Loss of iron to the Pt-container in melting experiments with basalts and a method to reduce it. Contrib. Mineral. Petrol. **67**, 221–225.

Keesman, I., Matthes, S., Schreyer, W. & Seifert, F. (1971). Stability of almandine in the system FeO-(Fe_2O_3)-Al_2O_3-SiO_2-(H_2O) at elevated pressures. Contrib. Mineral. Petrol. **31**, 132–144.

Kushiro, I., (1964). The system diopside-forsterite-enstatite at 20 kilobars. Carnegie Inst. Wash. Yearbk. **63**, 101–108.

Kushiro, I., Shimizu, N. & Nakamura, Y., (1972). Compositions of coexisting liquid and solid phases formed upon melting of natural garnet and spinel lherzolites at high pressures: a preliminary report. Earth Planet. Sci. Lett. **14**, 19–25.

Langmuir, C.H. & Hanson, G.N., (1981). Calculating mineral-melt equlibria with stoichiometry, mass balance and single-component distribution coefficients. In "Thermodynamics of Mineral and Melts", R.C. Newton, A. Navrotsky & B.J. Wood (ed.). New York, Springer-Verlag, 247–271.

Maaløe, S. & Petersen, T.S., (1976). Phase relations governing the derivation of alkaline basaltic magmas from primary magmas at high pressures. Lithos **9**, 243–252.

Maaløe, S. & Wyllie, P.J., (1979). The join grossularite-pyrope at 30kb and its petrological significance. Amer. J. Sci. **279**, 288–301.

Masson, C.R., (1965). An approach to the problem of ionic distribution in liquid silicates. Proc. Roy. Soc. Lond. **A287**, 201–221.

Mysen, B.O., (1975). Partitioning of iron and magnesium between crystals and partial melts in peridotite upper mantle. Contrib. Mineral. Petrol. **52**, 69–76.

Mysen, B.O. & Boettcher, A.L., (1975a). Melting of a hydrous mantle: I. Phase relations of a natural peridotite at high temperatures and pressures with controlled activities of water, carbon dioxide and hydrogen. J. Petrol. **16**, 520–548.

Mysen, B.O. & Boettcher, A.L., (1975b). Melting of a hydrous mantle: II. Geochemistry of crystals and liquids formed by anatexis of mantle peridotite at high temperatures and high pressures as a function of controlled activities of water, carbon dioxide and hydrogen. J. Petrol. **16**, 549–593.

Mysen, B.O. & Kushiro, I., (1977). Compositional variations of coexisting phases with degree of melting of peridotite in the upper mantle. Amer. Mineral. **62**, 843–865.

Nathan, H.D. & Van Kirk, C.K., (1978). A model of magmatic crystallisation. J. Petrol. **19**, 66–94.

Nehru, C.E. & Wyllie, P.J., (1975). Compositions of glasses from St. Pauls peridotite partially melted at 20kb. J. Geol. **83**, 455–471.

Nielsen, R.L. & Drake, M.J., (1979). Pyroxene–melt equilibria. Geochim. Cosmochim. Acta **43**, 1259–1272.

Nielsen, R.L. & Dungan, M.A., (1983). Low pressure mineral–melt equilibria in natural anhydrous mafic systems. Contrib. Mineral. Petrol. **84**, 310–326.

O'Hara, M.J., (1963a). The join diopside–pyrope at 30 kilobars. Carnegie Inst. Wash. Yearbk. **62**, 116–119.

O'Hara, M.J., (1963b). Melting of garnet peridotite at 30 kilobars. Carnegie Inst. Wash. Yearbk. **62**, 71–76.

O'Hara, M.J., (1968). The bearing of phase equilibria studies in synthetic and natural systems on the origin and evolution of basic and ultrabasic rocks. Earth Sci. Rev. **4**, 69–133.

O'Hara, M.J. & Mercy, E.L.P., (1963). Petrology and petrogenesis of some garnetiferous peridotites. Trans. Roy. Soc. Edin. **65**, 251–314.

Ohtani, E., Irifune, T. & Fujino, K., (1981). Fusion of pyrope at high pressures and rapid crystal growth from the pyrope melt. Nature **294**, 62–64.

Presnall, D.C., Brenner, N.L. & O'Donnel, T.H., (1973). Drift of Pt/Pt10Rh and W3Re/W25Re thermocouples in single stage piston–cylinder apparatus. Amer. Mineral. **58**, 771–777.

Presnall, D.C., Dixon, J.R., O'Donnel, T.H & Dixon, S.A., (1979). Generation of mid–ocean ridge tholeiites. J. Petrol. **20**, 3–25.

Rhodes, J.M. & Dawson, J.B., (1975). Major and trace element chemistry of peridotite inclusions from the Lashaine volcano, Tanzania. Phys. Chem. Earth **9**, 545–557.

Richardson, S.W., Bell, P.M. & Gilbert, M.C., (1968). Kyanite–sillimanite equilibrium between 700° and 1500°C. Amer. J. Sci. **266**, 513–541.

Ringwood, A.E., (1975). Composition and petrology of the earths mantle. McGraw–Hill, New York.

Roeder, P.L. & Emslie, R.F., (1970). Olivine–liquid equilibrium. Contrib. Mineral. Petrol. **29**, 275–289.

Saxena, S.K. & Eriksson, G., (1983). Theoretical computation of mineral assemblages in pyrolite and lherzolite. J. Petrol. **24**, 538–555.

Saxena, S.K. & Eriksson, G., (1985). Anhydrous phase equilibria in earth's upper mantle. J. Petrol. **26**, 378–390.

Scarfe, C.M., Mysen, B.O. & Rai, C.S., (1979). Invariant melting behaviour of mantle material: partial melting of two lherzolite nodules. Carnegie Inst. Wash. Yearbk. **78**, 498–501.

Stern, C.R. & Wyllie, P.J., (1975). Effect of iron absorption by noble-metal capsules on phase boundaries in rock melting experiments at 30kb. Amer. Mineral. **60**, 681–689.

Stolper, E., (1980). A phase diagram for mid-ocean ridge basalts: Preliminary results and implications for petrogenesis. Contrib. Mieral. Petrol. **74**, 13–27.

Sweatman, T.R. & Long, J.V.P., (1969). Quantitative electron-probe microanlysis of rock-forming minerals. J. Petrol. **10**, 332–379.

Takahashi, E., (1986). Melting of a dry peridotite KLB-1 up to 14GPa : Implications on the origin of peridotitic upper mantle. J. Geophys. Res. **91**, 9367–9382.

Takahashi, E. & Kushiro, I., (1983). Melting of a dry peridotite at high pressures and basalt magma genesis. Amer. Mineral. **68**, 859–879.

Takahashi, E. & Scarfe, C.M., (1985). Melting of peridotite to 14GPa and the genesis of komatiite. Nature **315**, 566–568.

Thompson, A.B., (1979). Metamorphism in a model mantle I. Predictions of P-T-X relations in $CaO-Al_2O_3-MgO-SiO_2$. In "The Mantle Sample: Inclusions in Kimberlites and other volcanics", F.R. Boyd & H.O.A. Meyer (ed.). Amer. Geophys. Un., Washington, 15–28.

Thompson, R.N. & Kushiro, I., (1972). The oxygen fugacity within graphite capsules in piston-cylinder apparatus at high pressures. Carnegie Insi. Wash. Yearbk. **71**, 615–616.

Williams, D.W. & Kennedy, G.C., (1969). Melting curve of diopside to 50 kilobars. J. Geophys. Res. **74**, 4359–4366.

Wood, B.J. & Holloway, J.R., (1984). A thermodynamic model for subsolidus equilibria in the system $CaO-MgO-Al_2O_3-SiO_2$. Geochim. Cosmochim. Acta **48**, 159–176.

Yoder, H.S.Jr., (1975). Generation of basaltic magma. National Academy of Sciences, Washington.